

# Sheffield Hallam University

*The non-linear analysis of masonry arches.*

MALLINDER, P. A.

Available from the Sheffield Hallam University Research Archive (SHURA) at:

<http://shura.shu.ac.uk/20006/>

## A Sheffield Hallam University thesis

This thesis is protected by copyright which belongs to the author.

The content must not be changed in any way or sold commercially in any format or medium without the formal permission of the author.

When referring to this work, full bibliographic details including the author, title, awarding institution and date of the thesis must be given.

Please visit <http://shura.shu.ac.uk/20006/> and <http://shura.shu.ac.uk/information.html> for further details about copyright and re-use permissions.

ROBERTSON'S LIBRARY  
70ND STREET  
SHEFFIELD S1 1WB

6771  
06

TELEPEN

100228049 4



ProQuest Number: 10697313

All rights reserved

INFORMATION TO ALL USERS

The quality of this reproduction is dependent upon the quality of the copy submitted.

In the unlikely event that the author did not send a complete manuscript and there are missing pages, these will be noted. Also, if material had to be removed, a note will indicate the deletion.



ProQuest 10697313

Published by ProQuest LLC (2017). Copyright of the Dissertation is held by the Author.

All rights reserved.

This work is protected against unauthorized copying under Title 17, United States Code  
Microform Edition © ProQuest LLC.

ProQuest LLC.  
789 East Eisenhower Parkway  
P.O. Box 1346  
Ann Arbor, MI 48106 – 1346

# **THE NON-LINEAR ANALYSIS OF MASONRY ARCHES**

P.A. Mallinder

A thesis submitted in partial fulfilment of the  
requirements of  
Sheffield Hallam University  
for the degree of Doctor of Philosophy

1988

T H E N O N - L I N E A R A N A L Y S I S

O F

M A S O N R Y A R C H E S

*Submitted by Peter Alan Mallinder to The Council for National Academic Awards for the degree of Master of Philosophy. Sponsored by Sheffield City Polytechnic and in collaboration with South Yorkshire County Council. Submitted in partial fulfillment of the requirements for the degree of Master of Philosophy, December 1988.*

"Some of the problems of arch analysis cannot be solved by either rational or empirical methods alone. They are problems in probability in which the range of uncertainty of certain fundamental variables is a matter for observation, but the probable uncertainty in the results consequent upon the accidental combination of these variables can scarcely be determined by experiment"

*Professor Hardy Cross,*

*University of Illinois.*

# C O N T E N T S

LIST OF FIGURES .....	I 5
LIST OF TABLES .....	I 7
LIST OF PLATES .....	I 8
ACKNOWLEDGEMENTS .....	I 10
ABSTRACT .....	I 11
CHAPTER 1 - INITIAL CONSIDERATIONS .....	1
1.1 Introduction .....	1
1.2 The Arch Form .....	5
1.3 Historical Résumé .....	11
1.4 Modern-day Arch Assessment .....	14
1.4.1 The Work Of Professor Pippard And The MEXE Method .....	14
1.4.2 Professor Heyman's 'Mechanism' Approach .....	22
1.4.3 Finite Element Analysis .....	27
1.5 Summary .....	30
CHAPTER 2 - FIELDWORK .....	33
2.1 Introduction .....	33
2.2 Darfield And Burying Lane Bridges .....	33

2.3	Bridge At Kettlewell, North Yorkshire .....	35
2.4	Bradberry Balk Lane Bridge, South Yorkshire .....	37
2.5	Ribblehead Viaduct, North Yorkshire .....	40
2.6	Bolton Mill Bridge, South Yorkshire .....	42
2.7	Bridge Near Argeles, France .....	44
2.6	Rivelin Mill Bridge, Sheffield, South Yorkshire .....	46
2.9	Summary .....	47
CHAPTER 3 - CONSTITUTIVE MODEL .....		53
3.1	Introduction .....	53
3.2	Stroke-controlled Core Test Programme .....	53
3.3	General Formulation .....	60
3.3.1	Introduction .....	60
3.3.2	Uncracked Section .....	63
3.3.3	Cracked Section .....	68
3.4	Solution Procedures .....	73
3.4.1	Introduction .....	73
3.4.2	Typical PSTRESS1 Input/Output .....	74
3.5	Limit State Interaction Diagram .....	81
3.5.1	Uncracked Section .....	81
3.5.2	Cracked Section .....	84
3.5.3	Axial Force/Bending Moment Interaction Diagram .....	86
3.5	Summary .....	89
CHAPTER 4 - MASONRY ARCH BRIDGE ANALYSIS .....		92
4.1	Introduction .....	92
4.2	Static Mechanism Model Assumptions .....	93

4.3	Static Mechanism Model Topology .....	96
4.4	Limit State Equations Including Load Dispersal Through Fill	96
4.5	Limit State Equations For Arch Barrel Only .....	102
4.6	Computer Program MECHARCH .....	103
4.6.1	Program MECHARCH .....	103
4.6.2	Load Dispersal Through Fill Medium .....	105
4.7	MECHARCH Validation .....	107
4.7.1	MECHARCH Analysis Applied To Bridgemill Full-scale Test .....	107
4.7.2	MECHARCH Analysis Applied To A Comparability Study ....	110
4.7.3	MECHARCH Analysis Applied To Two Further Full-scale Tests .....	113
4.7.4	MECHARCH Analysis Applied To Liverpool University Model Test .....	117
4.8	Serviceability Model .....	119
4.8.1	Introduction .....	119
4.8.2	Initial Serviceability Model .....	119
4.8.3	General Solution Of The Matrix Equations .....	128
4.8.4	Initial Serviceability Case Studies .....	129
4.8.5	Development Of The Serviceability Model .....	132
4.8.6	SERVARCH Vs Bridgemill Full-scale Test .....	136
4.9	Summary .....	140
CHAPTER 5 - COMMENTS AND CONCLUSIONS .....		142
5.1	Preliminary Assessment .....	142
5.2	Secondary Factors .....	144
5.3	Suggestions For Further Work .....	145

APPENDIX 'A' - SOFTWARE LISTING ..... A 1

APPENDIX 'B' - PUBLICATIONS ..... A 8

APPENDIX 'C' - NOMENCLATURE ..... A 20

APPENDIX 'D' - BIBLIOGRAPHY ..... A 23

# L I S T O F F I G U R E S

Figure	Title	Page
1.1	Cumulative Numbers Of Public Road Bridges In The United Kingdom .....	2
1.2	Arch Terminology .....	9
1.3	Pippard's Elastic Analysis .....	16
1.4	Typical Heyman Collapse Model .....	25
1.5	Typical Finite Element Mesh .....	28
2.1	Demolition Of Bradberry Balk Lane Bridge .....	39
3.1	Typical Load-deflection Response From A Rivelin Mill Core .....	58
3.2	Idealised Parabolic Stress-strain Law .....	62
3.3	Topology For Uncracked Sections .....	64
3.4	Topology For Cracked Sections .....	69
3.5	Typical PSTRESS1 Graphical Output For An Uncracked Masonry Section .....	75
3.6	Typical PSTRESS1 Graphical Output For A Cracked Masonry Section .....	77
3.7	Typical PSTRESS1 Graphical Output Depicting Stress And Strain Plots After Solution .....	78
3.8	Ultimate Failure Stress And Strain Plots For The Example Given In The Text .....	80
3.9	Limit State Interaction Diagram .....	87

3.10 Numerically Derived Moment-Maximum Strain	
Locus For $n=0.45$ .....	90
4.1 Topology .....	97
4.2 Left Substructure .....	98
4.3 Right Substructure .....	99
4.4 Typical Graphical Output From Computer Program SPREAD .....	106
4.5 Topology .....	120
4.6 Case Studies .....	131
4.7 FLEXARCH - NIARCH - SERVARCH Development .....	134

# L I S T O F T A B L E S

Table	Title	Page
4.1	Bridgemill Analyses .....	109
4.2	Comparability Study Results .....	112
4.3	Prestwood And Torksey Bridges - Basic Data .....	114
4.4	Prestwood And Torksey Results .....	116

# L I S T O F P L A T E S

Plate	Title	Page
1.1	Vaulting To York Minster's Roof .....	7
1.2	A Typical Flying Buttress At York Minster .....	7
2.1	Darfield Bridge, After Passage Of Mining Wave, As At July, 1966. ....	34
2.2	Burying Lane Bridge, After Passage Of Mining Wave, As At November, 1975. ....	34
2.3	Bridge At Kettlewell, North Yorkshire, Damaged By Frost Action. ....	36
2.4	Close-up Showing Internal Construction .....	36
2.5	Bradberry Balk Lane Bridge During Course Of Demolition ....	38
2.6	A Typical Voussoir From Above Bridge, Cleaved Into Four For Transit. ....	38
2.7	Ribblehead Viaduct .....	41
2.8	Typical Cracking On Ribblehead's Masonry Piers .....	41
2.9	Bolton Mill Bridge, South Yorkshire, Showing Overall Poor Condition .....	43
2.10	Crown Of Bolton Mill Bridge - Note Inscription .....	43
2.11	A Part Demolished French Multi-span Bridge .....	45
2.12	Note Increase In Parapet/Spandrel Wall Thickness (Background, Right) In This Same Example Of French Practice .....	45

2.13 Rivelin Mill Bridge, Sheffield, During Strengthening Programme .....	48
2.14 A View Of Rivelin Mill's Intrados Showing Roughness Of Voussoirs .....	49
2.15 Rivelin Mill: Note Angle Of Voussoirs To Springers Due To Skew .....	50
2.16 Rivelin Mill: Rough Nature Of Inner Face Of Spandrel Wall Apparent .....	51
2.17 Rivelin Mill Bridge, Sheffield, With Sample Of Spalled Voussoir In Foreground. The Cigarette Packet Is Used To Give A Visual Indication Of Scale. Cores Taken From This Sample Were Used In A Series Of Stroke-controlled Compression Tests .....	52
3.1 50mm Cores Taken From A Rivelin Mill Bridge Voussoir .....	55
3.2 Rock From The Same Source After Point Load Testing .....	55
3.3 The Point Load Testing Apparatus .....	56
3.4 The 'Stiff', Stroke-controlled Rock Core Testing Apparatus. ....	57
3.5 A Core Ready For Testing .....	59
3.6 A Failed Core From Rivelin Mill Bridge After Testing .....	61
4.1 Prestwood Bridge On The Point Of Collapse .....	95

## A C K N O W L E D G E M E N T S

The author would like to take this opportunity to express his appreciation to Dr. N. W. Taylor, Director of Studies, particularly for the production of equations (3.45) to (3.66), to Mr. J. Ducker, Second Director of Studies, and to Mr. B. L. Davies, External Supervisor, for their help and guidance.

Appreciation is also expressed to Mr. D. A. Richardson for his contribution to the geotechnical experimentation.

# A B S T R A C T

( P. A. Mallinder )

## THE NON-LINEAR ANALYSIS OF MASONRY ARCHES

The objective of the research programme has been to investigate the problems besetting the national masonry arch bridge stock and to propose enhanced means of appraisal accordingly. The programme has involved site assessments and limited experimentation together with limit state and serviceability analyses. All theoretical and empirical studies have been mounted as micro-computer software and are supported by computer graphics. Throughout, the accent is on engineering requirements in practice; the almost universal absence of as-built drawings and the involvement of natural materials whose mechanical properties are highly variable are to be noted from the outset.

Initial considerations relating to the arch form, its historical context and present masonry arch assessment methods are set out in Chapter 1. Fieldwork studies are presented in Chapter 2.

The concept that masonry has finite compressive strength is accordingly considered in Chapter 3 which includes experimentation establishing the appropriate constitutive properties with respect to natural rock. A general moment-thrust response modelling is established and an original non-linear limit-state moment-thrust interaction diagram is determined.

Limit state and serviceability masonry arch bridge models of innovatory form are included in Chapter 4. These models follow from the studies of Chapter 3 and are novel in their own right. However, the critical arguments upon which they are based demand that these models be seen as prototypes of enhanced models whose features have now been established.

Overall conclusions are discussed in Chapter 5 wherein the practical factors affecting the nature of masonry arch bridges are juxtaposed with the engineering requirements imposed upon them. Modern assessment methods must afford output that is safe without being overconservative. The findings of the research programme are in keeping with this. Supporting documentation is given in the Appendices.

## CHAPTER 1

### INITIAL CONSIDERATIONS

#### 1.1 INTRODUCTION

The arch is one of the oldest structural principles known to man. Its usefulness first became apparent to the civilisations of pre-history, thousands of years ago. Throughout almost the whole of our ascent to technological mastery, the arch reigned supreme as the only structural form capable of spanning appreciable distances without the need for materials of tensile strength. The art of arch exploitation reached its zenith in the middle ages with the construction of magnificent cathedrals throughout Europe. It was not until comparatively modern times that the world's first non-masonry arched bridge at Ironbridge, Staffordshire, heralded the end of the era. The rapid progress of the industrial revolution ensured that by the beginning of the 20th Century the masonry arch was virtually obsolete, having been replaced by flat bridges of steel and reinforced concrete. Such is the durability and longevity of masonry arch structures, however, that even though virtually none have been constructed for the last sixty years or more, they still account for the largest single group of public road bridges in the United Kingdom<sup>(1)</sup>. Figure 1.1 gives indication of our inheritance of these old masonry bridges.

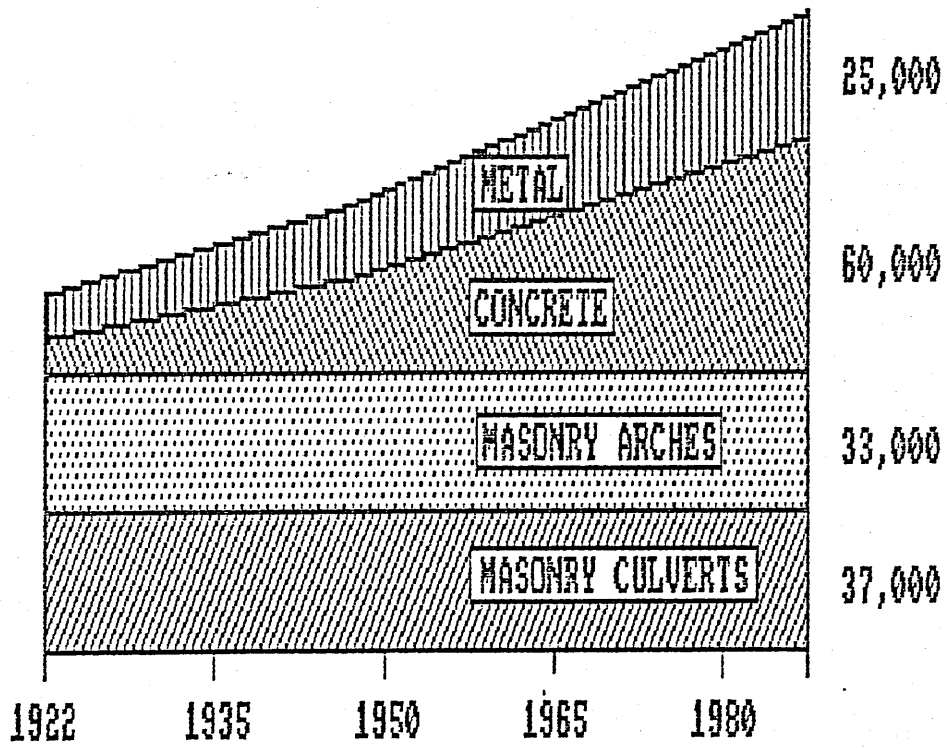


Figure 1.1

Cumulative Numbers of Public Road Bridges in the United Kingdom

Their continued abundance among the country's bridgestock gives rise to serious problems for several reasons. First of all, none of them were "designed" in the modern sense. Most would probably have had no calculations at all applied to their construction - merely having been built to conform to traditional proportions - and even the ones that were the subject of calculations would have often had these based upon simple empirical theory or even rules of thumb. Additionally, records of their dimensions, internal structure and so forth have rarely survived. The second problem is that the loading that was envisaged at the time revolved about the horse and cart - a far cry from the modern 38 tonne heavy goods vehicle. The final problem is simply that of old age and progressive deterioration. Even structures as durable and with such reserves of strength as these do eventually fail. The current position is therefore that, although no new masonry arch bridges are today being built, there is a great need to develop modern techniques aimed at determining the strength of these existing structures when subjected to present day highway loading. The emphasis has thus moved from design to assessment<sup>(2,3,4)</sup>.

There are two main schools of thought with respect to modern masonry arch analysis. The first, chronologically, is almost entirely due to the work of Professor Heyman<sup>(5,6,7,8)</sup> of Cambridge University and concerns limit state philosophy. His approach assumes infinite compressive strength for the arch material and deems failure to occur upon the formation of four mechanistic hinges (or "plastic hinges", according to some sources). Promise is shown by the technique, it being supported by observations of failure modes of this type in

practice<sup>(9)</sup>, although actual numerical predictions of collapse loads are often not as good as one would hope. Whilst basically appropriate to many arch configurations, further development is undoubtedly necessary to achieve consistent and accurate results. The second school of thought is concerned with evaluation of full load-displacement path histories employing finite element analysis<sup>(4,10,11)</sup>, a technique familiar to structural engineers. Perhaps surprisingly, the results from this approach have often been disappointing. Again the reason is that the modelling is not sufficiently representative of reality, and short of a massive increase in complexity this may remain so.

It is worthy of note that contemporary research in this field has been primarily devoted to the prediction of an ultimate collapse load for an arch, whereas in practice it is the service load capacity of the arch that is of relevance to the bridge owner. It is possible that the latter may be determinable from a collapse value by simply factoring down, but at present the relationship between the two states is a matter for conjecture.

The author has attempted to make contributions to the current state of knowledge in predominantly three areas. Firstly, a detailed theoretical study of the fundamental engineering properties of masonry has been undertaken and the results, apart from being of value in their own right, have been utilised in the remainder of the work. Secondly, a refinement of the mechanism-type analysis has been developed, using the results of the above studies, whereby the

"infinite compressive strength" assumption is replaced by actual masonry constitutive properties. An item of computer software has been written to carry out the analysis and to arrive at an ultimate collapse load prediction. The third area of application is again computer based. Essentially, an iterative, piecewise linear flexibility analysis is performed with adjustments being made to the arch model during each cycle to allow for the attendant degradation of structural stiffness. The procedure is continued until a hinge is deemed to have developed. In the latter case, then, the objective is the study of arch behaviour up to such a notional "serviceability" limit state and is complementary to the previously described ultimate limit state studies. However, it is considered possible that that a first hinge could form very early during the loading regime and that this would cause revision of the notional serviceability definition<sup>(7)</sup>.

The various techniques developed have been compared against full scale and model tests and the results are discussed and conclusions drawn. Throughout, attention is focussed upon single span, non-skewed arch forms with non-laminated arch barrels.

## 1.2 THE ARCH FORM

The Romans constructed the first proper roads and bridges in the British Isles but of the latter only piers and foundations have

survived. The oldest surviving British bridges are mediæval arched river crossings. A few of these date from the 12th Century but thereafter ever increasing numbers of arch bridges survive up to the end of the 19th Century, and indeed there exist some examples dating from the early 20th Century.

As a constructional material, bricks were used by the Romans but they were not used again in Britain until their re-introduction in the 13th Century. The earliest examples of arch bridges in Britain are therefore invariably of stone.

The most common arch profile is segmental - Roman arches were in fact semi-circular, in the mistaken belief that only vertical reactions could result<sup>(12)</sup>. Until the 15th Century the pointed style was also common, a product of the Gothic school of architecture. During this period greater consideration was given to aesthetic qualities than to likely structural performance, with the inevitable result that many arches collapsed on removal of the centering.

Many fine examples of mediæval architecture still exist. Plate 1.1 depicts the magnificent York Minster - widely recognised as one of the master works of western architecture - where instances of the exploitation of the arch principle abound<sup>(13)</sup>. Plate 1.2, for example, shows one of the Minster's many flying buttresses. Yet a further development of the arch principle can be seen elsewhere in the construction of domes. These are merely three-dimensional arches, and instead of the need to provide strong abutments to resist the arch's

Plate 1.1  
Vaulting To  
York Minster's Roof

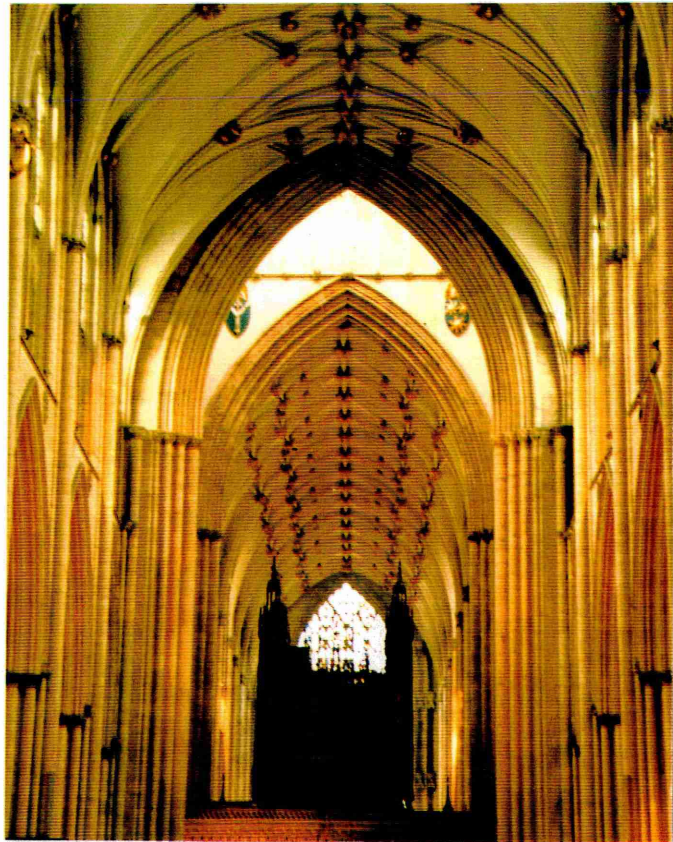


Plate 1.2  
A Typical Flying Buttress  
At York Minster



horizontal thrust, a continuous ring beam is provided around the dome's base. The aim of the present studies is, however, to consider arches in their more usual form, particularly in their application to bridges, and consequently their action and construction in such cases will be briefly described. Figure 1.2 enables the main structural components to be observed. The main "working" structural component of an arch is the ring (or barrel) which is composed of discrete, wedge-shaped masonry components termed "voussoirs" - as many of the early studies of arch behaviour were conducted by the French, then so are many of the terms used of French extract. The voussoirs are usually, but not necessarily, cemented together. The main purpose of this is to provide a good bedding between adjacent voussoirs, rather than for the purpose of transmitting tensile forces since the arch ring is essentially, and most importantly, a compression-only structural element. Indeed, it was the advent of true tensile structural materials that heralded the end of the masonry arch.

In order to provide a relatively level deck surface, a layer of fill material is placed over the arch ring, possibly together with a waterproof membrane. Good fill material is relatively incompressible, inorganic and inert; in practice, fill is often of lesser quality. In addition to "levelling up" the top of the arch, the fill also provides a permanent dead load. As is sometimes the case with arches, a counter-intuitive phenomenon exists here. That is, with most bridges a large dead load is undesirable as it means that, for a given bridge, less live load may be carried. The opposite is true of arch bridges. Within reason, a greater dead load mobilises more

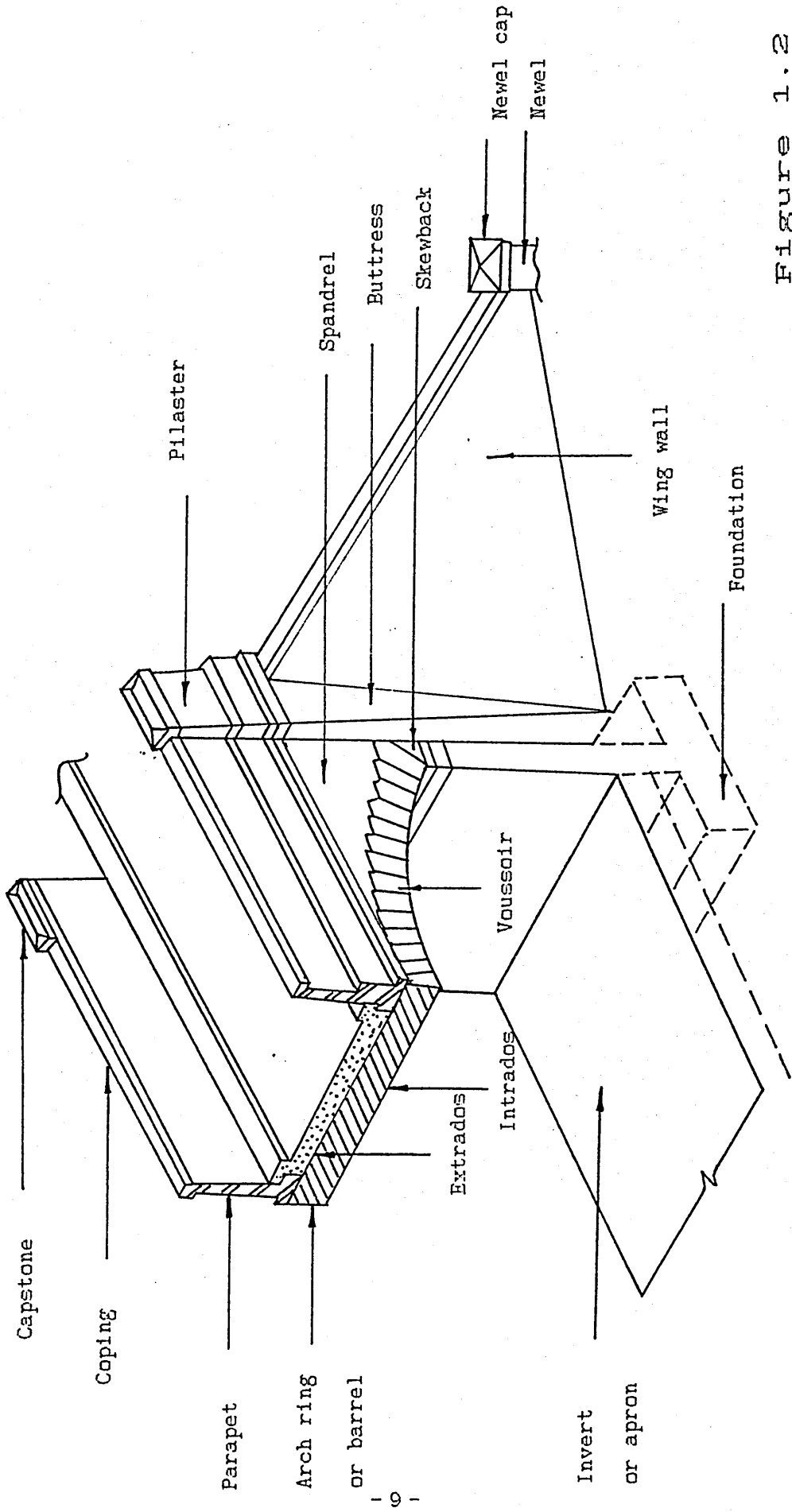


Figure 1.2

Arch Terminology

pre-compression in the arch ring - in much the same way as prestressing tendons put pre-compression into a beam - and thus the arch is able to resist more live load bending. With the prestressed beam analogy, a limiting value on the amount of prestress available is quickly reached as a result of limiting compression. Owing to the massive cross-section present in an arch ring, its respective compression upper limit is very high indeed, and thus the arch will benefit from large depths of fill above it.

There is a second advantage in deep fill. As a live load passes over the arch, perhaps in the form of near-point loads from wheels and so forth, the fill has the effect of dispersing the load such that by the time it reaches the arch ring, it has become a distributed load of some kind. All structures find point loads more onerous than distributed loads of the same total magnitude, but this is even more true of the arch. The reason is that, again counter-intuitively, the critical load position for an arch is around the quarter point - unlike for a simple beam, where the critical point is obviously midspan. This being the case, if a point load applied at the right hand quarter point is dispersed by the fill, some of the load shed may find its way towards the left quarter point and this would actually provide a *relieving* effect, rather than contributing to collapse as would be the case with an equivalent beam.

To properly perform its function, the fill must be restrained from lateral movement and this is the role of the spandrel walls. These simply sit astride the arch ring, debatably providing it with an edge

stiffening effect, and often giving rise to problems of a local failure kind<sup>'14'</sup> (rather than a global failure of the arch) due to the lateral pressures that they experience. Spandrels may tilt, slide or bulge and in doing so help allow the adjacent fill to rut and settle.

The final component of an arch is the abutment. All arch rings (even semi-circular ones) gain part of the reaction for their large compressive forces from the horizontal direction. Thus they not only exert a vertical force on their abutments, but a significant horizontal one also, though it may generally be said that the steeper the arch, the lower the horizontal component is likely to be.

These then, are the main elements of a masonry arch. Although the function of each of them is simple to describe, and arches may be constructed relatively easily by primitive means and by unskilled labour, the formal action of each element, and the interaction between them, is exceedingly complex to fully comprehend.

### 1.3 HISTORICAL RÉSUMÉ

In the year 1676 Hooke<sup>'12'</sup> propounded the first theory of arch mechanics. He drew an analogy between a flexible hanging catenary and a rigid inverted catenary. It was left to Gregory in 1697 to develop the postulation that an arch would only be "safe" if an inverted catenary could be included within its thickness.

La Hire (1695) was next to contemplate the problem. By constructing a force polygon for the individual voussoir weights he was able to determine the thrust in an arch. As a result of this he was better able to design adequate abutments to resist this thrust.

Couplet's memoir of 1730 stated that an arch would not collapse if the chord of half the extrados did not cut the intrados but lay within the thickness of the arch. He then examined the semi-circular arch subjected to self-weight only and assumed that it collapsed by breaking into four pieces. He developed a cubic equation relating the ratio of arch depth,  $d$ , to the mean radius,  $r$ , and postulated that the minimum value of the ratio  $d/r$  was 0.107. Unfortunately, Couplet's work was forgotten but later much of the same ground was covered by Coulomb.

In the year 1800 Boistard tested a series of model arches featuring dry-jointed voussoirs. One of the models tested was of the very shallow Pont de Nemours, possessing a span to rise ratio of no less than sixteen. Boistard's aims were threefold. Firstly, he wished to observe models of failure under various load conditions; secondly to determine the minimum abutment requirements for resisting horizontal arch thrust and finally to obtain an estimate of the forces exerted on centering during construction. During one of his tests on a semi-circular arch of forty eight voussoirs he observed that it was possible to construct the arch almost up to the quarter points without centering. This ability of semi-circular arches to support themselves

was quite likely utilised by the Romans and other arch builders of antiquity.

In 1826 Navier was the first to suggest that if the line of thrust lay within the middle third of the voussoirs then none of the arch could be in tension. Following this, Professor Moseley showed in 1835 that, if the arch ring was unable to resist tension, the line of thrust must lie everywhere within the arch ring. Later, in 1846, Snell was to raise the question of the possibility of material failure affecting the position of the line of thrust.

Also in 1846 Barlow<sup>(15)</sup> demonstrated, by means of a model, that Moseley must be correct. The model employed voussoirs with curved contact faces such that only one contact point was possible. When loaded, the voussoirs "rolled" against one another until equilibrium was reached whereupon the thrust line (joining the contact points) could be observed. Barlow pointed out that, provided the arch was sufficiently deep to contain the thrust line, then many thrust lines were possible. He also raised the important point that, because the assumptions of infinite compressive strength and perfect joints were unrealistic, then the lines of thrust must not be allowed to approach the edges of the arch ring. This note of warning has a bearing on the later, much more recent work carried out by Professor Heyman<sup>(5,6,7,8)</sup>, and is a feature of the author's constitutive studies.

In the year 1845 Villarceau presented a treatise to the Academie des Sciences in France in which he developed a design method which

required the centre line of the voussoirs to coincide with one of the possible thrust lines for the load condition, thereby achieving a safe design. By solving the resulting numerical equations Villarceau thus produced the first definite design tool. Professor Heyman, in modern times, has suggested that much of Villarceau's work is still valid and would result in an economical and safe design.

In 1879 Castigliano<sup>(16)</sup> developed the concept of structural analysis by the strain energy method and was to apply this technique to two arches. However, with the gradual introduction during the nineteenth century of new materials such as cast and wrought iron, the era of masonry arch construction was drawing to a close and with it much of the interest in arch mechanics. In the future, interest would eventually be rekindled but not, as previously, would it be centred on analysis for the purpose of subsequent design, but rather upon the assessment of existing arches required to carry loads far in excess of those envisaged by their designers, generations before.

#### 1.4 MODERN-DAY ARCH ASSESSMENT

##### 1.4.1 The Work Of Professor Pippard And The MEXE Method

In the 1930's, Professor Pippard<sup>(17)</sup>, of the Castigliano "elastic" school, conducted model experiments and analyses that were to form the basis of arch assessment, in various guises, for the next fifty years. In particular, the Department of Transport's own approach<sup>(2,3)</sup>

is still largely based on his work and for this reason the background will be considered in some detail.

Professor Pippard limited consideration to the case of a two-pinned arch<sup>(17)</sup> on the basis that although masonry arch bridges are nominally doubly encastre, hinges form at the abutments very early during the loading regime due to very slight spreading of the latter. Furthermore, he was only to consider arches of parabolic profile with a ratio of quarter point rise to crown rise of 3 to 4 subjected to a central point load, as illustrated in Figure 1.3. Analysis of this singly redundant system was based on strain energy. Letting  $M_x$  denote the bending moment at abscissa  $x$ , then the strain energy,  $U$ , may be given as

$$U = 2 \int_0^{1/2} \frac{M_x^2 ds}{2EI} \quad \dots (1.1)$$

where  $ds$  denotes an element of arc length of arch ring,  $EI$  refers to flexural rigidity and  $H$  denotes the horizontal reaction.

$H$  can be evaluated employing the principle that  $dU/dH = 0$ , if  $H$  does no work, such that

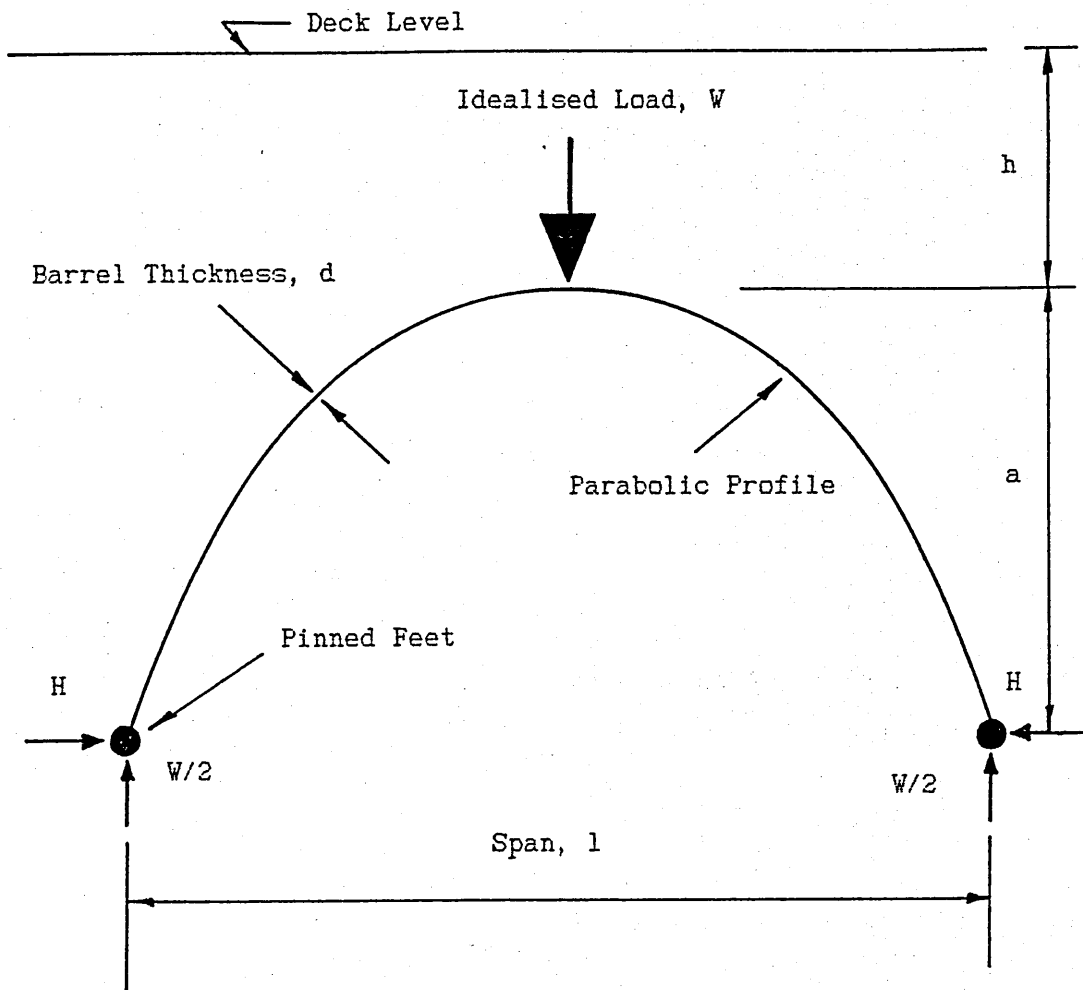


Figure 1.3  
Fippard's Elastic Analysis

$$\int_0^{1/2} \frac{M_x dM_x ds}{EI dH} = 0 \quad \dots (1.2)$$

To effect a simplification, Pippard adopted the relationship

$$I = I_0 \frac{ds}{dx}$$

where I represents the second moment of area of the arch ring at x, and I<sub>0</sub> the same at the crown (Figure 1.3); this implies that the arch ring thickness increases towards the springings. This yields

$$\int_0^{1/2} \frac{M_x dM_x dx}{dH} = 0 \quad \dots (1.3)$$

noting that the horizontal component of force is constant throughout an arch ring. Manipulation affords H<sub>1</sub>, the thrust at the crown due to live load to be

$$H_1 = 25W(1/a)/128 \quad \dots (1.4)$$

with the bending moment at the crown due to live load, M<sub>1</sub>, becoming

$$M_1 = -7Wl/128 \quad \dots (1.5)$$

These values must now be superimposed on the corresponding values arising from the dead loads due to the arch ring and the fill. Pippard assumed that the effective width of the bridge was  $2h$ , suggesting a  $45^\circ$  live load dispersal at the crown. It is furthermore assumed that the arch ring and fill material have equivalent specific weights (denoted by  $\rho$ ) with the fill possessing zero strength and thereby imposing a purely vertical load on the arch ring. A second strain energy analysis now provides the thrust at the crown,  $H_d$ , due to dead load to be

$$H_d = \rho l^2 h (a/21 + (h+d)/4) / a \quad \dots (1.6)$$

and the bending moment at crown,  $M_d$ , due to dead load

$$M_d = \rho l^2 a h / 168 \quad \dots (1.7)$$

Combining equations 1.4 to 1.7 (superposition of live and dead load effects) yields the horizontal thrust, which is constant across the arch, to be

$$H = (\rho l h (a/21 + (h+d)/4) + 25W/128) l / a \quad \dots (1.8)$$

and the bending moment at the crown

$$M_{\text{crown}} = (\rho l a h / 42 - 7W/32) l / 4 \quad \dots (1.9)$$

Pippard now suggests two possible limiting criteria. As W increases, either the thrust line at the crown rises and tension develops, this tension being limited by a "middle half" rule such that

$$W_{lim \text{ tens}} = (32\rho lh(2a^2+4ad+2ld(h+d)))/(21(28a-25d)) \quad \dots (1.10)$$

or, it may instead be the case that a certain limiting value of compressive stress, f, is reached, whereupon

$$W_{lim \text{ compr}} = (256fhd/l+128\rho lh(a/28/d-1/21-(h+d)/4/a))/(25/a+42/d) \quad \dots (1.11)$$

Pippard then draws upon his experimental work<sup>(17)</sup> to conclude that the former approach (the "middle half") is the most appropriate. Based upon this work, Pippard was later to produce safe load tables for arches. By assuming a parabolic profile with a span to rise ratio of four and knowing the span, the arch ring thickness and the depth of cover to the crown, together with values for the arch ring and fill specific weights, it was possible to read off the maximum possible safe central point load from the tables.

Pippard, in conjunction with Baker, was later to put forward four possible modes of arch failure:

1. Development of excessive tensile stress in the jointing material.

2. Development of excessive compressive stress in the voussoir material.
3. By the sliding of one voussoir over another.
4. By spreading of the abutments.

The formation of a "mechanism" was not specifically mentioned - note the "elastic" nature of the method - although this type of failure had been observed in the model tests<sup>(17)</sup>. Presumably, since the development of excessive tensile/compressive stresses must precede the formation of a mechanism, conditions 1 and 2 above would cover this eventuality.

During the second world war it became necessary to route heavy military traffic, such as tanks, over public road bridges and, especially in times of emergency, a simple, quick means of estimating arch bridge carrying capacity was required. The Military Engineering Experimental Establishment (MEXE) thus developed a technique based on the earlier work of Pippard. After the war, the MEXE method, as it has come to be known, was adopted by the Department of Transport and by this stage it incorporated a nomogram to evaluate its only "mathematical" element.

The MEXE method was issued to local authorities in various memoranda over the years, the latest of these being the current Departmental Standard BD21/84<sup>(2)</sup> and its accompanying Advice Note, BA16/84<sup>(3)</sup>. Both of these documents were issued in 1984. In addition to MEXE,

they permit the application of alternative analyses with certain conditions.

MEXE itself is quick and simple to apply, a desirable prerequisite considering the number of arch bridges that require assessment at regular intervals. It initially enables the calculation of a "provisional axle load" utilising the span, arch and fill thickness at the crown - this is done by means of a nomogram (or a formula). The provisional axle load is then modified by a series of factors that are meant to compensate for the deviation of the real arch from the assumed ideal. These factors adjust for span to rise ratios other than four to one, for the shape of the arch, for the type of arch and fill materials, for the state of the joints and for the overall condition. The resulting "modified axle load" now represents a permissible axle load for a two-axled bogie. The permissible axle load for single axle and tri-axles may then be calculated from this and allowances made for the case where a bogie axle may "lift off" due to road surface irregularities or to a hump-back bridge. A weight restriction may then be applied to the bridge if the calculation suggests that "construction and use" vehicles cannot be allowed unrestricted passage. Great reliance is placed on the judgement of the bridge inspector in arriving at the various condition factors. Furthermore, the MEXE method is thought to be too conservative<sup>(12)</sup>, particularly so for longer spans. The Departmental Standard and Advice Note do, however, permit the use of alternative techniques.

#### 1.4.2 Professor Heyman's "Mechanism" Approach

Professor Heyman's approach is often termed "plastic", though this is not used in the same sense as when, say, it is applied to structural steelwork analyses, since in the present context one is dealing with a brittle material. Heyman observes that "plastic" analysis of arches dates back to the 18th century and therefore pre-dates elastic methods. The objective is to determine the ultimate limit state loading on the basis that a four hinge mechanism will initiate a collapse.

The approach is founded on the following basic assumptions:

1. The arch ring material is infinitely strong in compression, or the stress levels are so low that compression failure is rendered unlikely.
2. The arch ring material possesses zero tensile strength.
3. No sliding (shear failure) is likely between voussoirs.
4. Live loads are transmitted from the deck surface down to the level of the arch ring without any dispersal.

Assumption 1 is essentially unsafe, of course, but is considered to be close to the truth in this context and is therefore more reasonable than it might at first appear. In essence it implies that the "thrust line" is able to approach the very edge of the arch ring before failure occurs. Common sense dictates that this cannot be so, and that failure must occur slightly sooner. Just how much sooner will be

considered in greater detail in Chapter 3. For the present, however, it can be said that the result of this assumption must be to give the method a tendency to predict a slightly higher ultimate strength for any given arch than is actually the case. It also has the implication that no knowledge at all is needed regarding the constitutive properties of the arch material. This is in contrast to other methods where some form of stress-strain relationship is required

The second assumption regarding zero tensile strength is, at least for cemented arch rings, also untrue but in the absence of any other reliable data, a reasonable one that is often applied in general masonry design.

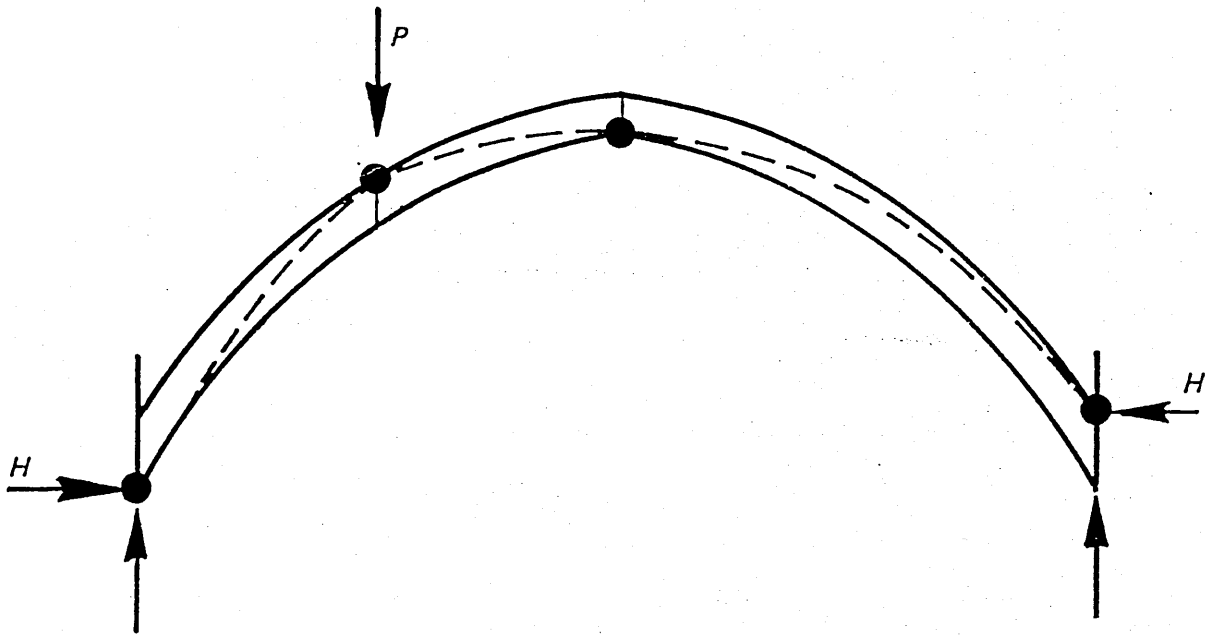
The shear failure assumption is again debatable. Punching shear failure was not observed in the Bridgemill full-scale load test<sup>(3)</sup>. However, punching of an individual voussoir, perhaps overlain by an isolated piece of rock fill is feasible - Rivelin Mill bridge described in Chapter 2 exhibited an individual punched voussoir - but the author would tend to agree that a global failure initiated by punching shear under normal traffic loads is extremely unlikely.

To ignore the dispersal of live loads through the arch fill material is quite a substantial approximation. While accepting that determination of the exact pattern of loading that the arch ring experiences from an arrangement of loads at deck level is not simple, almost any kind of dispersal assumption is likely to yield more accurate results, particularly when the load is remote from the crown.

However, Heyman's assumption in this respect is at least "safe" in that it will result in the prediction of lower ultimate strengths than in actuality, since a concentrated load of a given magnitude is more onerous than a "smeared" load of the same total magnitude.

It will be seen that the two main approximations inherent in the method, namely infinite compressive strength and the absence of live load dispersal, tend to work in opposite directions and therefore to cancel. The amount of "cancelling" will depend upon many parameters, geometrical and constitutive, and will vary from one study to another.

From this point, Heyman next divides the arch fill and barrel into vertical 'slices' and assumes that the weight of each of these slices is applied as a point load to the arch. The live loading is similarly treated as one or more point loads and the resulting thrust line through the arch ring constructed by a geometrical method. Failure of the arch is deemed to occur when the thrust line just touches the extremities of the ring in four positions, these four positions being termed "hinges", with four hinges being necessary to convert the doubly encastre arch into a mechanism. It is notable that an inherent assumption here is that the natural state of all real masonry arches is encastre. This is in marked contrast to the earlier work of Pippard, and hence MEXE, wherein the arch is considered to be of the two-pinned form. Figure 1.4 depicts the salient features of the system topology involved.



'Plastic Hinges' Form At Each  
Of The Four Points Where  
The Thrust Line (Dotted)  
Touches The Arch Extremities

Figure 1.4  
Typical Heyman Collapse Model

With respect to the determination of the degree of safety of an existing arch under a prescribed pattern of loading, Heyman proposes that the thickness of an imaginary arch ring just enclosing the thrust line, divided by the thickness of the actual arch ring, be termed the "geometrical factor of safety". It should be noted that the geometrical factor of safety is not directly comparable to a "load factor". In other words doubling the load on an arch possessing a geometrical factor of safety of two may not cause collapse, whereas doubling the load on an arch possessing a load factor of two would indeed cause collapse. As far as the author is aware, no work has been done on the conversion of one system of notation to the other. Various other bodies have developed their own "mechanism models"<sup>(9,12,18,19)</sup> as this kind of behavioural modelling has become known.

Mechanism models have yielded promising results, but on occasions where the results have been poor, the usual explanation has been that arch-fill interaction has contributed significantly to the arch's strength. In other words, rather than merely acting as a vertical dead load and live load dispersal medium, the fill has exerted a passive restraint upon the barrel and thus inhibited hinge formation. It has been speculated<sup>(20)</sup> that this effect may considerably increase the strength of the structure and as a result of these observations the "state of the art" is typified by the incorporation of such arch-fill interaction effects into mechanism-type computer programs.

### 1.4.3 Finite Element Analysis

This modern approach employs a formal non-linear structural analysis procedure applicable throughout the loading regime. This involves the allowance for the complexities associated with the lack of tensile strength and crack propagation. Figure 1.5 shows a typical finite element modelling mesh. The two finite element computer programs that have been written to date (in the United Kingdom, at least) are due to Dr. Crisfield of the Transport and Road Research Laboratory<sup>(4)</sup>, and Professor Sawko and Mr. Towler of Liverpool University<sup>(11)</sup>. The former of these two programs was developed from earlier programs specifically written for the analysis of thin shells. Reference 4 describes the theory in some detail, then goes on to validate the program against a published theoretical study<sup>(21)</sup> due to Sawko and Towler. This study took the form of the application of various alternative analytical techniques (MEXE, Pippard's elastic, Heyman, Sawko/Towler) to a series of *hypothetical* arch bridges with the intention of observing the scatter of results from the rival techniques. To this list of comparisons Crisfield adds his own results (both 10 and 20 element model versions) for one of the arches under study. As a demonstration of the effectiveness of Crisfield's own program the exercise is unfortunately rather limited. The comparison is entirely theoretical and the "true" solution is therefore unknown. Nevertheless, it shows a wide range of predicted ultimate loads ranging from 63kN (Heyman lower bound) to 119kN (Sawko & Towler) with Crisfield falling somewhere in between. It would also

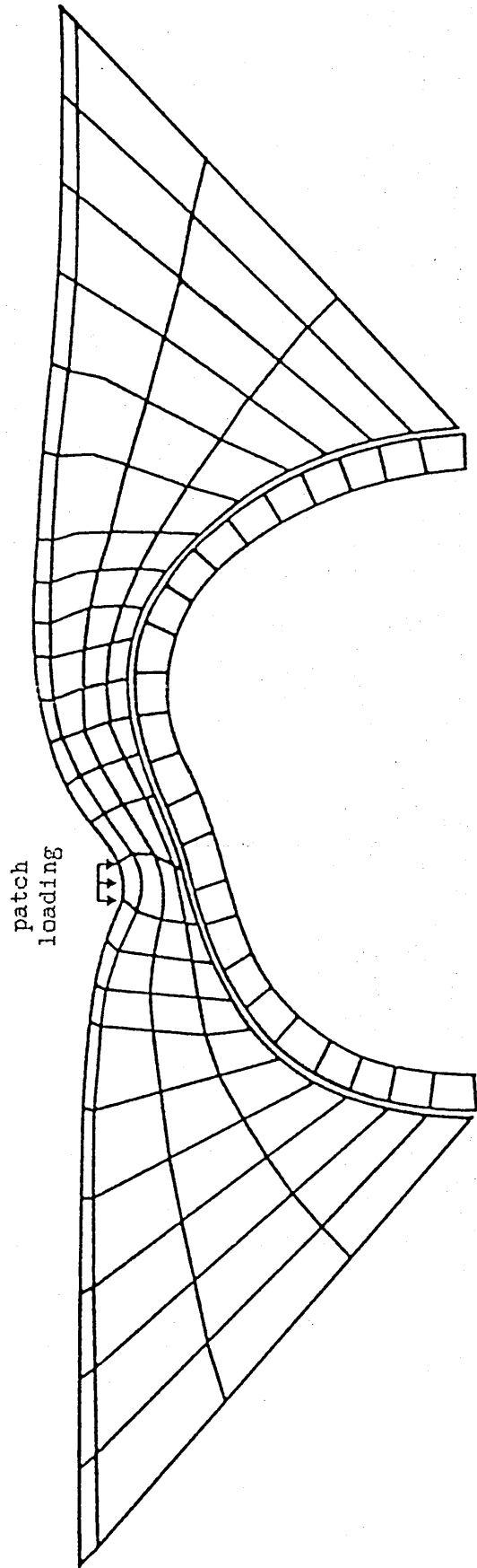


Figure 1.5 Typical Finite Element Mesh<sup>12</sup>

appear, as Crisfield points out, that the MEXE result quoted in the exercise is suspect and should be ignored.

When Crisfield's program was applied to a full-scale load test - Bridgemill, Girvan - it predicted ultimate collapse at somewhere between 1500kN and 2700kN, depending upon the parameters chosen for densities, material compressive strength and so forth. The actual collapse load recorded was in fact in excess of 3100kN. In the absence of further data it has to be said that the results given by the program, in its present form, do not appear particularly promising.

The second finite element program, due to Sawko and Towler, was novel in the respect that the modelling incorporated parabolic stress-strain characteristics for the arch ring material. This kind of relationship was becoming accepted at that time due to the work of Hodgkinson and Powell<sup>(22)</sup> in the field of brickwork and is developed herein by the author.

To attempt to validate this program, two brickwork arches of four metres span were constructed in the laboratories of Liverpool University and these were tested both with respect to "serviceability" and to destruction. A résumé of the results so obtained was published in Proceedings of the 6th International Brick Masonry Conference<sup>(10)</sup>, Rome, 1982. In predicting collapse loads, the program appears to give quite good results, the authors quoting results for the two collapse tests within +21% and -13% of "actual" values. However, for the

serviceability tests, the nature and criteria for which are not quoted, the published paper gives a theoretical value of 980kN against actual values of 120kN (crown load, no fill over crown) and 140kN (crown load, 250mm fill over crown). These values, unless in error, are far less encouraging!

A final point to remember regarding Sawko and Towler's series of model tests is that the arch barrels were tested in a "pure" form, in other words the dead load due to fill was applied by weights placed on a stepped extrados, and the live load was applied directly to the arch ring itself. By this means, two of the largest and most intractable sources of complexity were eliminated: no arch-fill interaction could possibly have been present and furthermore dispersal of the live load through the fill could not occur. In this rare instance, two of Heyman's assumptions actually existed! For these reasons, the model tests are valuable in providing data free from two of the usual fill-related variables, in contrast to the full-scale test data available in which all the variables act (and interact) at once. This difference will later be taken advantage of in the development of the author's own analyses.

## 1.5 SUMMARY

It is widely accepted that the present utilitarian arch assessment tool, MEXE, is over-conservative, particularly so in the case of

longer spans. Furthermore, it is not applicable to many real life masonry arches, skewed decks, for example. The consequences of this are that the authority responsible for the safety and maintenance of a particular structure may be forced prematurely to apply weight restrictions or to carry out unnecessary "strengthening" works. It would quite clearly be of great benefit to possess a more accurate assessment tool.

Before Heyman's "mechanism" work became popular, it was widely believed that a comprehensive finite element analysis would prove to be the arch panacea, a throwback to the early 1970's when this kind of analysis was thought to be universally applicable. This is not the present case although the potential exists to develop a comprehensive, three dimensional finite element computer simulation. However, the effort required to develop it and the cost in computer time to run it are daunting. Even if such a program were available, it would not represent a day-to-day design office tool, since its running cost would be prohibitive considering the number of arch bridge assessments that need to be made on a regular basis. Mechanism analysis, on the other hand, is relatively simple and easy to apply. Its main drawback at present is that it is relatively undeveloped, and does not model all the phenomena known to exist. Additionally, the author considers that it is quite conceivable that not all arches would necessarily fail by the formation of a mechanism, especially so in the case of low span to rise arches with thick arch rings under deep fill.

Having described the nature of the problem and having reviewed the historical and topical attempts at its solution, consideration will now be given to a series of actual structures with the intention of studying their performance in service and the typical problems experienced.

## CHAPTER 2

### FIELDWORK

#### 2.1 INTRODUCTION

During the course of this study various masonry arch structures have been visited with the object of gaining background information and also to inspect and study various aspects of masonry arch distress.

#### 2.2 DARFIELD AND BURYING LANE BRIDGES

Some researchers in the field of masonry arch bridges are of the opinion that these structures are so "massive" that they remain unaffected by subsidence of the abutments, such as that caused by mineral extraction<sup>(23)</sup>. Plates 2.1 and 2.2, taken from the personal records of Mr. B. L. Davies, formerly South Yorkshire County Council's Chief Bridge Engineer, amply demonstrate this opinion to be incorrect. Both of the bridges illustrated were subjected to mining subsidence. They were both previously in a sound condition.

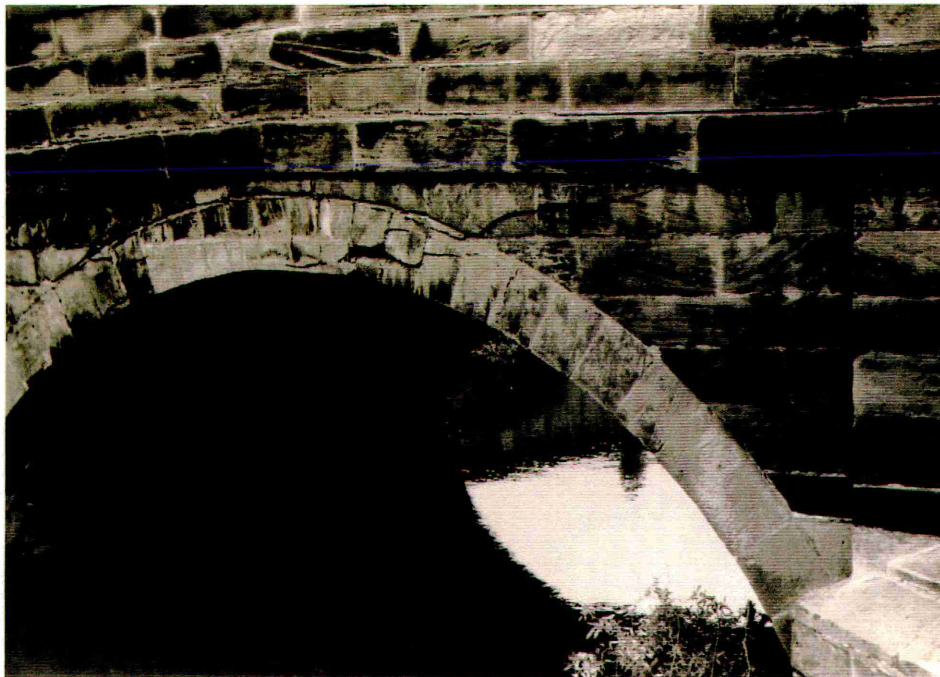


Plate 2.1 Darfield Bridge, After Passage Of Mining Wave, As  
At July, 1966.



Plate 2.2 Burying Lane Bridge, After Passage Of Mining Wave,  
As At November 1975

### 2.3 BRIDGE AT KETTLEWELL, NORTH YORKSHIRE

The failure of one of the spandrel walls of this bridge was reported in *New Civil Engineer*<sup>(14)</sup>, 28th February, 1985. The failure was considered as having probably been caused by the freeze/thaw cycle. Plate 2.3 shows the extent of the collapse (the bridge being taken out of service as a result) and Plate 2.4 reveals close-up details of the internal construction left exposed by the missing stonework. It is clear from the latter Plate that, at least in this instance, the arch barrel thickness internally is the same as that of the exposed voussoirs at the edges - this is not always the case.

The minimal fill cover to the barrel at the crown position is also apparent and, interestingly, "strata" lines are visible in the fill material, made noticeable by layers of material of differing size. This gives clues as to how the fill was originally placed. It would seem that layers of varying thickness, thin at the crown, thicker at the springing, were used to maintain a balanced load despite the fact that the centering would still have been in place to support the arch. One can imagine that by adopting this practice less substantial centering would be sufficient and also that any variations in the supply of fill material would be evened out across the whole span.

Repairs to the bridge were estimated at £100,000. The bridge had been under regular inspection prior to the failure but yet no advance signs of distress had been evident. This particular bridge gives an example

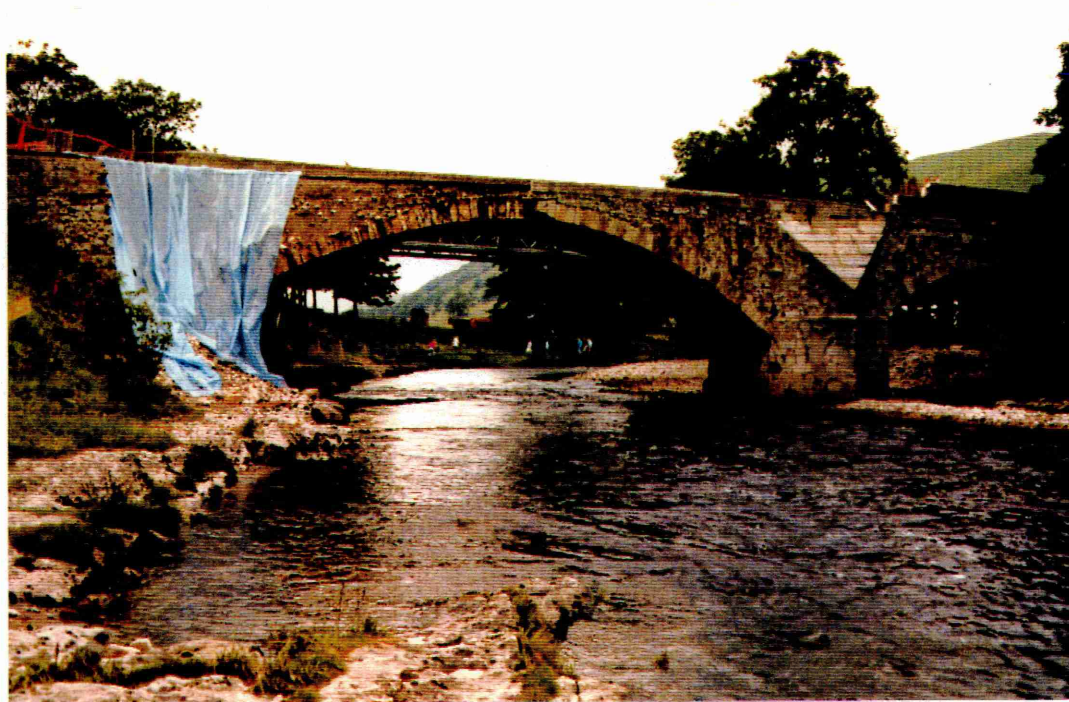


Plate 2.3 Bridge At Kettlewell, North Yorkshire, Damaged By  
Frost Action.



Plate 2.4 Close-up Showing Internal Construction.

of a local element failure rather than a global failure of the entire arch. Local failure problems such as this are much more common than overall, ultimate failure situations.

#### 2.4 BRADBERRY BALK LANE BRIDGE, SOUTH YORKSHIRE

Constructed circa 1800 over the Dearne and Dove canal, this bridge was in generally sound condition but its demolition was necessary in order to make way for the Wombwell Bypass improvement scheme in July 1985. The opportunity was therefore taken to obtain measurements, rock samples and fill samples.

The arch barrel was constructed of stone voussoirs to an elliptical profile (Plate 2.5). Geotechnical sources suggest that the voussoir stone is quite distinct from the stone used elsewhere in the bridge. One of the voussoirs, cleaved for easier transit, is depicted in Plate 2.6 alongside a one metre rule for scale purposes. Typical voussoir weight was 300kgf.

The same wall thickness was carried down from the parapet wall to the spandrels while the adjoining embankment gravity retaining wall was of similar construction but additionally backed up by roughly mortared stones and also battered back towards the retained side. Figure 2.1 gives the overall dimensions of the bridge.

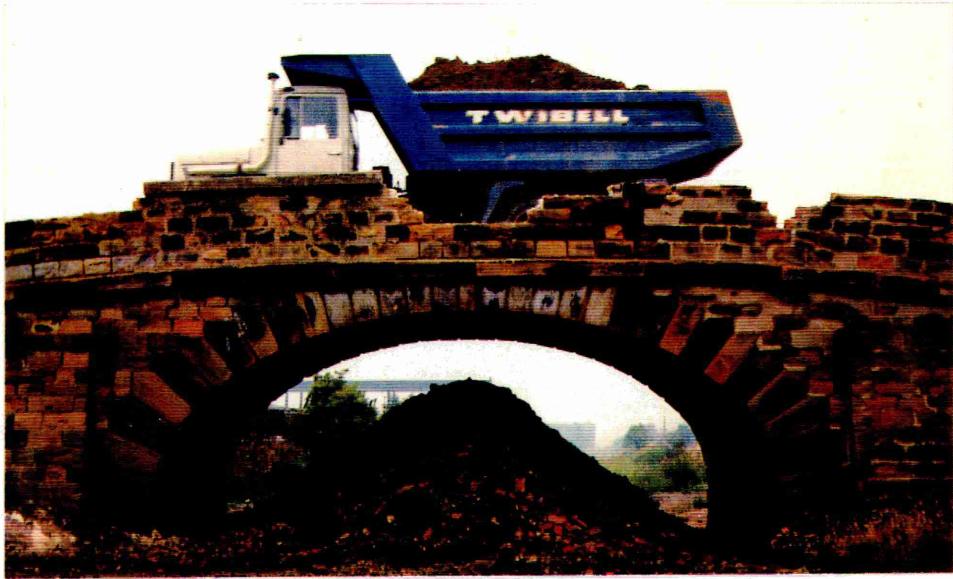
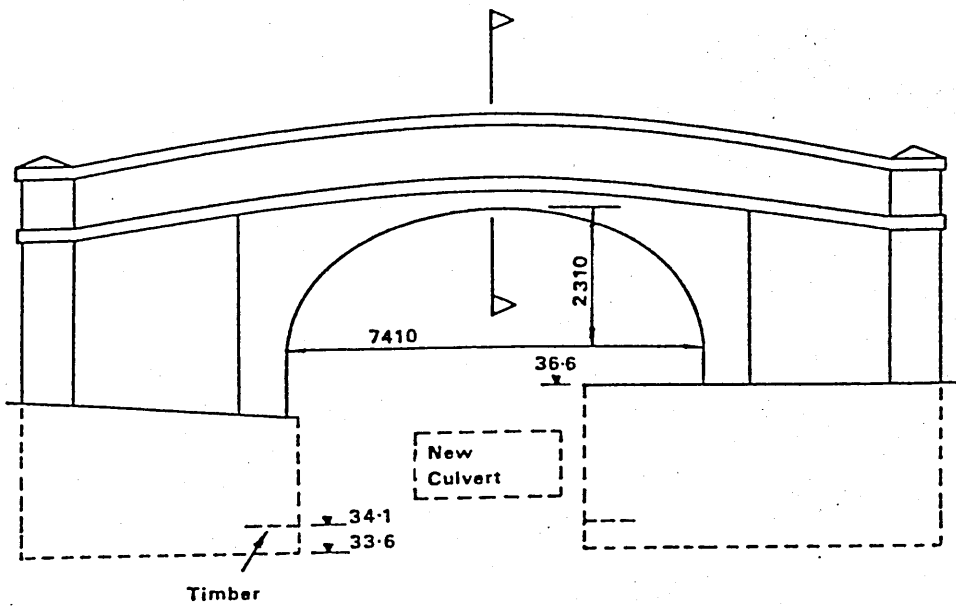


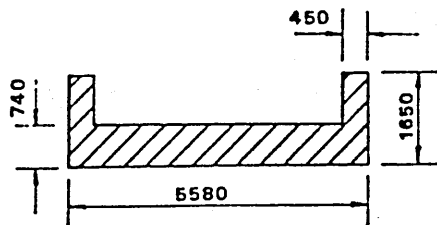
Plate 2.5 Bradberry Balk Lane Bridge During Course Of Demolition.



Plate 2.6 A Typical Voussoir From Above Bridge, Cleaved Into Four For Transit.



EAST ELEVATION



CROSS SECTION AT CROWN

Dimensions in mm.

Levels in m. above o.d.

DEMOLITION OF BRADBERRY BALK LANE BRIDGE

Figure 2.1

The fill material consisted of local head deposits and local industrial waste. At the time of inspection (Monday, 29th July, 1985) the fill was surprisingly dry, despite the prevailing torrential weather conditions; the bituminous carrigeway surfacing was obviously serving as an efficient waterproofing medium.

## 2.5 RIBBLEHEAD VIADUCT, NORTH YORKSHIRE

Plate 2.7 gives an overall impression of this well-known and controversial multi-span arched viaduct and also shows the structure in the context of its bleak, exposed setting. Although its twenty-four spans appear from afar to be entirely formed of stone, the working arch barrel material is in fact brickwork. Clearly, a close-up inspection of the intrados was not possible without special access equipment, but even from ground level it was apparent that there was a great deal of water staining accompanied by the emanation of white leachate substances.

The piers, constructed of stone, showed abundant evidence of serious cracking of a rather unusual nature (Plate 2.8). The cracks did not generally follow the perpendicular bed joints but passed through the blocks themselves. It seems unlikely that the cracks were due to applied load, neither live nor dead, as they did not particularly occur in key, highly stressed areas but at random. The best explanation is probably that the deck waterproofing has broken down



Plate 2.7 Ribbleshead Viaduct

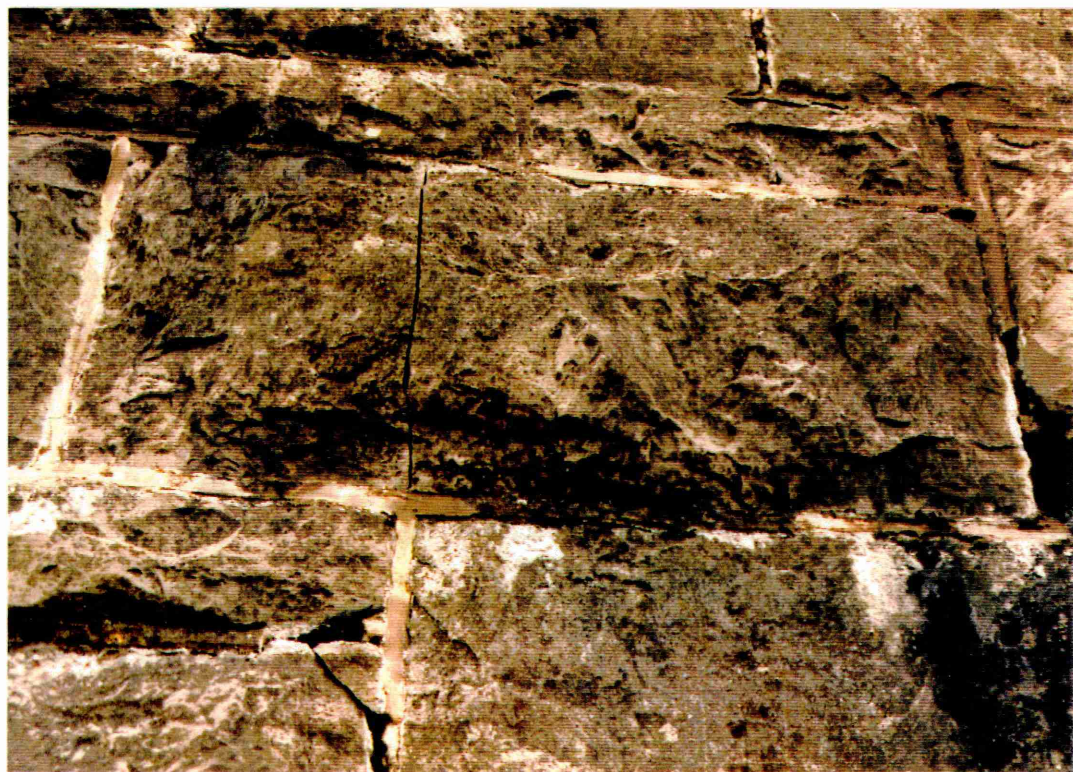


Plate 2.8 Typical Cracking On Ribbleshead's Masonry Piers

allowing water to percolate down inside the piers - the staining on the intrados reinforces this hypothesis. From there on, possibly expanding pier fill in conjunction with freezing and thawing cycles (remember the exposed location) have served to burst the blocks outwards. There is possibly also an inherent flaw in the stone contributing to the problem as one would have expected the mortar to fail before the stone given the relatively weak lime mortars in use at the time of construction.

All in all, a rather perplexing problem and, being multi-span, it would appear not one to fall strictly within the remit of the present studies. Official sources have costed the repairs to Ribbleshead viaduct at £4 million<sup>(12)</sup>.

## 2.6 BOLTON MILL BRIDGE, SOUTH YORKSHIRE

This bridge was taken out of service as a matter of urgency in 1976. Plates 2.9 and 2.10 serve to illustrate the overall poor condition of the structure. Bulging spandrels, open joints and cracked masonry can all be seen. In 1976 it was noted from beneath the bridge that a hinge could actually be observed during the passage of traffic. A further interesting feature concerning the hinge is that it occupied a segment of barrel encompassing several voussoirs, the voussoirs within this segment 'rolling' in turn as loading traversed the bridge. The arch was in fact extremely flexible and the constant relative movement



Plate 2.9 Bolton Mill Bridge, South Yorkshire, Showing Overall Poor Condition.



Plate 2.10 Crown Of Bolton Mill Bridge - Note Inscription

of the voussoirs was grinding material from the voussoir bearing surfaces. Not surprisingly, the bridge was immediately closed and a temporary culverted diversion constructed alongside.

Owing to the presence of services within the deck, the bridge was not demolished and neither were repairs attempted. The diversion was made permanent and the bypassed bridge still stands.

## 2.7 BRIDGE NEAR ARGELES, FRANCE

Plates 2.11 and 2.12 show a partially demolished multi-span arch bridge from which it is possible to see details of the internal construction - such opportunities are comparatively rare. The bridge appears to have been extremely well constructed. The single most interesting feature can be seen in Plate 2.12. Here a massive increase in thickness is evident as one moves down from the parapet wall to the spandrel wall. This feature would not normally have been apparent without recourse to the drilling of trial holes through the wall. A point to bear in mind, however, is that details of French and English practice may have differed as this feature has not been observed elsewhere.

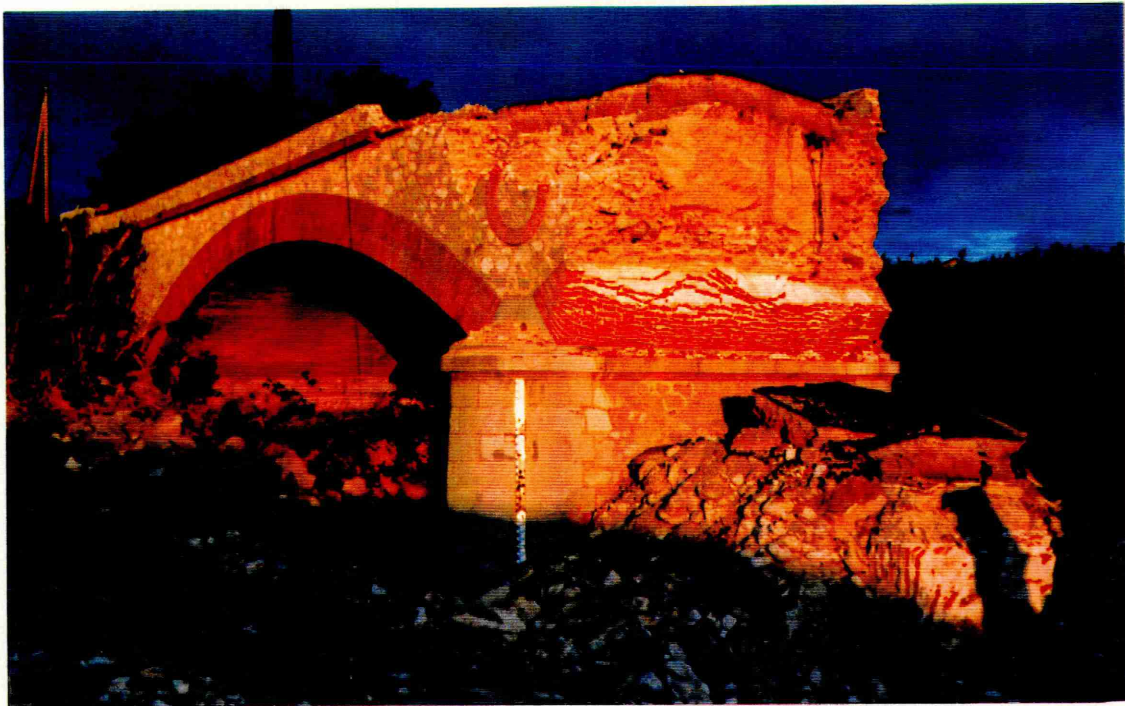


Plate 2.11 A Part-demolished French Multi-span Bridge.

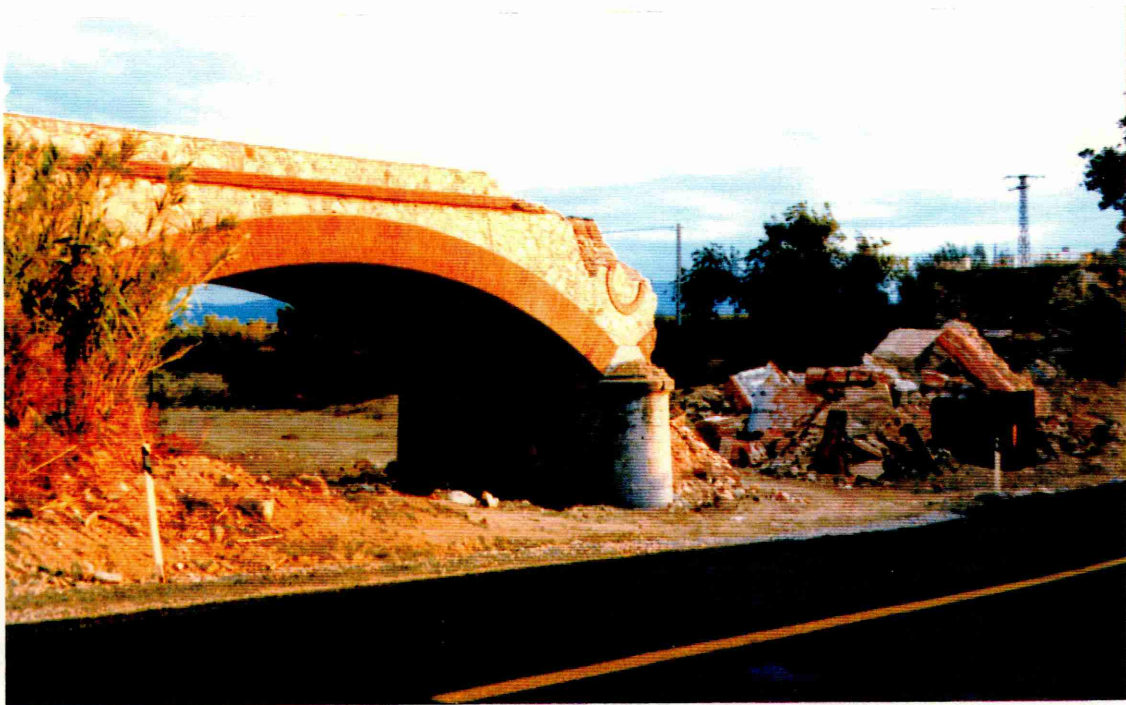


Plate 2.12 Note Increase In Parapet/Spandrel Wall Thickness (Background, Right) In This Same Example Of French Practice.

## 2.8 RIVELIN MILL BRIDGE, SHEFFIELD, SOUTH YORKSHIRE

Rivelin Mill Bridge carries the A57 trans-pennine Sheffield to Manchester trunk road over Rivelin Brook. As part of Sheffield City Council's rolling programme of bridge assessment, this highly skewed stone arch was inspected and a standard MBXE assessment carried out in accordance with BE3/73<sup>(24)</sup>. Depending upon the parameters chosen (as noted in Chapter 1, the method requires a large subjective input), it could be shown that a weight restriction should be imposed. Visual inspection tended to reinforce this result as, although the bridge superficially appeared in reasonable condition, loose voussoirs became apparent, including one that had been punched to hang below the barrel, and half of one other which resided in the river below! The problem mainly occurred adjacent to both external faces and was probably due in part to the high skew. Furthermore, the bridge was felt to vibrate under the passage of comparatively light highway traffic. A more detailed analysis was therefore performed using 'MECHARCH', the mechanism model analysis developed by the author in Chapter 4, with applied loading as required in BD21/84<sup>(2)</sup>. This revealed that the arch possessed an unacceptably low factor of safety against a mechanism-type collapse. A second analysis using the standard Heyman<sup>(6)</sup> mechanism technique was employed and this tended to reinforce the result. A programme of remedial works based upon a reinforced concrete saddle has been prepared in the offices of the author's employer and these works are in progress at the time of

writing. Plates 2.13 to 2.16 show the arch extrados and spandrel wall inner face masonry exposed by these works.

Plate 2.17 depicts a spalled section of voussoir taken from the river bed underneath the bridge, the bridge itself prior to the strengthening programme being visible in the background. A short series of uniaxial stroke-controlled rock core tests was carried out on samples obtained from this voussoir by employing a specially designed "stiff" testing apparatus. This feature is discussed in the following chapter.

## 2.9 SUMMARY

The masonry arch bridge form has been shown to be a complex system involving natural materials and the concomitant highly variable structural parameters. Age has led to this form suffering equally complex in-service problems. An analytical treatment will now be considered, but as an essential prerequisite, consideration will first be given to a study of basic masonry mechanics.



Plate 2.13

Rivelin Mill Bridge, Sheffield, During Strengthening Programme



Plate 2.14

A View Of Rivelin Mill's Extrados Showing Roughness Of Voussoirs



Plate 2.15

Rivelin Mill: Note Angle Of Voussoirs To Springers Due To Skew



Plate 2.16

Rivelin Mill: Rough Nature Of Inner Face Of Spandrel Wall Apparent

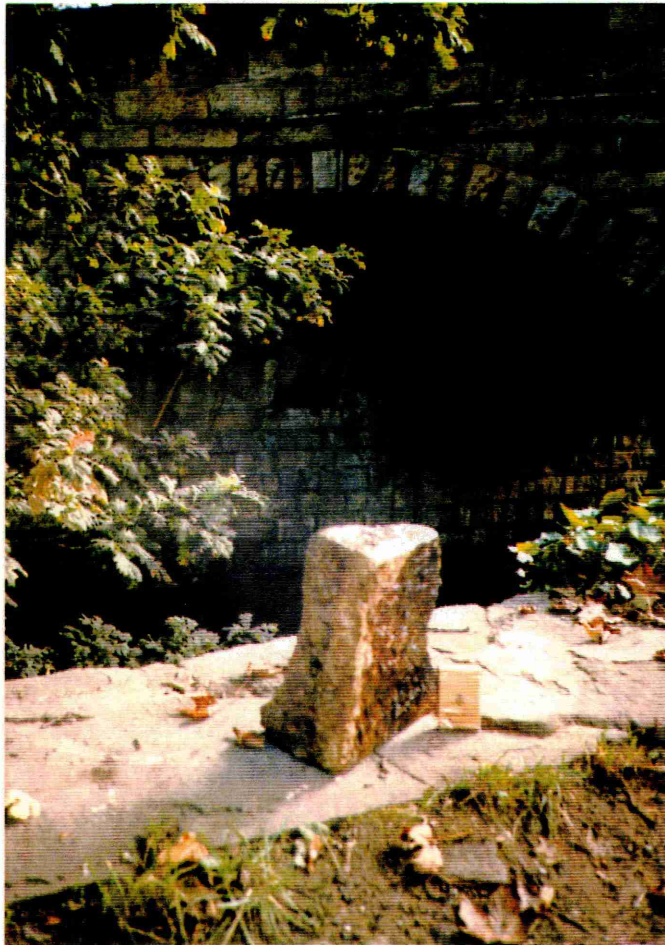


Plate 2.17 Rivelin Mill Bridge, Sheffield, With Sample Of Spalled Voussoir In Foreground. The Cigarette Packet Is Used To Give A Visual Indication Of Scale. Cores Taken From This Sample Were Used In A Series Of Stroke-controlled Compression Tests.

## CHAPTER 3

### CONSTITUTIVE MODEL

#### 3.1 INTRODUCTION

Masonry materials have traditionally been regarded as possessing linear stress-strain characteristics<sup>(25)</sup>; alternatively, infinite compressive strength has been assumed<sup>(5,6,7,8)</sup>. Relatively recent research<sup>(22)</sup> has, however, provided ample evidence that masonry exhibits strain softening under increasing stress and that this property may be more accurately modelled by means of a parabolic stress-strain relationship. It is proposed to employ these findings with the purpose of refining the analysis of masonry arch rings with respect to both serviceability and mechanistic models.

#### 3.2 STROKE-CONTROLLED CORE TEST PROGRAMME

A short series of stroke-controlled uni-axial rock core compression tests was undertaken on samples obtained from one of the masonry arches described in Chapter 2, Rivelin Mill Bridge, this series being the forerunner to a proposed larger and discrete programme of such

tests to be established at Sheffield City Polytechnic. Plate 3.1 shows some of the 50mm diameter cores taken from the damaged voussoir, recovered from the river bed beneath the bridge. Care was taken to ensure that the cores were orientated with their longitudinal axes along the line of thrust present in the bridge. The voussoir itself may be seen in the background. An aspect ratio of 2:1 was employed for the cores<sup>(25)</sup>. Plate 3.2 shows various pieces of the same rock after being subjected to point load testing - used to give initial data regarding likely strength. Plate 3.3 shows the point load testing equipment itself.

After sulphur capping to achieve smooth, parallel ends, the cores were tested in a specially stiffened testing apparatus (depicted in Plate 3.4) at a constant rate of strain equal to  $2 \times 10^{-5}$   $\text{secs}^{-1}$ , each test thereby being of some twenty minutes duration. A typical load-deflection response obtained from one of the cores is shown in Figure 3.1. It is inevitable that the sulphur caps would have had the effect of altering the load-deflection response but this method presented the most practical alternative, bearing in mind that this series of tests was partly intended to evaluate the feasibility of the stroke-controlled procedure and to test the previously untried, stiffened testing rig in this role. Plate 3.5 depicts a typical core sample installed between the platens ready for testing.

With reference to Figure 3.1, if the reverse curve immediately after the origin is neglected, it will clearly be seen that a curve of approximately parabolic shape has been obtained and that the tracing

Plate 3.1

50mm Cores Taken From A

Rivelin Mill Bridge Voussoir

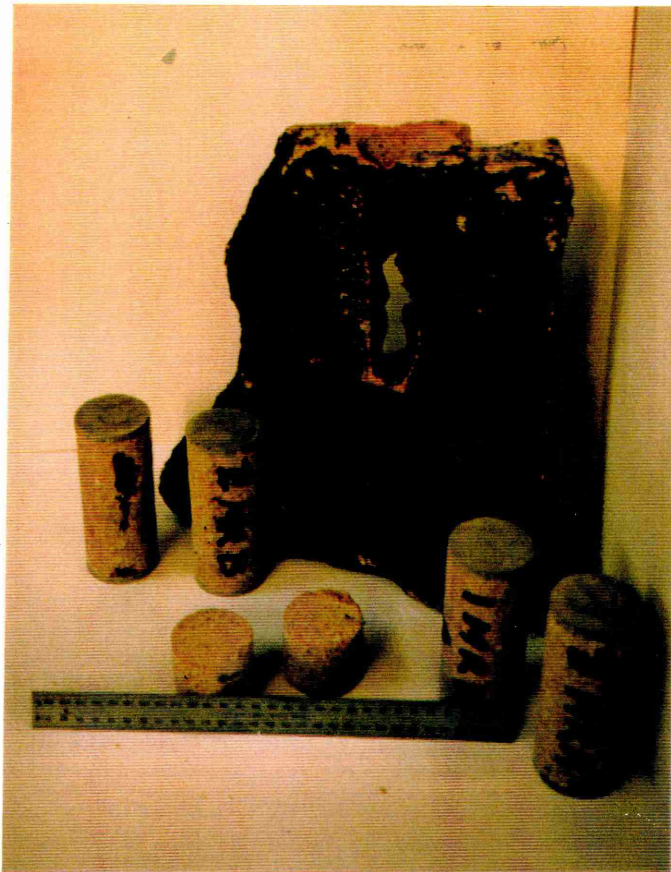
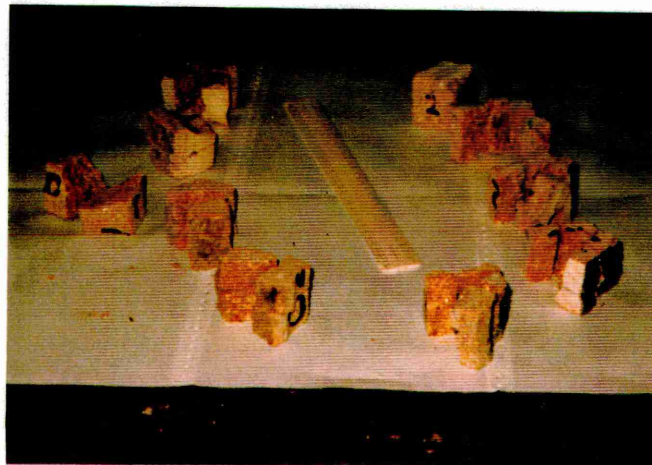


Plate 3.2

Rock From The Same Source

After Point Load Testing



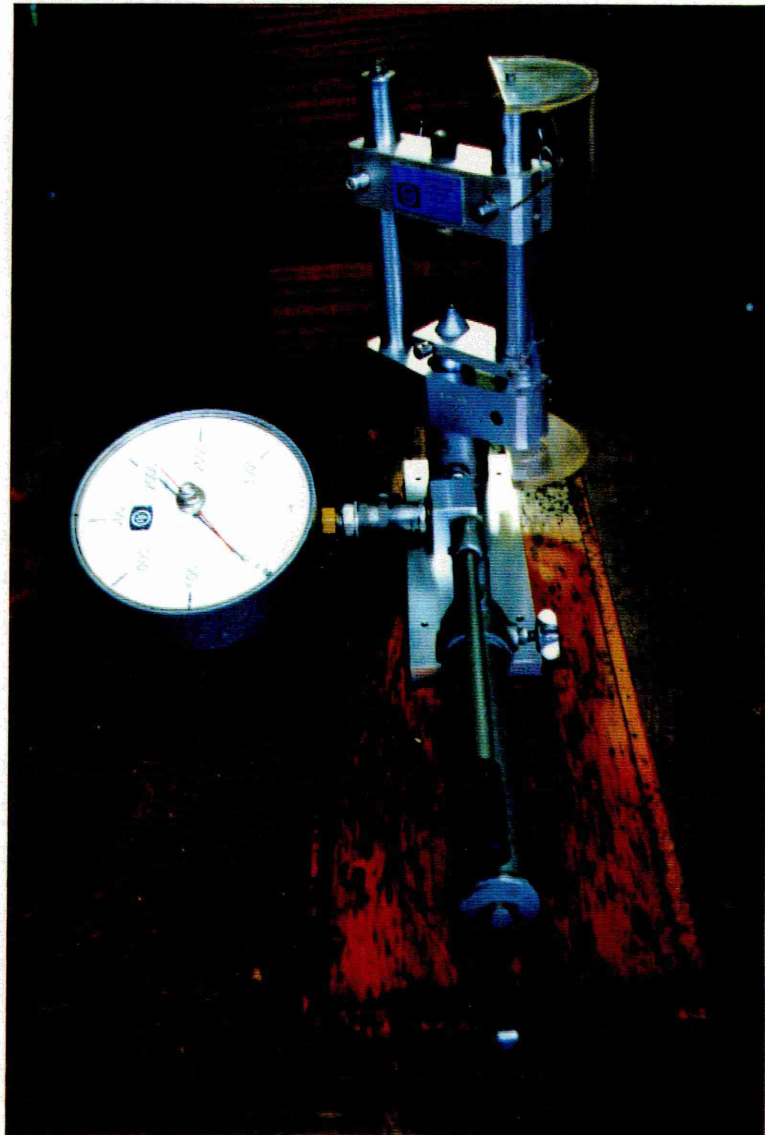


Plate 3.3

The Point Load Testing Apparatus

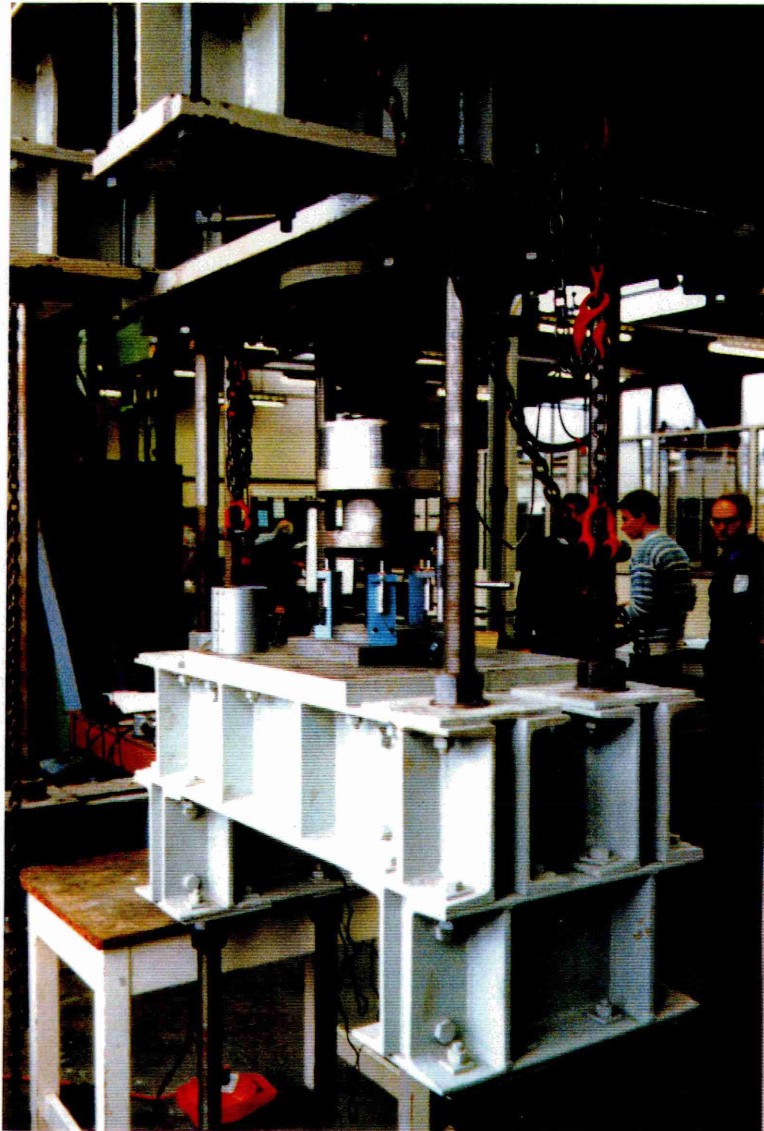
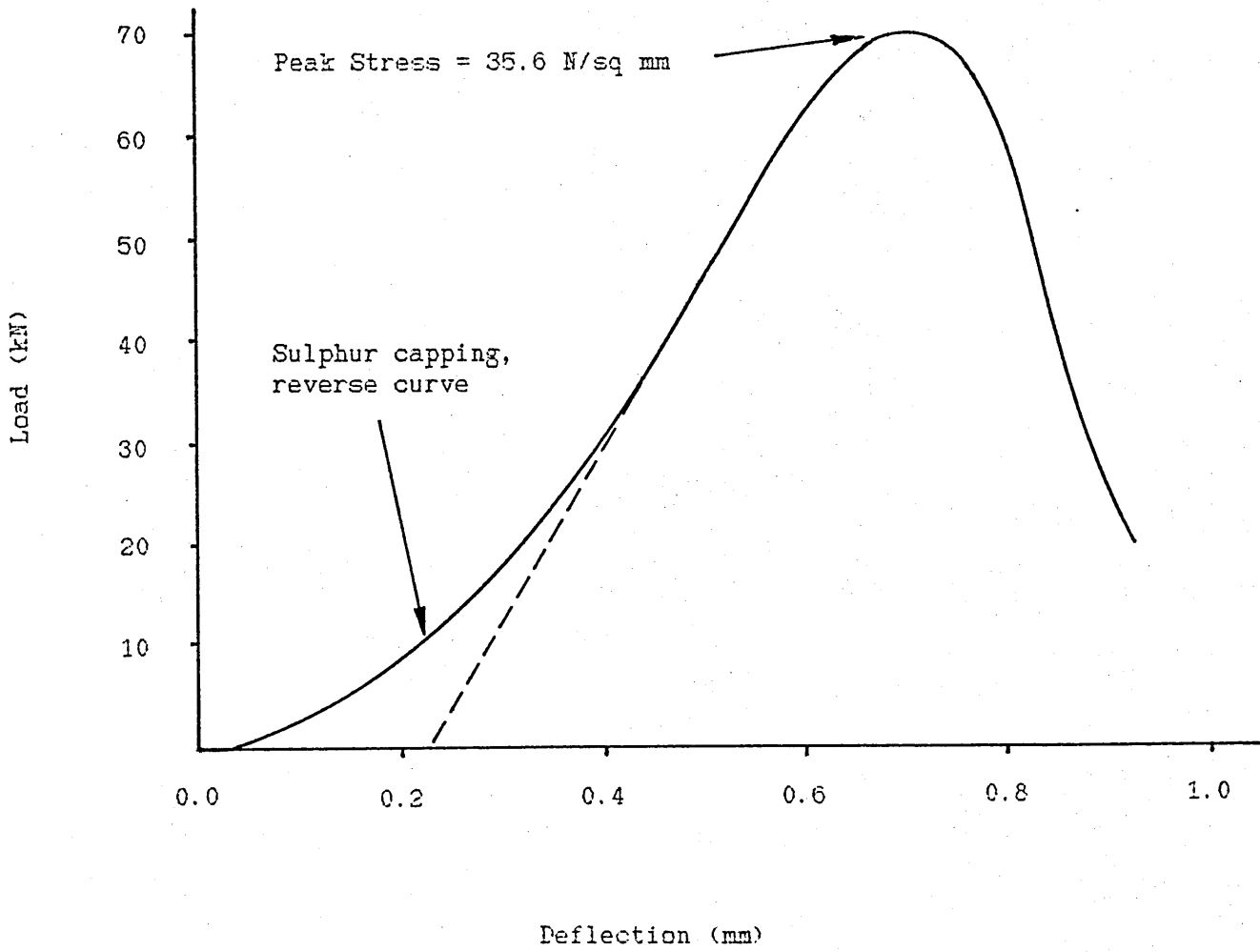


Plate 3.4

The "Stiff", Stroke-controlled Rock Core Testing Apparatus



N.B. A second test gave a peak stress of 36.5 N/mm<sup>2</sup>

Figure 3.1

Typical Load-Deflection Response from a Rivelin Mill Core

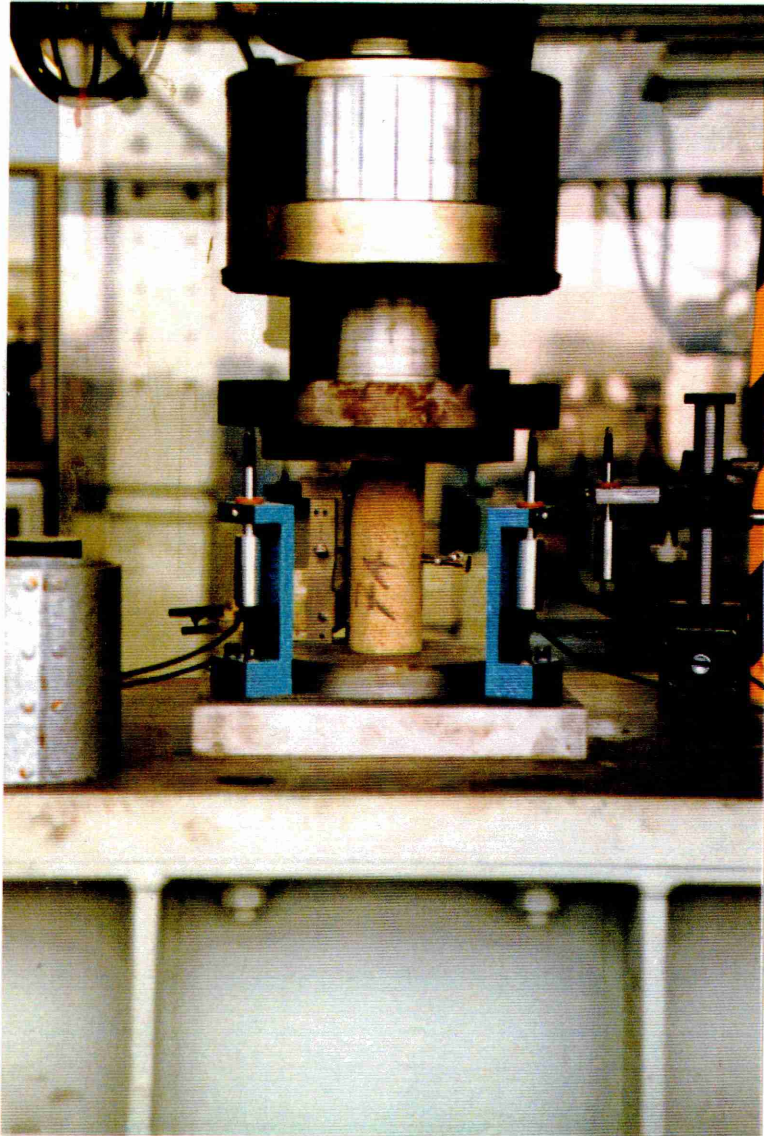


Plate 3.5

A Core Ready For Testing

of the falling branch, the response after maximum load, has been possible for a considerable distance. The reverse curve at the outset is due to bedding-in, particularly with respect to the sulphur capping which suffered extrusion. A failed core is depicted in Plate 3.6 - the squashing of the cap at one end is apparent. Further conclusions on, or investigations of, this kind of laboratory testing are not possible from this limited branch of the present arch studies. However, the at least qualitative confirmation of an idealised parabolic, stress-strain law for rock, as opposed to the previously well documented similar law for brickwork, is very encouraging and supports the present studies. Quantitatively, the peak stress of 35.6 N/mm<sup>2</sup> can be considered to typify the respective data; the voussoir rock was coarse and comparatively weak.

### 3.3 GENERAL FORMULATION

#### 3.3.1 Introduction

The general form of the stress-strain relationship to be adopted, neglecting bedding-in, and the accompanying notation are shown in Figure 3.2. The general equation of the curve is given by

$$\sigma/\sigma_m = 2\epsilon/\epsilon_m - (\epsilon/\epsilon_m)^2 \quad \dots (3.1)$$

where  $\sigma_m$  and  $\epsilon_m$  denote the peak stress and corresponding peak strain, respectively. It is to be noted that the tensile strength is



Plate 3.6

A Failed Core From Rivelin Mill Bridge After Testing

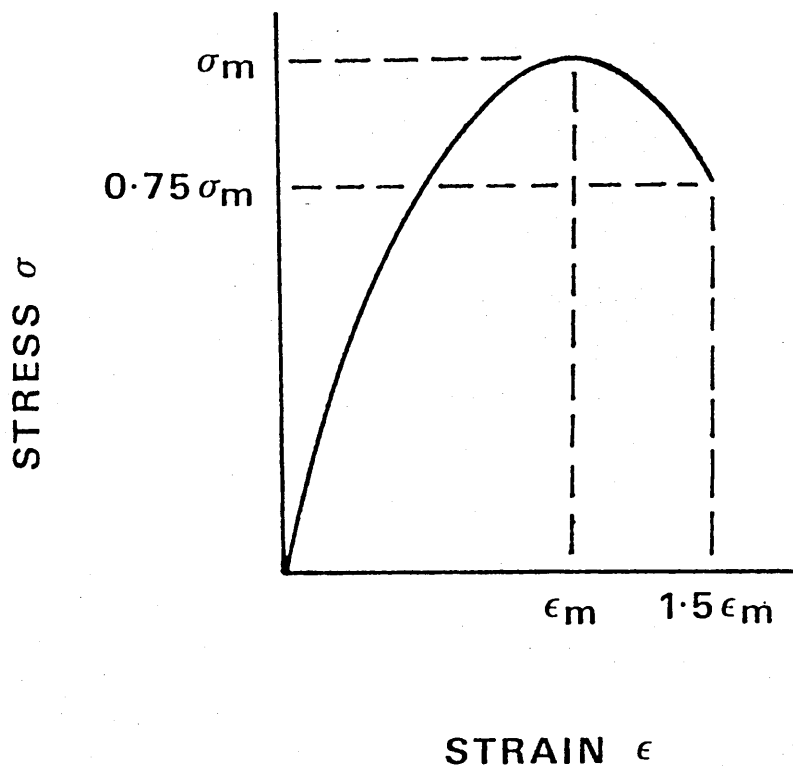


Figure 3.2

Idealised Parabolic Stress-Strain Law

considered to be negligible. An analytical procedure will now be established to model the behaviour of a rectangular masonry section under imposed axial thrust with co-existent uniaxial bending moment.

### 3.3.2 Uncracked Section

Consider first an uncracked section as denoted in Figure 3.3.

Clearly, axial thrust  $P$  is given by

$$P = \int_{-d/2}^{d/2} \sigma b dy \quad \dots (3.2)$$

where  $b$  denotes the section's depth and  $b$  its width, and bending moment  $M$  is given by

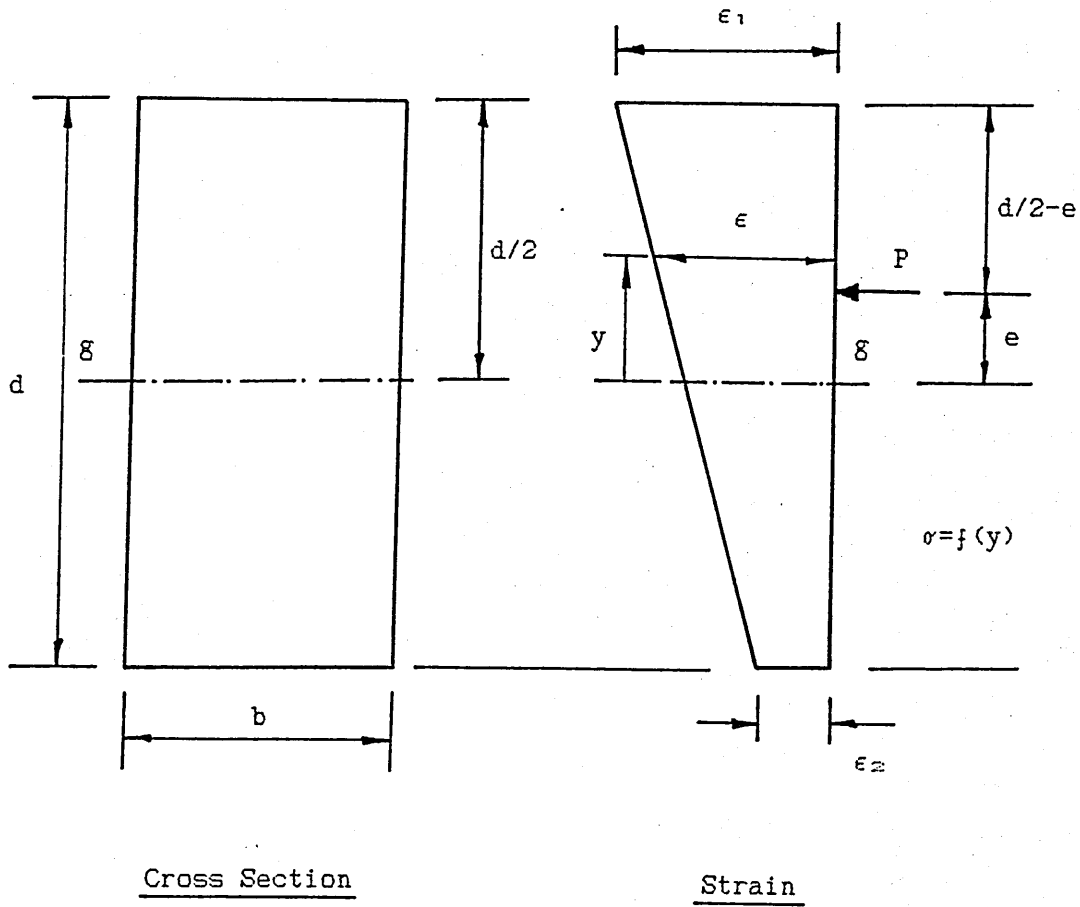
$$M = \int_{-d/2}^{d/2} \sigma b y dy \quad \dots (3.3)$$

Furthermore, for plane sections

$$\epsilon = k_1 + k_2 y \quad \dots (3.4)$$

where  $k_1$  and  $k_2$  are constants and  $y$  is a variable denoting the distance from the centroidal axis of the section to the point under consideration.

$$1.5\epsilon_m \gg \epsilon_1 \gg \epsilon_2 \gg 0$$



$$\text{At } \epsilon = \epsilon_1, \sigma = \sigma_1$$

$$\epsilon = \epsilon_2, \sigma = \sigma_2$$

Figure 3.3

Topology For Uncracked Sections

$$\text{At } \epsilon = \epsilon_2, y = -d/2 \quad \dots (3.5)$$

$$\text{and at } \epsilon = \epsilon_1, y = d/2 \quad \dots (3.6)$$

Rewriting 3.4

$$\epsilon_2 = k_1 - k_2 d/2 \quad \dots (3.7)$$

and

$$\epsilon_1 = k_1 + k_2 d/2 \quad \dots (3.8)$$

such that

$$k_1 = (\epsilon_2 + \epsilon_1)/2 \quad \dots (3.9)$$

with

$$k_2 = (\epsilon_2 - ((\epsilon_2 + \epsilon_1)/2))2/d \quad \dots (3.10)$$

or

$$k_2 = 2/d(\epsilon_1/d - \epsilon_2/d) \quad \dots (3.11)$$

$$\therefore \epsilon = (\epsilon_1 + \epsilon_2)/2 + y/d(\epsilon_1 - \epsilon_2) \quad \dots (3.12)$$

Substitution of equation 3.12 into equation 3.1 yields

$$r = \sigma_m (2/\epsilon_m ((\epsilon_1 + \epsilon_2)/2) + y/d(\epsilon_1 - \epsilon_2)) - ((\epsilon_1 + \epsilon_2)/2 + y/d(\epsilon_1 - \epsilon_2)) / \epsilon_m)^2) \dots (3.13)$$

Hence, employing equation 3.2

$$P = \int_{-d/2}^{d/2} \sigma_m b (2/\epsilon_m ((\epsilon_1 + \epsilon_2)/2) + y/d(\epsilon_1 - \epsilon_2)) - ((\epsilon_1 + \epsilon_2)/2 + y/d(\epsilon_1 - \epsilon_2)) / \epsilon_m)^2) dy \dots (3.14)$$

Integration and substitution of the limits gives

$$P = \sigma_m b d (-1/3 (\epsilon_1 / \epsilon_m)^2 + \epsilon_1 / \epsilon_m - 1/3 (\epsilon_1 \epsilon_2 / \epsilon_m^2) + \epsilon_2 / \epsilon_m - 1/3 (\epsilon_2 / \epsilon_m)^2) \dots (3.15)$$

Similarly, from equation 3.3

$$M = \int_{-d/2}^{d/2} \sigma_m b (2y/\epsilon_m ((\epsilon_1 + \epsilon_2)/2) + y/d(\epsilon_1 - \epsilon_2) - y((\epsilon_1 + \epsilon_2)/2 + y/d(\epsilon_1 - \epsilon_2)) / \epsilon_m)^2) dy \dots (3.16)$$

Integration and substitution of the limits gives

$$M = \sigma_m b d^2 / 6 (-1/2 (\epsilon_1 / \epsilon_m)^2 + \epsilon_1 / \epsilon_m - \epsilon_2 / \epsilon_m + 1/2 (\epsilon_2 / \epsilon_m)^2) \dots (3.17)$$

For specified parameters P and M, equations 3.15 and 3.17 must be solved simultaneously to provide a solution for  $\epsilon_1$  and  $\epsilon_2$ , the respective maximum strains. Equation 3.15 may also be rearranged to give

$$(\epsilon_1/\epsilon_m)^2 = 3\epsilon_1/\epsilon_m - (\epsilon_1\epsilon_2/\epsilon_m^2) + 3\epsilon_2/\epsilon_m - (\epsilon_2/\epsilon_m)^2 - 3P/(\sigma_m bd) \quad \dots (3.18)$$

Equation 3.17 may be rearranged similarly to give

$$(\epsilon_1/\epsilon_m)^2 = 2(\epsilon_1/\epsilon_m - \epsilon_2/\epsilon_m + 1/2(\epsilon_2/\epsilon_m)^2 - 12M/(\sigma_m bd^2)) \quad \dots (3.19)$$

Equations 3.18 and 3.19 may now be equated to provide an expression for  $\epsilon_1/\epsilon_m$ , and this may be substituted into equation 3.17 to provide a polynomial of degree 4 in  $\epsilon_2$

$$\begin{aligned} 0 = & \sigma_m bd^2/6(-1/2((2(\epsilon_2/\epsilon_m) - 5\epsilon_2/\epsilon_m + 3P/(\sigma_m bd) - 12M/(\sigma_m bd^2))/(1 - \\ & \epsilon_2/\epsilon_m))^2 + (2(\epsilon_2/\epsilon_m) - 5\epsilon_2/\epsilon_m + 3P/(\sigma_m bd) - 12M/(\sigma_m bd^2))/(1 - \epsilon_2/\epsilon_m) - \\ & \epsilon_2/\epsilon_m + 1/2(\epsilon_2/\epsilon_m)^2) - M \quad \dots (3.20) \end{aligned}$$

Various iterative solution routines are available to provide a value for  $\epsilon_2$ . Thereafter, back-substitution is used to obtain a corresponding value for  $\epsilon_1$ .

### 3.3.3 Cracked Section

Now consider the situation prevailing should the section become cracked in tension. Equations 3.2 and 3.3 are still applicable, subject to revised integral limits in accordance with the topology of Figure 3.4 - note the effective depth,  $d'$ . From Figure 3.4 it may be seen that, for plane sections

$$\epsilon = k_1 + k_2 y' \quad \dots (3.21)$$

where  $k_1$  and  $k_2$  are again constants and  $y'$  is a variable denoting the distance from the centroidal axis of the section remaining uncracked to the point under consideration;  $d'$  is the depth of the uncracked section.

$$\text{At } y' = d'/2, \epsilon_1 = k_1 + k_2 d'/2 \quad \dots (3.22)$$

$$\text{and at } y' = -d'/2, \epsilon_0 = k_1 - k_2 d'/2 \quad \dots (3.23)$$

thus

$$k_1 = k_2 d'/2 \quad \dots (3.24)$$

and substitution into equation 3.22 gives

$$\epsilon_1 = k_2 d'/2 + k_2 d'/2 \quad \dots (3.25)$$

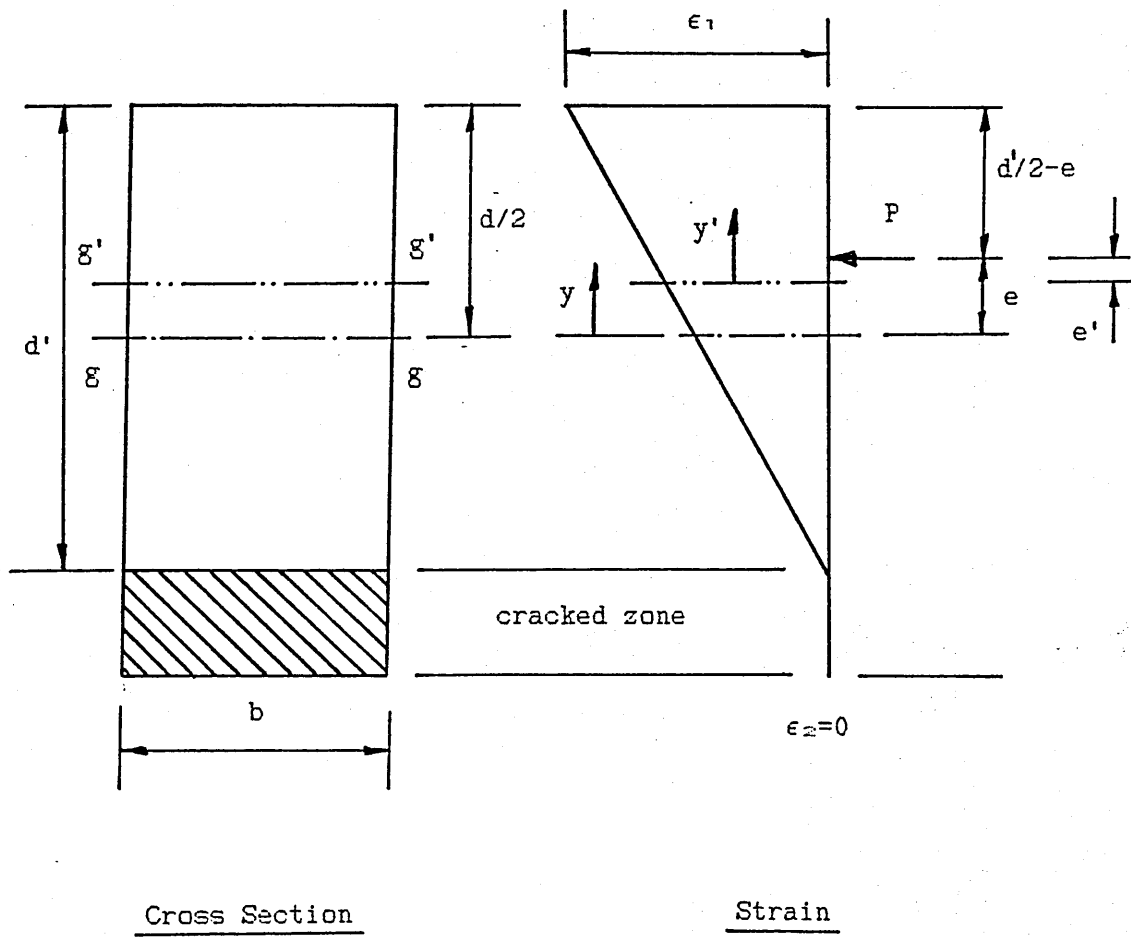


Figure 3.4  
Topology For Cracked Sections

such that

$$\epsilon_1 = k_2 d' \quad \dots (3.26)$$

with

$$k_2 = \epsilon_1 / d' \quad \dots (3.27)$$

and

$$k_1 = \epsilon_1 / d' \cdot d' / 2 \quad \dots (3.28)$$

or

$$k_1 = \epsilon_1 / 2 \quad \dots (3.29)$$

Hence

$$\epsilon = \epsilon_1 / 2 + \epsilon_1 y' / d' \quad \dots (3.30)$$

Substitution of equation 3.30 into equation 3.1 yields

$$\sigma = \sigma_m (2(\epsilon_1 / 2 + \epsilon_1 y' / d') / \epsilon_m - (\epsilon_1 / 2 + \epsilon_1 y' / d')^2 / \epsilon_m^2) \quad \dots (3.31)$$

Hence, employing equation 3.2 but with  $d'$  replacing  $d$  in the limits,

$$P = \int_{-d'/2}^{d'/2} \sigma_m b (2(\epsilon_1/2 + \epsilon_1 y'/d')/\epsilon_m - (\epsilon_1/2 + \epsilon_1 y'/d')^2/\epsilon_m^2) dy' \quad \dots (3.32)$$

Integration and substitution of the limits gives

$$P = \sigma_m b d' / 3 (3\epsilon_1/\epsilon_m - (\epsilon_1/\epsilon_m)^2) \quad \dots (3.33)$$

Similarly, from equation 3.3, and again with  $d'$  replacing  $d$  in the limits

$$M' (\equiv Pe') = \int_{-d'/2}^{d'/2} \sigma_m b (2\epsilon_1/\epsilon_m (1/2 + y'/d') y' - (\epsilon_1/\epsilon_m)^2 (1/2 + y'/d')^2 y') dy' \dots (3.34)$$

Integration and substitution of the limits gives

$$M' = \sigma_m b (d')^2 / 12 (2\epsilon_1/\epsilon_m - (\epsilon_1/\epsilon_m)^2) \quad \dots (3.35)$$

Equations 3.33 and 3.35 must be solved simultaneously to provide a solution for the cracked section case. From equation 3.33

$$(d')^2 = 9P^2 / (\sigma_m^2 b^2 (3\epsilon_1/\epsilon_m - (\epsilon_1/\epsilon_m)^2)^2) \quad \dots (3.36)$$

And from equation 3.35

$$(d')^2 = 12M' / (\sigma_m b (2\epsilon_1/\epsilon_m - (\epsilon_1/\epsilon_m)^2)) \quad \dots (3.37)$$

Equating equations 3.36 and 3.37 provides a polynomial

$$4\sigma_{mb}M' = (3\epsilon_1/\epsilon_m - (\epsilon_1/\epsilon_m)^2)^2 - 3P^2(2\epsilon_1/\epsilon_m - (\epsilon_1/\epsilon_m)^2) = 0 \quad \dots (3.38)$$

Before this may be solved,  $M'$  must also be eliminated. Now,

$$M' = Pe' \quad \dots (3.39)$$

and, transforming

$$e' = e - ((d-d')/2) \quad \dots (3.40)$$

Hence

$$M' = P(e - ((d-d')/2)) \quad \dots (3.41)$$

But, from equation 3.36

$$d' = 3P / (\sigma_{mb}(3\epsilon_1/\epsilon_m - (\epsilon_1/\epsilon_m)^2)) \quad \dots (3.42)$$

Substitution of equation 3.42 into equation 3.41 gives

$$M' = P(e - ((d - (3P / (\sigma_{mb}(3\epsilon_1/\epsilon_m - (\epsilon_1/\epsilon_m)^2)))) / 2)) \quad \dots (3.43)$$

This may now be substituted into equation 3.38 to yield a polynomial of degree four in  $\epsilon_1$

$$0 = 4\sigma_m b P \left( e - \left( \frac{d - (3P / (\sigma_m b (3\epsilon_1 / \epsilon_m - (\epsilon_1 / \epsilon_m)^2)))}{2} \right) (3\epsilon_1 / \epsilon_m - (\epsilon_1 / \epsilon_m)^2) \right)^2 - 3P^2 (2\epsilon_1 / \epsilon_m - (\epsilon_1 / \epsilon_m)^2) \quad \dots (3.44)$$

Having solved for  $\epsilon_1$ , back substitution may be employed to determine the corresponding value of  $d'$  from equation 3.42.

### 3.4 SOLUTION PROCEDURES

#### 3.4.1 Introduction

There are several standard iterative routines available for the solution of polynomials, including those attributable to Bairstow and Newton-Raphson and also the half-interval search type of routine. Owing to the fact that the nature of the polynomials under consideration was unknown, and also that they would certainly exhibit multiple turning points, the author decided to purpose-write his own solution routines rather than to rely on pre-written "black box" type procedures. This approach enabled a "feel" for the problem to be developed and also helped a better understanding of the data trends. It furthermore enabled computer graphics to be employed to give a better illustration of exactly what was taking place.

The two software items developed, one applicable to an uncracked section and the other to a cracked section, were packaged together and entitled PSTRESS1. Both are basically half-interval search routines outputting a simple graphical representation of the polynomial to the

computer visual display unit. By this means all roots present may be examined and evaluated as required. In addition, having extracted the appropriate roots, the masonry cross-section can be graphically displayed together with computed stress and strain plots. It will perhaps be useful to illustrate the nature of PSTRESS1 at this juncture.

### 3.4.2 Typical PSTRESS1 Input/Output

Figure 3.5 depicts a typical page of screen output from PSTRESS1 resulting from an uncracked analysis of the following masonry cross section:

Cross sectional dimensions	: 1000 mm wide
	: 300 mm deep
Peak material stress, $\sigma_m$	: 16 N/mm <sup>2</sup>
$\epsilon_m$ corresponding to $\sigma_m$	: 0.0024
Applied axial compression (P)	: 1200 kN
Applied bending moment (M)	: 110 kNm

This depth of section was chosen as being perhaps representative of the voussoir depth of a small arch bridge and the width of one metre is the "one metre strip" often used by engineers. The  $\sigma_m$  and  $\epsilon_m$  values are similarly intended to be fairly typical<sup>(27)</sup>. The  $\sigma_m$  value and the cross-sectional area provide a squash load for the section of 4800 kN, and with this in mind the P and M values above were chosen. It may be observed from the graphical output that, within the range

AXIAL FORCE = 1200000 NEWTONS, MOMENT = 110000 NEWTON METRES

\*\*\* SOLUTION:  $\epsilon_1=0.00100$   $\epsilon_2=-0.00029$  AT POLY.=0.41699 \*\*\*

CHECK:  
COMPUTED P=1200.00956 kN  
COMPUTED M=110.00072 kNm  
C FOR COPY?C

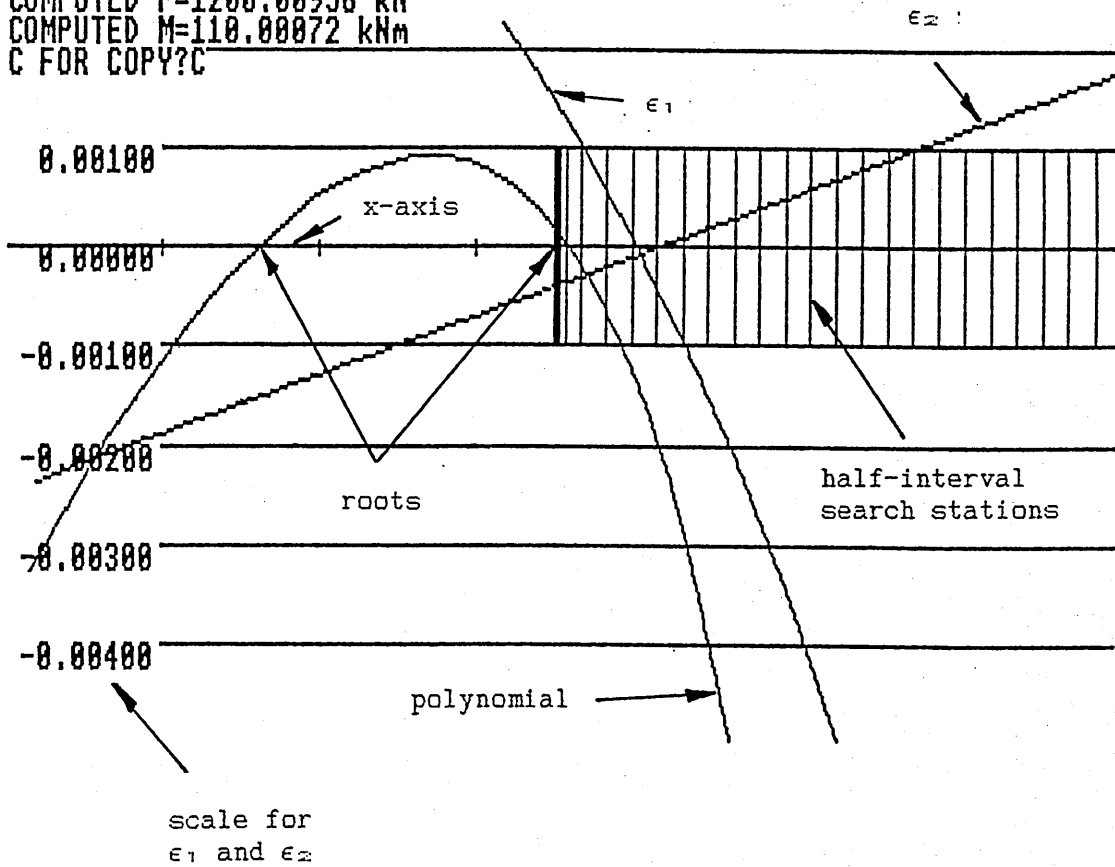


Figure 3.5

Typical PSTRESS1 Graphical Output For An Uncracked Masonry Section

shown, there are two roots. Of these, the leftmost root is trivial in that  $\epsilon_1$  is enormously positive and  $\epsilon_2$  is negative. It may therefore be concluded that this root has a non-physical interpretation. Having thus decided that the rightmost root is the one required, it is apparent that whilst  $\epsilon_1$  is sensibly positive,  $\epsilon_2$  is slightly negative and hence the section must in fact crack to generate an equal and opposite internal reaction to the externally applied forces. This being the case, the "uncracked" analysis just performed is in fact invalid, and therefore control within the software now passes to a second analysis based upon the cracked section mathematics previously described.

The new graphical output from the cracked section analysis is depicted in Figure 3.6. Again, within the range visible there are two roots. The leftmost root provides another trivial solution ( $\epsilon_1=0$ ), but the rightmost root at last affords the required solution,  $\epsilon_1=0.00133$ , and hence that  $d'$  (the depth of section left uncracked) is 165mm.

Having found "a" correct solution, the PSTRESS1 proceeds to plot the appropriate stress and strain diagrams for the section and these are shown in Figure 3.7. One will note the curved boundary to the stress plot - this is a consequence of the parabolic stress-strain law. The deep crack (some 45% of the section) is also to be noted, yet the section is still well below failure. In fact, maintaining the axial force constant at 1200kN but incrementing the bending moment produces an eventual limiting failure for this particular section of masonry at 131.5kNm.

AXIAL FORCE = 1200000 NEWTONS, MOMENT = 110000 NEWTON METRES

\*\*\* SOLUTION:  $d'=0.16558$   $E1=0.00133$  AT POLY. $=-37888$  \*\*\*

CHECK:

COMPUTED  $P=1200.00000$  kN

COMPUTED  $M'=29.34977$  kNm

GIVING A COMPUTED  $M=110.00000$  kNm

C FOR COPY?C

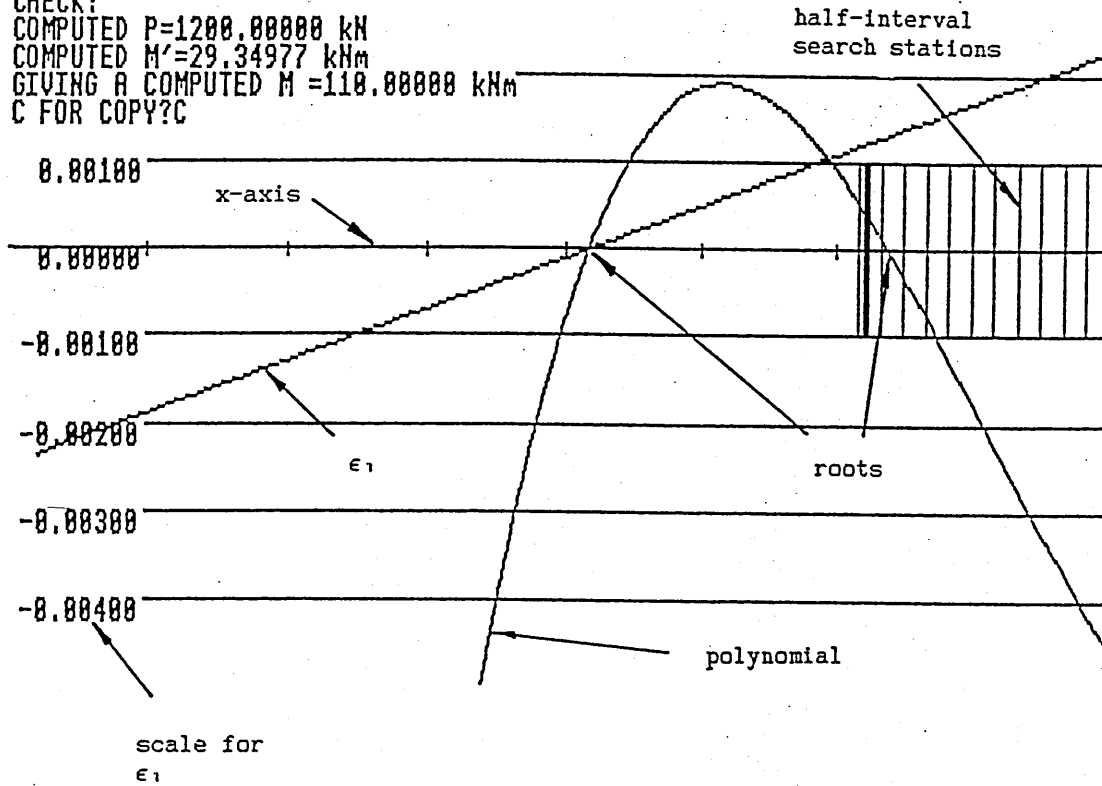
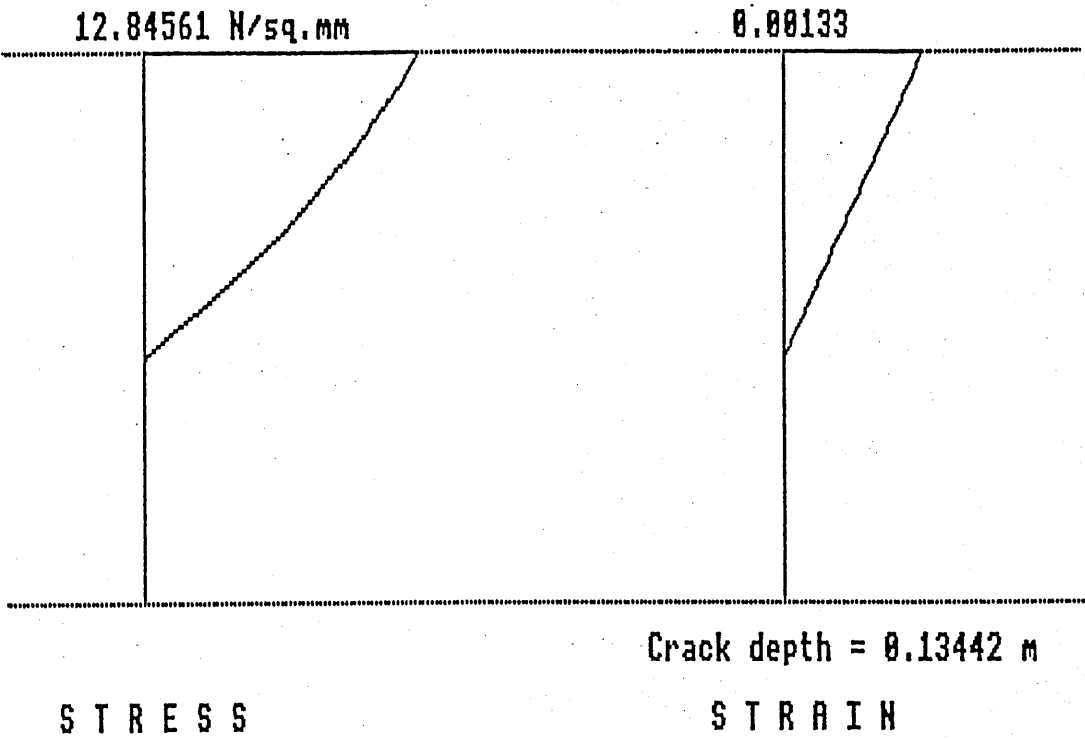


Figure 3.6

Typical FSTRESS1 Graphical Output For A Cracked Masonry Section



\*\*\* CRACKED ANALYSIS \*\*\*

Figure 3.7

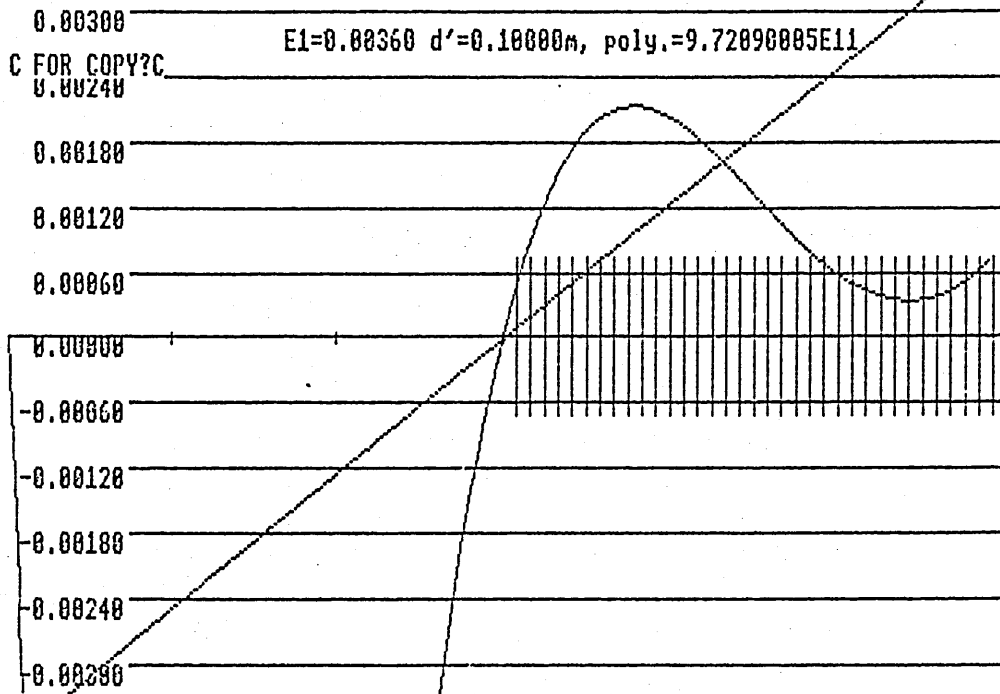
Typical PSTRESS1 Graphical Output Depicting Stress And Strain Plots  
After Solution

At failure, the rightmost arm of the locus (see Figure 3.8a) curves upwards again and lifts off from the x-axis. This leaves only trivial solutions and hence the section is deemed to have failed. There may in fact be up to four roots for any particular problem (only the first two have been shown in the above example), and one would expect that only one of these would provide a physically sensible solution. In general this is true, but a novel phenomenon is theoretically possible under conditions approaching the limit state. Under such circumstances, *two* entirely viable solutions may exist, though in a physical sense one is far more probable than the other. This phenomenon is entirely due to the adoption of a parabolic stress-strain characteristic and in particular to the presence of the falling branch. The effect will be described more fully in the next section which relates to limit state considerations.

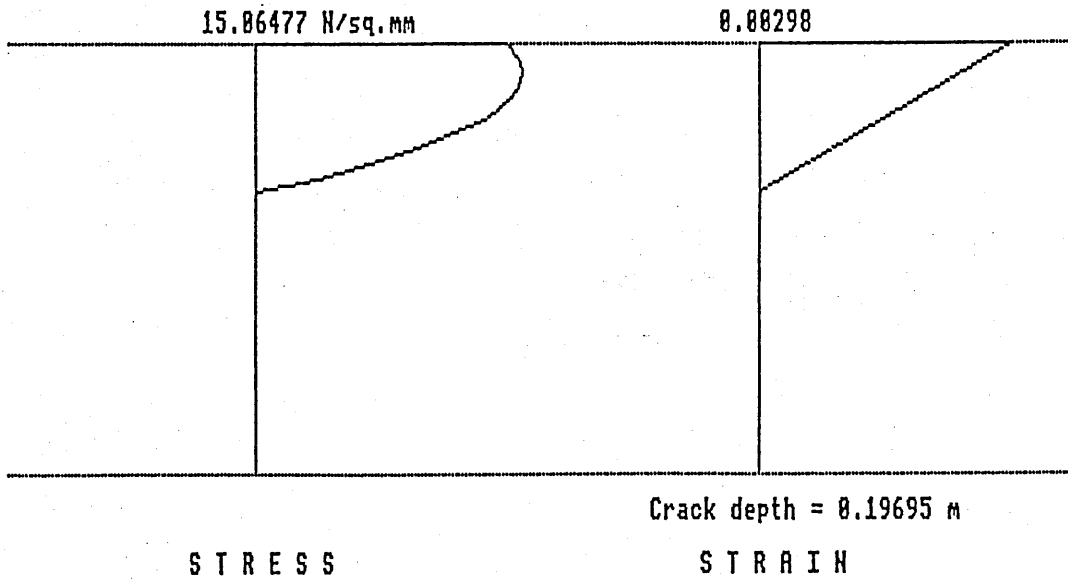
The stress and strain plots produced by PSTRESS1, on the point of failure, are depicted in Figure 3.8b. At this condition the crack extends through nearly two thirds of the section. An interesting feature is the separation of maximum effects - the peak stress occurs within the section and not at the extreme fibres undergoing maximum strain.

Appendix 'B' provides a full program listing of PSTRESS1, written in BBC 'BASIC'. The ability to determine limit state characteristics using the above numerical approach is to be noted; this feature will be further discussed in the ensuing.

Axial force = 1200000.0 Newtons, Bending moment = 133000.0 Newton metres



(a) PSTRESS1 Plot Depicting Post-failure Condition



(b) Ultimate Failure Stress And Strain Plots

For The Example Given In The Text

Figure 3.8

### 3.5 LIMIT STATE INTERACTION DIAGRAM

#### 3.5.1 Uncracked Section

The limit state (in this context the *ultimate* prefix is assumed) is determined by obtaining the maximum force,  $P=P_m$ , that the masonry section can withstand at any given value of bending moment,  $M$ . This is achieved by employing

$$\partial P / \partial \epsilon_1 = 0 \quad \dots (3.45)$$

in conjunction with prescribed values of  $M(\epsilon_2)$ .

However, to evaluate this "static" limit state would require extensive and very complex mathematical manipulation and a conservative simplification is therefore employed using equation 3.45 with prescribed values of  $\epsilon_2(M)$ . This alternative approach results in a "kinematic" limit state and a closed-form algorithm<sup>(28)</sup>. Further, it is to be noted that the "formal" static state, whilst not being amenable to closed form solution, can be determined numerically from the previously described computer program PSTRESS1. It will be shown that the variations between the numerically defined formal static state and the closed form kinematic limit state interaction curves are small, and comparison using numerical data from PSTRESS1 shows that the proposed course of action provides a kinematic solution that is in all cases conservative in terms of thrust/moment values. Given the inherent nature of the material under study, an approximation of this

kind - ie the formulation of a kinematic rather than the more formal static limit state - is considered justified.

Developing the kinematic formulation, then, and employing equation 3.45 in conjunction with prescribed  $\epsilon_2(M)$  values with respect to equations 3.14 and 3.16 generates the limiting condition for an uncracked section

$$\epsilon_1 = (3\epsilon_m - \epsilon_2)/2 \quad \dots (3.46)$$

recalling  $\epsilon_1 \leq 1.5\epsilon_m$ ,  $\epsilon_2 \geq 0$ .

The appropriate expression for  $F_m$  is obtained by back-substituting equation 3.46 into equation 3.14 which affords

$$F_m = \sigma_m b d / 4 (3 + 2(\epsilon_2 / \epsilon_m) - (\epsilon_2 / \epsilon_m)^2) \quad \dots (3.47)$$

The corresponding limit state bending moment  $M_m$  is determined by substituting equation 3.46 into equation 3.16 such that

$$M \equiv M_m = \sigma_m b d^2 / 16 (1 - 2(\epsilon_2 / \epsilon_m) + (\epsilon_2 / \epsilon_m)^2) \quad \dots (3.48)$$

Equations 3.47 and 3.48 thereby afford the requisite limit state interaction locus subject to the delineation of the range of validity of the uncracked case studies.

Intuition demands that the squash load  $P_s$  represents an upper bound on  $P_m$  with

$$\left. \begin{array}{l} P_m \\ M_m = 0 \end{array} \right| = P_s = \sigma_m b d \quad \dots (3.49)$$

wherein a uniform axial stress distribution  $\sigma_1 = \sigma_2 = \sigma_m$  acts across the entire section. Equation 3.49 is fully supported by the present studies, employing, with respect to equation 3.47

$$\partial P_m / \partial \epsilon_2 = 0 \quad \dots (3.50)$$

then back-substitution yields

$$\left. \begin{array}{l} \epsilon_2 \\ P_m = P_s \end{array} \right| = \epsilon_m \quad \dots (3.51)$$

which affords equation 3.49 upon substitution into equations 3.47 and 3.48. The lower bound value for  $P_m$  with respect to the uncracked section studies is obtained by setting  $\epsilon_2 = 0$ . At this state, equation 3.46 gives

$$\epsilon_1 = 3\epsilon_m/2 \quad \dots (3.52)$$

which accords with the limiting permissible extreme fibre strain. Further, substitution into equation 3.47 identifies the lower bound of  $P_m$  to be

$$P_m = 0.75\sigma_m bd \quad \dots (3.53)$$

at which state equation 3.48 gives

$$M_m = \sigma_m bd^2/16 \quad \dots (3.54)$$

Introducing the non-dimensional parameter  $n = P_m/P_s$ , then equations 3.47 and 3.48 afford the limit state locus for the section in the range  $0.75 \leq n \leq 1$ .

### 3.5.2 Cracked Section

It is now necessary to determine the limit state locus for  $0 \leq n \leq 0.75$ . The approach is similar to that employed in the previous study. Equation 3.45 remains valid although for the cracked section this is employed in conjunction with prescribed values of bending moment  $M(d')$ . Applying equation 3.45 to equation 3.33 generates the explicit limiting condition

$$\epsilon_1 = 1.5\epsilon_m \quad \dots (3.55)$$

The corresponding limiting stress condition being simply

$$\sigma_1 = 0.75\sigma_m \quad \dots (3.56)$$

Back-substituting equation 3.55 into equations 3.33 and 3.35 gives

$$P_m = 3\sigma_m b d' / 4 \quad \dots (3.57)$$

and

$$M_m = \sigma_m b d' (6d - 5d') / 16 \quad \dots (3.58)$$

respectively. The above expressions thereby define the limit state interaction locus for  $0 \leq n \leq 0.75$ ; these expressions interface with equations 3.47 and 3.48, affording the values given in equations 3.53 and 3.54, at  $n = 0.75$ . At the lower bound,  $n = 0$ , equations 3.57 and 3.48 afford

$$n = P_m = d' = M_m = 0 \quad \dots (3.59)$$

Intuition suggests that a turning point is present in the interaction locus  $0 \leq n \leq 0.75$ . Employing

$$\partial M_m / \partial P_m = \partial M_m / \partial d' \cdot \partial d' / \partial P_m = 0 \quad \dots (3.60)$$

Then, from equations 3.57 and 3.58

$$\left. \begin{array}{l} d' \\ \partial M_m / \partial P_m = 0 \end{array} \right| = 3d/5 \quad \dots (3.61)$$

with a maximum turning point at  $n = 0.45$ . The absolute maximum bending moment the section can resist is, therefore, from equation 3.58

$$M_m \Big|_{n = 0.45} \equiv M_m = 9\sigma_m b d^2 / 80 \quad \dots (3.62)$$

### 3.5.3 Axial Force/Bending Moment Interaction Diagram

Noting the identities of equation 3.49 and 3.62, and introducing the non-dimensional parameter  $m = M_m/M_s$ , then the interaction diagram can be conveniently represented in n-m space. For this purpose, equations 3.47, 3.48, 3.57 and 3.58 are written in the form

$$n = (3 + 2(\epsilon_z/\epsilon_m) - (\epsilon_z/\epsilon_m)^2) / 4 \quad \dots (3.63)$$

$$m = 5(1 - 2(\epsilon_z/\epsilon_m) + (\epsilon_z/\epsilon_m)^2) / 9 \quad \dots (3.64)$$

$$n = 0.75(d'/d) \quad \dots (3.65)$$

$$m = 5(d'(6d - 5d')/d^2) / 9 \quad \dots (3.66)$$

The kinematic interaction diagram thus defined is depicted by the solid line in Figure 3.9. For comparison, a numerically derived static limit state locus is depicted by the dotted line. The latter was obtained using computer program PSTRESS1, as exemplified in Section 3.4.2. It will be noted that the closed form kinematic locus is everywhere within the static locus and indeed the two are very close. It is suggested, therefore, that the former represents an acceptable working measure of a masonry section's capacity for most practical applications. Figure 3.9 also shows three straight lines

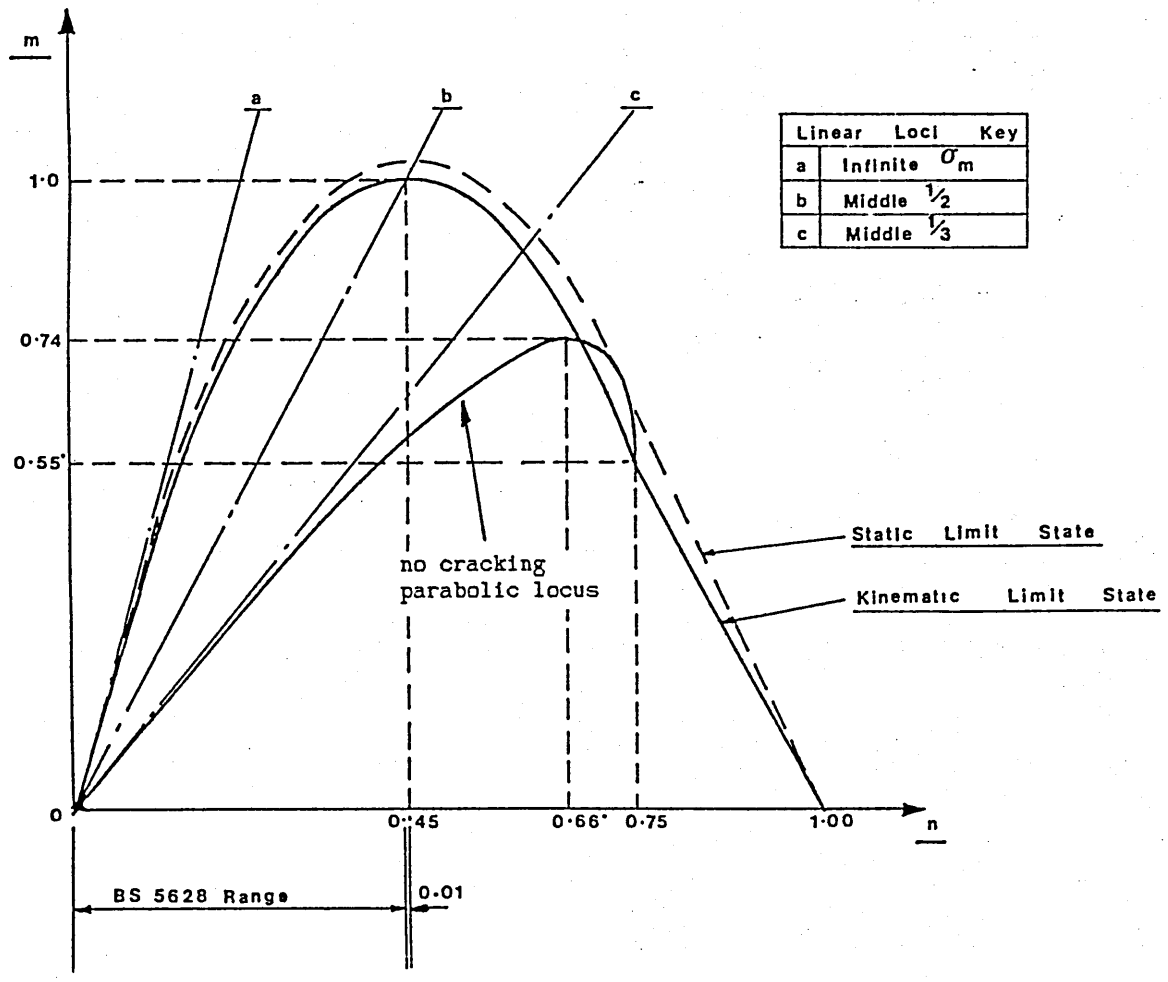


Figure 3.9

Limit State Interaction Diagram

representing, respectively, a material with infinite compressive strength, a section obeying the linear theory middle-half rule and a section obeying the linear theory middle-third rule.

The "infinite compressive strength" line is significant in that it represents the properties usually assumed in an arch mechanism-model material. The differences between such a hypothetical material and a real material are clearly apparent. It may be seen that the difference increases with increasing values of  $n$ . Thus, at  $n = 0$ , the error in assuming an incompressible material is nil, but at  $n = 0.2$  the error is in effect to overestimate the moment capacity of the section by approximately 22%. Depending upon the particular states of stress present in an arch at the ultimate limit state, this discrepancy may be significant. Note that this "line" can be shown to be tangential to the kinematic limit state locus.

The line depicting the linear middle half rule is also interesting in that both the kinematic and static loci peak along this line. In simple terms, then, this means that the absolute maximum bending moment capacity available from any masonry section occurs at the linear middle-half law condition.

The third line in Figure 3.9 depicts the linear middle-third rule and can be shown to be tangential to the parabolic-law no cracking criterion. The former provides the basis of the masonry design code of practice, B.S. 5628<sup>(23)</sup>, the latter being obtained by prescribing  $d=d'$  ( $\epsilon_2=0$ ) in equations 3.33 and 3.35.

Finally, as mentioned earlier (Section 3.4.2), under certain conditions there are theoretically *two*, equally valid, stress and strain distributions possible for a given externally applied moment/thrust pair. This condition may only arise in the narrow band between the static and kinematic loci on the interaction diagram. This duality phenomenon may be best explained by reference to Figure 3.10. This shows  $\epsilon_1/\epsilon_m$  plotted against  $m$ , all at a fixed value of  $n = 0.45$ . Because the curve so produced is (partially) double valued in  $m$ , there are always two possible solutions (at least) in the vicinity of the static limit state. Both respective solutions possess physical meaning and refer to pre- and post- static conditions. However, beyond  $\epsilon_1/\epsilon_m = 1.5$  the second root is deemed non-physical and hence the region in which two *valid* roots may be said to exist is limited to the zone between the curve's absolute peak (the static limit state) and the point at which  $\epsilon_1/\epsilon_m = 1.5$ . This latter value relates to the kinematic limit state, there also being some state possessing the same  $P_m$ ,  $M_m$  values but at a lower strain status as exemplified in Figure 3.10.

### 3.5 SUMMARY

Accepting that masonry materials exhibit parabolic stress-strain laws, then it is obvious that fundamental understanding of the consequences is necessary for the study of masonry arches and the study of masonry structures in general. Particularly towards the ultimate limit state

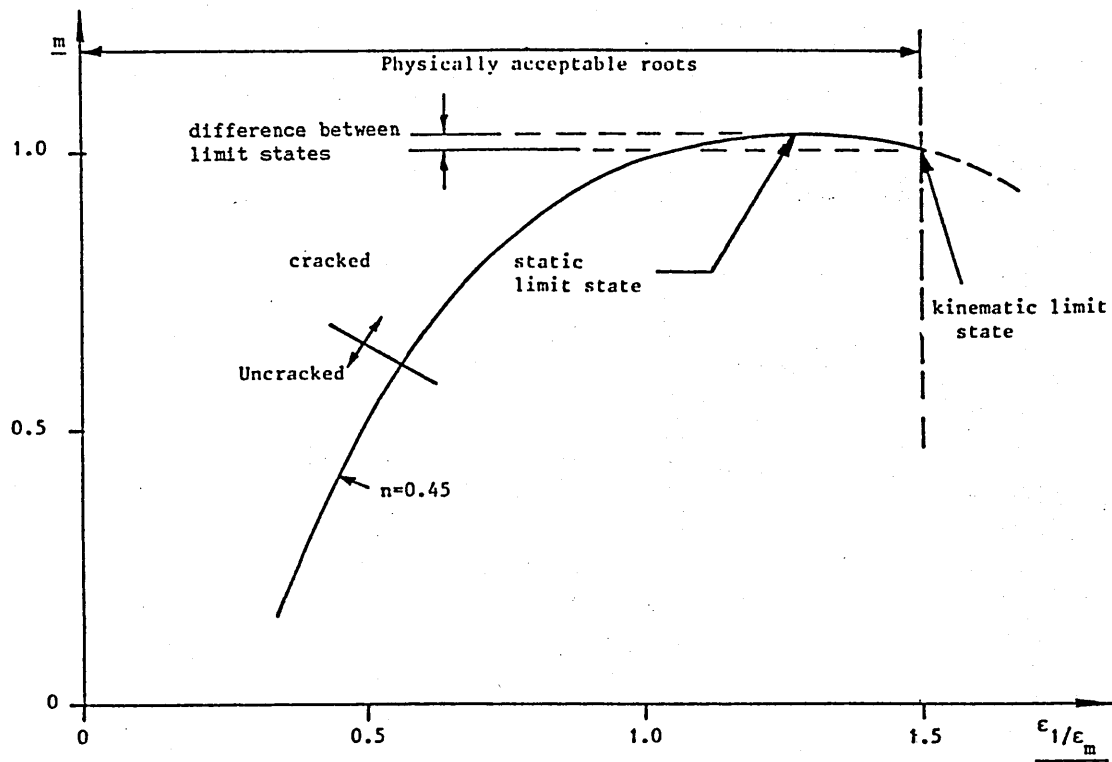


Figure 3.10

Numerically Derived Moment-Maximum Strain Locus For  $n=0.45$

condition, significant differences have been shown to exist between the properties of linear-law and parabolic-law materials. The theory outlined in this chapter predicts the separation of maximum stress and strain effects prior to failure and also enables the section to be "solved" regarding stresses, strains and likely crack depths for any viable loading. Further, a limit state interaction diagram has been formulated which enables the analyst to dispense with the non-conservative infinite compressive strength dictum. The need for such a refinement has been suggested<sup>(18)</sup> but a proper means to achieve it has not previously been forwarded, as far as the author is aware.

It is now proposed to set out two alternative masonry arch bridge analysis schemes, one relating to (ultimate) limit state considerations and the other to general serviceability considerations. Both schemes employ the foregoing constitutive modelling.

## CHAPTER 4

# MASONRY ARCH BRIDGE ANALYSIS

### 4.1 INTRODUCTION

A static mechanism analysis is first presented for both arch rings per se and for arch ring/fill systems. This analysis enables solution for the case of an external quarter point load. This loading configuration is considered to be the critical loading case<sup>(S.28)</sup> for most masonry arch bridges. The procedure is computerised and compared against both full-scale and model validation data.

An attempt is also made to establish a serviceability model on the basis of a doubly encastre arch subject to any pattern of transverse loading with the serviceability limit being equated to the formation of the first hinge. Given the complexity of the analysis, the attempt is primarily designed to highlight specific problems in a general masonry arch bridge model.

#### 4.2 STATIC MECHANISM MODEL ASSUMPTIONS

- a) The mechanical arch is considered to consist of a single structural element, the arch ring, supporting a homogeneous, level and isotropic fill material.
- b) The fill is taken to impart a purely vertical load on the arch ring and also to act as a dispersal agent for the applied live load. Any strengthening of the arch barrel due to its interaction either actively or passively with the fill (so called "arch-fill interaction") is not allowed for, this being an extremely complex effect in its own right.
- c) A one metre strip of arch is analysed, a collapse load for the whole arch being obtained by multiplying the resulting figure by the overall width of the arch.
- d) The arch barrel is taken to possess a constant radial thickness.
- e) For the purpose of determining dead load, a single value for specific weight is employed, this being intended to include for both the fill material and the arch barrel material.

- f) Spandrel wall edge stiffening effects are considered to be of a secondary nature.
- g) The profile of the arch is deemed to be segmental, other profiles being treated by approximation.
- h) Collapse is presumed to be due to the formation of four mechanistic hinges.
- i) The hinges are located beneath the quarter point live load, at the crown and at each springing. This simplification is generally in accordance with typical collapse patterns presented by other workers in this field<sup>(4,5)</sup> and indeed a very similar system of hinges may be observed in Plate 4.1. which depicts the collapse of Prestwood bridge during a full-scale load test<sup>(30)</sup>.
- j) Constitutive material properties are incorporated by means of the limit state moment-thrust interaction locus illustrated in Figure 3.9.



Plate 4.1

Prestwood Bridge On The Point Of Collapse

#### 4.3 STATIC MECHANISM MODEL TOPOLOGY

The essential features of the model are depicted in Figure 4.1 which relates to a typical one metre strip of arch. The dispersal of live load and the (approximately) linearly variably distributed load due to the fill are to be observed. Mechanical hinges are denoted by  $M_i (P_i)$  for  $1 \leq i \leq 4$ ,  $P_i$  defining the accompanying compression normal to the section at which  $M_i$  occurs.  $P_c$  denotes a one metre strip limit state knife edge total load. Using a live load dispersal based upon a Boussinesq distribution in two dimensions, the parameter  $p_c$  denotes the peak equivalent triangular load intensity (Figure 4.1). The specific weight of both the arch itself and of the fill is denoted by  $q$ .

A respective pair of sub-structure systems is illustrated in Figures 4.2 and 4.3.

#### 4.4 LIMIT STATE EQUATIONS - INCLUDING LOAD DISPERSAL THROUGH FILL

Being an overall mechanism study, the bridge is statically determinate and the following equilibrium statements are made available:

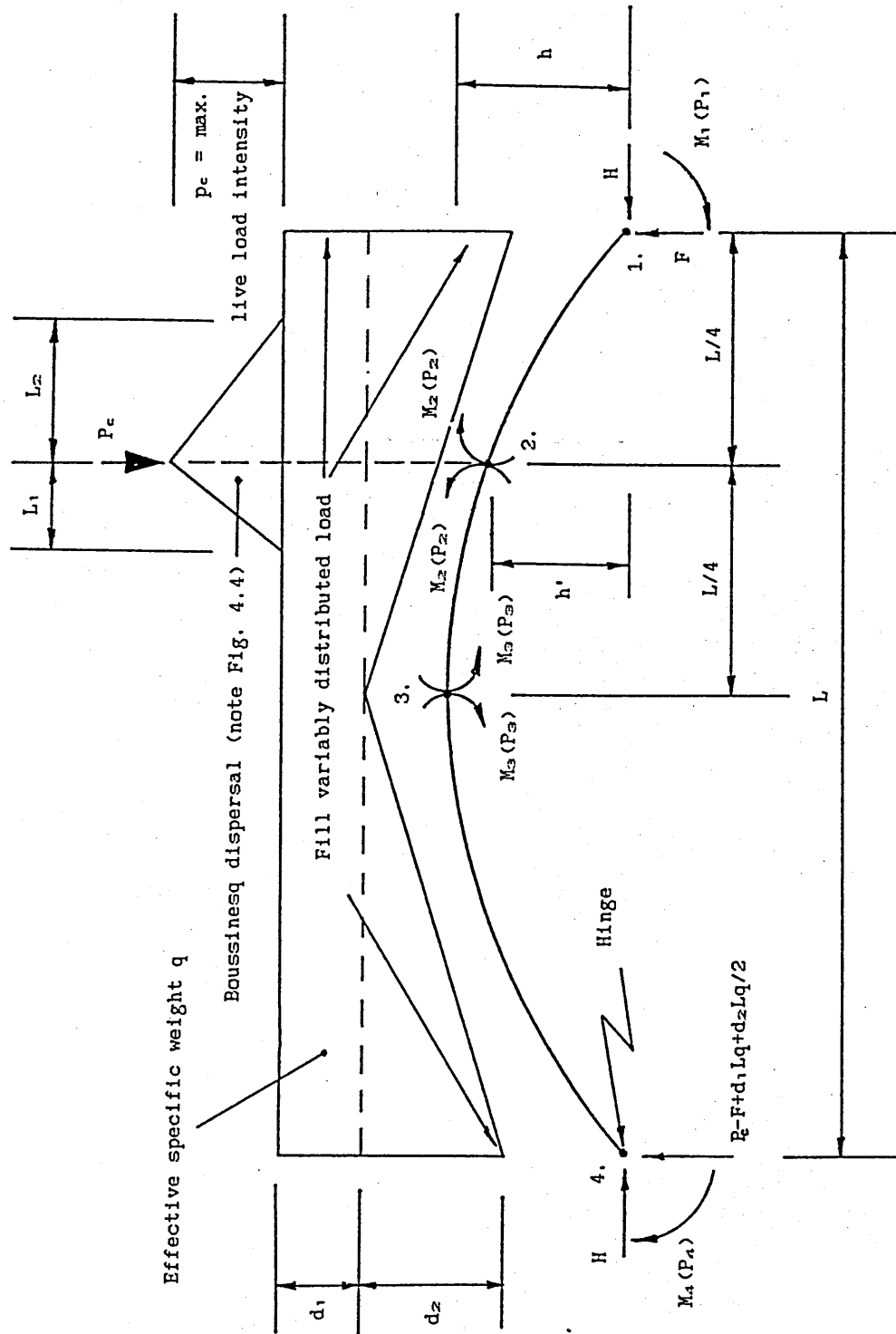


Figure 4.1

Topology

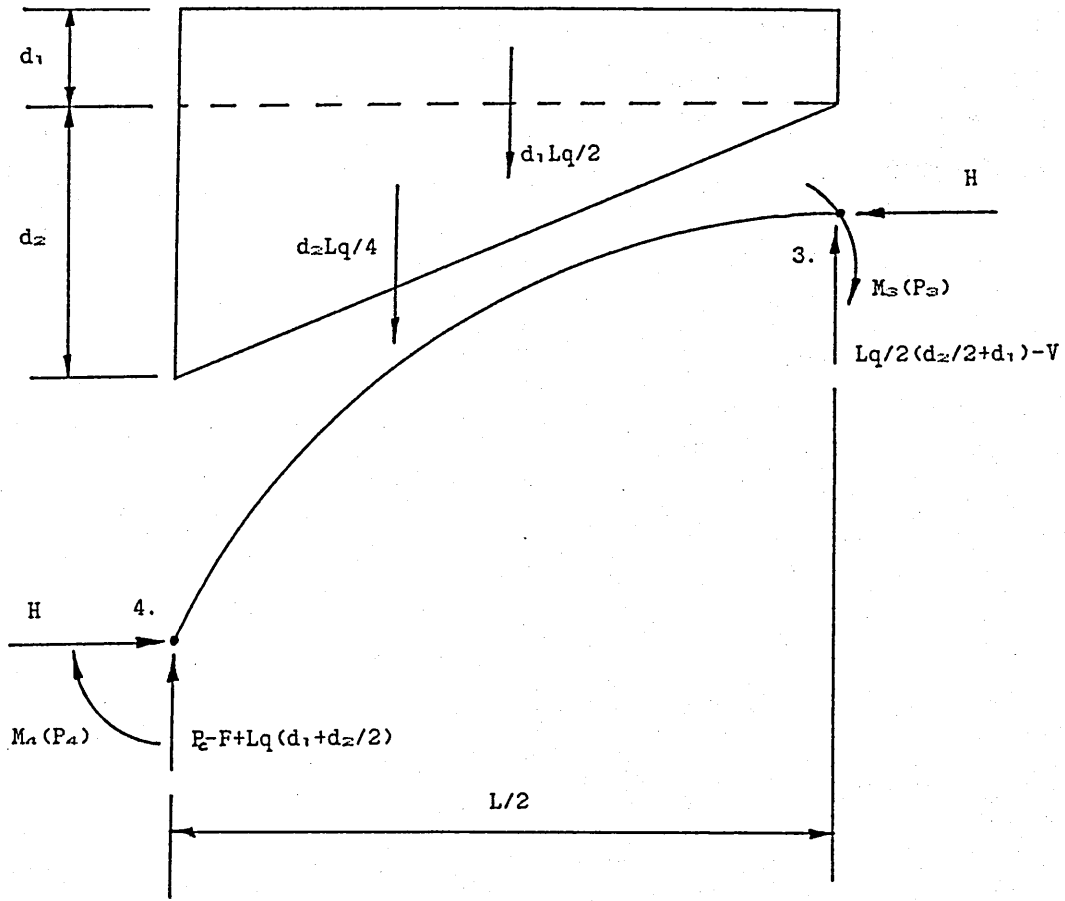


Figure 4.2

Left Substructure

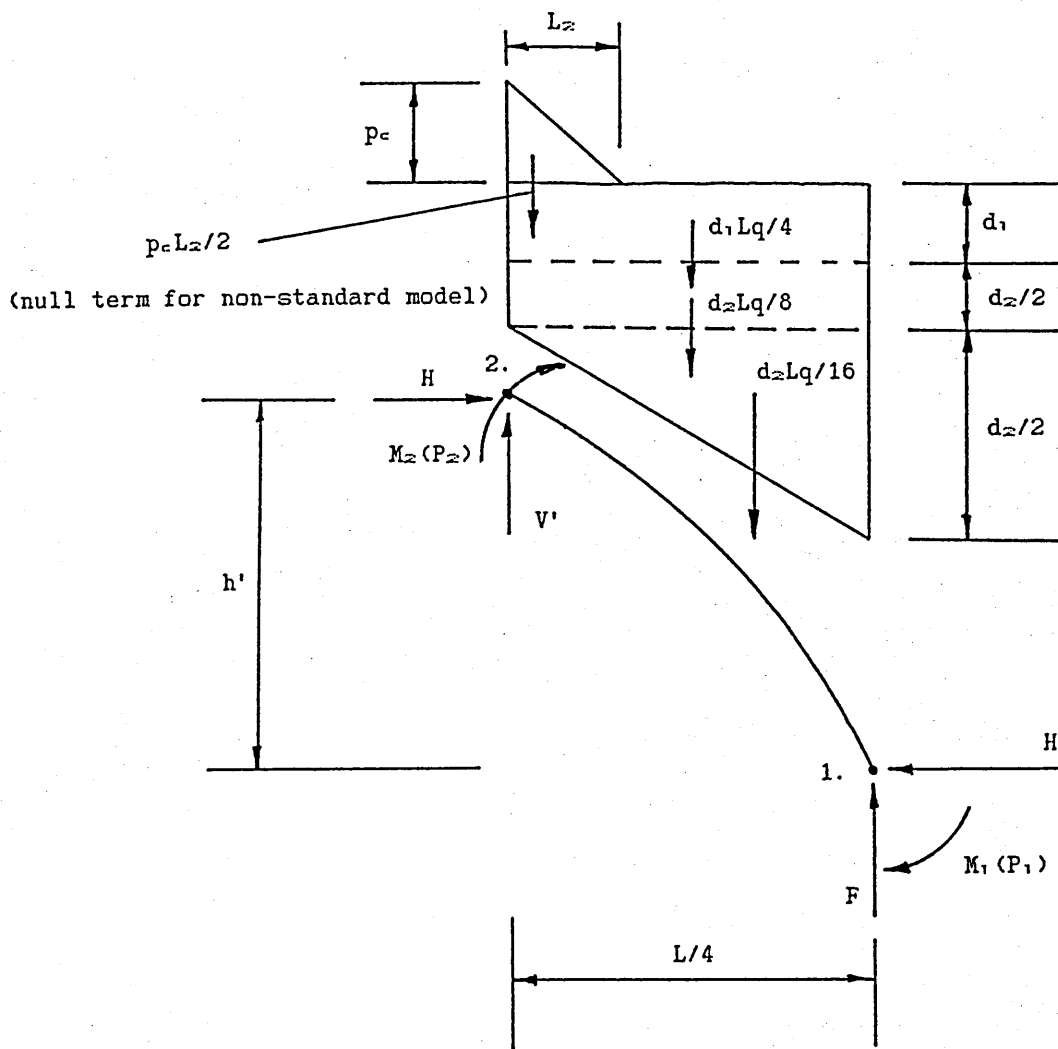


Figure 4.3

Right Substructure

Taking moments about the left springing (node 4) in Figure 4.1 yields

$$F = ((M_1 + M_4)/L) + (L_1 p_c / 2L) (3L/4 - L_1/3) + (L_2 p_c / 2L) (3L/4 + L_2/3) + Lq/4 (2d_1 + d_2) \quad \dots (4.1)$$

Taking moments about the crown (node 3), Figure 4.2

$$H = ((M_3 + M_4)/h) - L^2 q / 24h (3d_1 + 2d_2) + L/2h (P_c - F + Lq (d_1 + d_2/2)) \quad \dots (4.2)$$

The compression normal to the section at node 4 is given by

$$P_4 = ((P_c - F + Lq (d_1 + d_2/2))^2 + H^2)^{1/2} \cos \mu_4 \quad \dots (4.3)$$

With  $\mu_4$  denoting the angle between the resultant thrust and the tangent to the arch ring's centreline axis at node 4, this being given by

$$\mu_4 = \text{ABS}(\tan^{-1}(V_4/H_4) - (90 - \tan^{-1}(2(R-h)/L))) \quad \dots (4.4)$$

$V_4$  and  $H_4$  denoting the appropriate vertical and horizontal reactions, and  $R$  the arch's radius. The angular units are degrees,  $M_4$  being denoted in kNm units.

Taking moments about the quarter span point (node 2), Figure 4.3, provides

$$F = 4/L (Hh' + M_1 + M_2) + 2p_c L^2 / 3L + Lq/8 (d_1 + 5d_2/6) \quad \dots (4.5)$$

The normal compression is thereby

$$P_1 = (F^2 + H^2)^{1/2} \cos \mu_1 \quad \dots (4.6)$$

where  $\mu_1$  is derived similarly to  $\mu_4$ .

Resolving vertically, Figure 4.3

$$V' = Lq/16(4d_1 + 3d_2) - F + p_c L_2/2 \quad \dots (4.7)$$

The normal compression at node 2 is given by

$$P_2 = (H^2 + (Lq/16(4d_1 + 3d_2) - F + p_c L_2/2)^2)^{1/2} \cos \mu_2 \quad \dots (4.8)$$

Where  $\mu_2$  takes the form

$$\mu_2 = \text{ABS}(\tan^{-1}(V'/H)) - \text{ABS}(\tan^{-1}(L/(4(R^2 - L^2/16)^{1/2}))) \quad \dots (4.9)$$

Resolving forces at the crown (node 3), Figure 4.2

$$P_3 = H \quad \dots (4.10)$$

Finally, with reference to the limit state interaction locus, Figure 3.9

$$M_1 = f(P_1, d) \quad \dots (4.11)$$

for  $1 \leq i \leq 4$ , the relevant equations being simply based upon equations 3.57 and 3.58. Simultaneous and iterative solution of equations 4.1 to 4.11 provides a value for  $P_c$  at the limit state.

#### 4.5 LIMIT STATE EQUATIONS FOR ARCH BARREL ONLY

Several experimental tests have been carried out on arch rings per se<sup>(11)</sup>. That is, although a form of synthetic dead loading was applied to the arch ring, live loading was applied directly onto the arch barrel itself. Analysis of such cases requires no allowance for live load dispersal through the fill, and furthermore they are truly free from arch-fill interaction effects.

With respect to limit state modelling, the same equations as above apply subject to the following revision:

Equation 4.1 becomes

$$F = ((M_1 + M_2)/L) + 3P_c/4 + Lq/4(2d_1 + d_2) \quad \dots (4.12)$$

and equation 4.5 becomes

$$F = 4/L(Hh' + M_1 + M_2) + Lq/8(d_1 + 5d_2/6) \quad \dots (4.13)$$

The normal compression at node 2 (Figure 4.1), just to the right hand side of the point load, is thereby

$$P_z(1) = (H^2 + (Lq/16(4d_1 + 3d_2) - F)^2)^{1/2} \cos \mu_2 \quad \dots (4.15)$$

Consideration of the singularity existing at the point of application of the external load requires that the above expression be modified to afford the lower value of  $P_z$  present just to the left hand side of the point load. In other words, the bending moment capacity of the section is greater immediately to the right of the applied point load than it is immediately to the left due to the discontinuity present in the axial thrust at the point of application of the point load. This being the case, it is necessary to choose the lower of the two possible values of axial thrust. Hence

$$P_z(2) = (H^2 + (P_c + Lq/16(4d_1 + 3d_2) - F)^2)^{1/2} \cos \mu_2 \quad \dots (4.16)$$

## 4.6 COMPUTER PROGRAM MECHARCH

### 4.6.1 Program MECHARCH

A computer program, named MECHARCH and written in the "Basic" language, was prepared to carry out the above analyses and to solve the resulting simultaneous equations, thus providing the appropriate value for the external live point load necessary to produce a mechanism. Two versions of the program exist, one for a directly

applied point load and the other allowing for dispersal of the load through the arch fill medium. The main features of the program will now be described.

The program thereby analyses a typical one metre strip of a segmental arch structure and assumes mechanistic hinge positions as previously described in the foregoing analysis. In operation, the program asks for the "clear span" to be input by the user, and uses this figure in the analysis despite the fact that the span should really be measured to the "design line" along the centre line of the arch ring. However, the difference between the two is of the order of 2% and this correction is inappropriate considering the uncertainties present elsewhere in the analysis<sup>(19,31)</sup>. Alternatively, when the program requests the user to input the "clear rise" it does in fact make its own correction in this case by adding half the voussoir depth, giving the true rise to the design line. In the latter case the correction may easily be of the order of 15% and is therefore justified.

Regarding fill and voussoir density, MECHARCH does in fact employ a single density value (in kN/m<sup>3</sup> units) to represent the entire weight of materials above and including the arch ring itself. Given the usual uncertainties over the correct values to be used, even in the presence of laboratory tests on material won from trial holes as at the Bridgemill<sup>(32)</sup> full-scale test, the author considers it unrealistic to adopt separate values for the arch ring, the fill, the various carriageway layers and so forth.

The moment-thrust interaction diagram (Figure 3.9) is used to determine the states  $M_i(P_i)$  prevailing at each hinge position - an iterative application of MECHARCH being employed until these values are correct.

At this point a brief description of the method used to simulate load dispersal in one of the two versions of the program is necessary.

#### 4.6.2 Load Dispersal Through Fill Medium

Whereas the foregoing is common to both arches with fill over them and to those without, some special consideration is required with respect to load dispersal in the former case.

Load dispersal is simulated by standard theory attributable to Boussinesq<sup>(32)</sup> but with a modification to reduce the dispersal to two dimensions only and thus to make the simulation apt for knife edge type loading. The basic Boussinesq theory is handled by a further computer program named SPREAD. The output from SPREAD is in graphical form - Figure 4.4 depicts a typical sample - and it is a simple manual operation to scale-off the resulting load pattern's base dimensions to give an idealised equivalent triangular loading pattern (see Figure 4.1). In effect the triangle's area thus represented is equivalent to  $P_c$ . The base dimensions are then used as input to MECHARCH and serve to tell the program how far to spread the point load. During program running, the loading triangle's height is varied as MECHARCH iterates to find a solution, but the base dimensions remain constant.

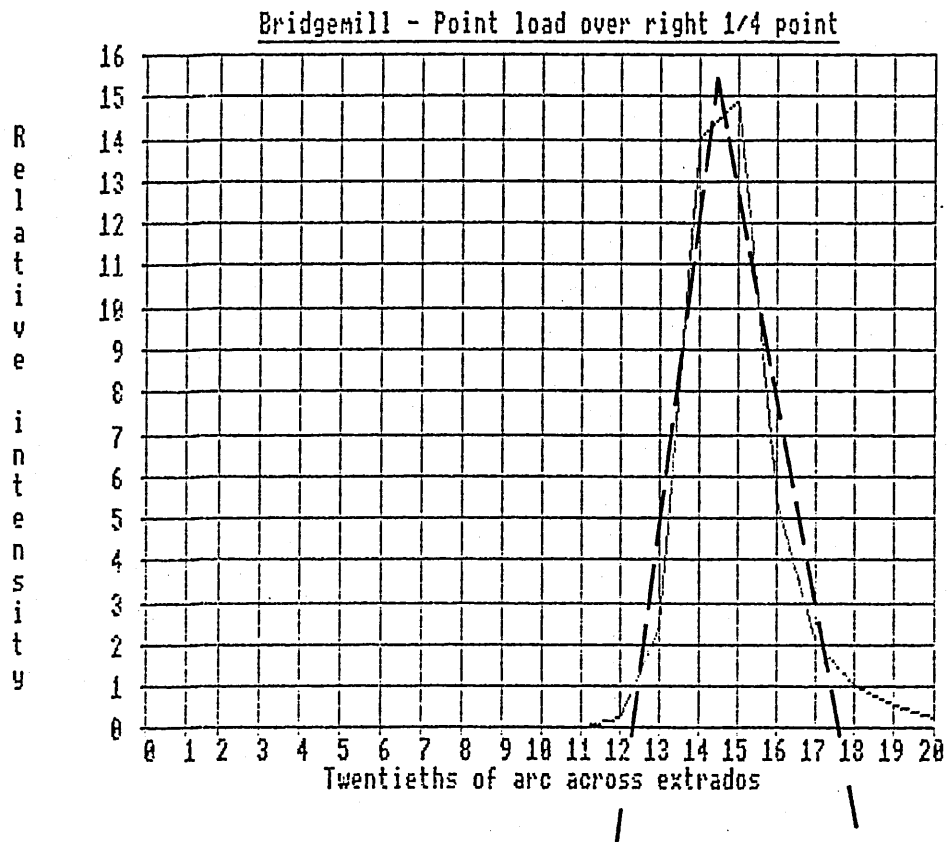


Figure 4.4

Typical Graphical Output From Computer Program SPREAD

(Note Manually Drawn "Give And Take" Lines)

## 4.7 MECHARCH VALIDATION

### 4.7.1 MECHARCH Analysis Applied to Bridgemill Full-scale Test

The masonry arch bridge at Bridgemill, Girvan, Scotland<sup>(2)</sup>, was loaded to destruction in 1984 as the first in a series of such tests sponsored by the Department of Transport. Knife edge quarter point live loading was applied to Bridgemill by means of four 200 tonne hydraulic jacks reacting against ground anchors installed in the river bed below. The four connecting tendons passed through holes cored in the deck by diamond bits. The load was equalised and distributed across the full deck width by means of short steel spreader beams and a 300mm thick concrete strip. The applied load was measured by load cells interposed between each jack and its spreader beam.

Piezo-electric crystal accelerometers for the measurement of acoustic emissions were mounted at each of the expected hinge points, one on the tension side of the voussoir and a complementary one on the compression side. Crucially, the tension sensor beneath the load point failed to work during the test and so the probable first indication of cracking due to live load was lost!

The input data to MECHARCH was as follows:

Profile:                   The arch is reported to have a shape somewhere between that of a parabola and that of a segment

of a circle, hence MECHARCH's segmental treatment is considered reasonable.

Span: 18.29m - this figure is actually the clear span, as noted above.

Rise: 2.84m (clear rise) + 0.3555 (voussoir thickness/2) = 3.195m.

Thickness: 0.711m - it is assumed that the internal barrel thickness is the same as the visible edge voussoir thickness. This is not always the case, e.g. Clare College Bridge<sup>(6)</sup>

Height of deck above springing: 3.753m - the deck is assumed level.

Fill density: Having duly considered the respective values quoted for these items in the Bridgemill report, a single figure of 20kN/m<sup>3</sup> is used as input to MECHARCH. This is intended to represent a weighted mean of the materials present, having due regard for the relative quantities involved.

Constitutive properties: The Bridgemill report quotes a mean maximum stress of 5 to 7 N/mm<sup>2</sup> and a mean Young's modulus of 5000 N/mm<sup>2</sup>.

Other researchers in the field using various techniques obtained the collapse load predictions for the Bridgemill test given in Table 4.1.

<u>Method</u>	<u>Source</u>	<u>Collapse Load (kN)</u>
Elastic analysis	Edinburgh University	unable to provide meaningful result
MEXE	Edinburgh University	1000 - 1500 (depending on factors chosen)
Heyman mechanism	Edinburgh University	2830
Finite element	T.R.R.L.	1500 - 2700 (depending on densities etc. chosen)
Model analysis	Edinburgh University	3890

TABLE 4.1  
BRIDGEMILL ANALYSES<sup>(9)</sup>

Recalling equations 4.1 to 4.11 together with Section 4.6, then the resulting output from MECHARCH provides a collapse load of 2808 kN for Bridgemill. This represents an "error" of -9.4%, being on the "safe" side of the true collapse load of 3100 kN.

This value compares well with those given in Table 4.1.

It is postulated that the main reason for the load obtained from MECHARCH being lower than the actual figure is almost certainly due to the contribution of arch-fill interaction, this effect strengthening the real bridge. It is, however, considered that the program is in actual fact providing a good estimate of the strength of Bridgemill's arch barrel alone, crucially subjected to load dispersal, and that the additional load carrying capacity of Bridgemill is due to an effect that the program makes no attempt to model. That this is probably the case will be later considered in Section 4.7.4 where MECHARCH is applied to one of Liverpool University's model arches where arch-fill interaction is not present.

#### 4.7.2 MECHARCH Analysis Applied to a Comparability Study

Sawko and Towler of Liverpool University undertook a comparability study<sup>(21)</sup> with the aim of testing their own finite element method of analysis against rivals in the field. It should be emphasised that this was an entirely theoretical study and that the arches used for this comparison were never constructed and hence which of the alternative analyses was nearest the "correct" result would never be

known. One of these comparisons, on a 6 metre span, 1.8 metre rise brickwork arch of barrel thickness 0.44 metres, was later also analysed by Crisfield<sup>(4)</sup> to compare his own technique against those reported by Sawko and Towler. The author proposes to do likewise in order to compare MECHARCH against the widest possible range of alternative methods.

A significant drawback in attempting to apply MECHARCH to the specimen arch is that Sawko and Towler do not quote material properties for the brickwork (eg.  $\sigma_{max}$ ) - most of the methods under comparison assuming infinite compressive strength, in any case. Crisfield was forced to assume properties (including fill density) in order to apply his finite element program and the author has also similarly assumed the following values:

$$\sigma_{max} = 2.5 \text{ N/mm}^2 \text{ (as Crisfield)}$$

$$\gamma_{fill, arch} = 19 \text{ kN/m}^3 \text{ (Crisfield uses } 1.8 \times 10^{-6} \text{ kg/mm}^3 \text{)}$$

Solution of the problem was achieved by proceeding in the manner described in Section 4.6.1., utilising Figure 3.9. The results from MECHARCH and the other methods are summarised in Table 4.2. In the absence of a "correct" value, this comparison exercise is of limited value, as has already been pointed out. It does, however, at least show that MECHARCH gives answers in the same ballpark as other, more established techniques.

<u>Method</u>	<u>Collapse Load (kN)</u>
Pippard elastic analysis	4
Heyman lower bound	63
Heyman upper bound	100
Sawko & Towler	119
MEXE	221*
Crisfield, 10 elements	95
Crisfield, 20 elements	85
Author's MECHARCH	108.9

\*As Crisfield points out<sup>(4)</sup>, there is some doubt as to whether Sawko and Towler interpreted MEXE properly in obtaining this figure. It should be treated with scepticism.

TABLE 4.2  
COMPARABILITY STUDY RESULTS

#### 4.7.3 MECHARCH Analysis Applied to Two Further Full-scale Tests

The Bridgemill full-scale arch bridge test was just the first in a series of such tests. At the time of writing, six of the series had been completed. However, some of these tests breach the assumptions set out in Section 4.2 and furthermore only limited data is available to the author for the more recent tests.

Of the six examples so far carried out, full and detailed information is available to the author for the first two, namely Bridgemill and Bargower, Bridgemill having been described in Section 4.7.1 above. Unfortunately Bargower cannot be employed by the author as the knife edge loading was applied at the third point in the full-scale test and MECHARCH, of course, is at present only applicable to quarter point loading. For the same reason the next in the series, Preston, is similarly unuseable. These bridges may have possessed features leading the TRRL to consider that third point loading was the more suitable. The fourth and fifth tests, Prestwood and Torksey respectively, are appropriate to the author's purpose although the data available for these two tests is very much more limited than that for Bridgemill. The last test in the current series, Shinafoot, is also inappropriate as the arch barrel thickness varied; from 390mm at the crown to 770mm at the springing.

The data presently available to the author on the Prestwood and Torksey tests is given in Table 4.3.

	<u>Span</u> <u>(mm)</u>	<u>Rise</u> <u>(mm)</u>	<u>Barrel Thick.</u> <u>(mm)</u>	<u>Crown Fill</u> <u>(mm)</u>	<u>Width</u> <u>(mm)</u>	<u>Coll. Load</u> <u>(kN)</u>
Prestwood	6550	1424	220	165	3800	228
Torksey	4902	1115	343	246	7045	1080

TABLE 4.3

PRESTWOOD AND TORKSEY BRIDGES - BASIC DATA

Regarding Table 4.3, both bridges were of segmental profile and were constructed of brick; no material properties are available, however. It should also be noted that the Prestwood arch was badly distorted before the test began and also that the deck possessed a longitudinal fall (see assumptions in Section 4.2). Finally, it is also understood that, on collapse, Torksey left both spandrels standing (literally only the barrel collapsed) and hence the width given above is that from parapet face to parapet face and this width only is used in the analysis.

Applying the same analytical procedure as before, again with the aid of Figure 3.9, the solutions obtained from MECHARCH are given in Table 4.4. MECHARCH's predictions are once more conservative. If one accepts that arch-fill interaction provides a general arch strengthening effect due to the inhibition of hinge formation, then the use of a method (like MECHARCH) that does not model the effect would naturally give rise to lower bound results. One may easily explain MECHARCH's results for Bridgemill and Prestwood in this way, but if the same is true for Torksey then it is to be observed that there is very little arch-fill contribution here! Against this it must be remembered that material properties have had to be assumed for the latter two arches and this must obviously have had an appreciable effect on the accuracy of the analyses. Nevertheless, it is noteworthy that lower bound solutions have consistently been obtained throughout.

	<u>MECHARCH Collapse Load (kN)</u>	<u>Test Collapse Load (kN)</u>
Prestwood	160	228
Torksey	1036	1080

TABLE 4.4

PRESTWOOD AND TORKSEY RESULTS

Consideration will now be given to a validation exercise where not only are the material properties accurately known, but that the stress-strain relationship is treated parabolically by the arch test's authors and that, furthermore, arch-fill interaction was not present.

#### 4.7.4 MECHARCH Analysis Applied to Liverpool University Model Test

Sawko and Towler of Liverpool University<sup>(11)</sup> conducted a series of arch tests on four metre span brick "models". Several of these tests relate to "serviceability", although exactly what is meant by this term is not defined. Only two actual arch failures were conducted, one with a crown knife edge load and the other with a quarter point knife edge load. This MECHARCH appraisal relates to the quarter point case. It is worth considering that these tests could be considered to relate not only to model tests, but also to full scale tests on arches typical of the small spans crossing culverts and streams.

The reader is referred to published matter<sup>(12)</sup> for a fuller description of the tests, but basically the model bridge spanned 4 metres (clear), with a segmental profile providing a central clear rise of one metre. A simulated fill dead load equivalent to 250mm of fill above the crown was employed. The dead loading was achieved by weights placed on a stepped extrados and consequently arch-fill interaction was not present. Similarly, the live load was applied directly to the arch barrel and hence dispersal of the load through the fill was similarly not present - the version of MECHARCH without live load dispersal was prepared for use in just this type of case.

Unfortunately, the assumed density of simulated fill is not quoted, merely its depth, but a typical figure of  $19 \text{ kN/m}^3$  has been taken for the input to MECHARCH. With regard to constitutive properties, Towler had tests conducted at the B.C.R.A. using samples of brickwork identical to those used in the arch. It was found that the material exhibited a stress-strain law that could be very well modelled parabolically with values of  $\sigma_m = 16 \text{ N/mm}^2$ , and  $\epsilon_m = 0.0034$ .

On running MECHARCH for this example it was found that the hinges formed occupy positions much nearer the origin in  $n, m$  space (Figure 3.9) than those in the Bridgemill test - typically at  $0.017P_m$  against  $0.200P_m$  (this accords with common sense as one would expect some scale effect to be present) - and MECHARCH predicts a collapse load of  $115.8 \text{ kN}$  for the model. This agrees remarkably well with the published value of  $117 \text{ kN}$ . By comparison, Sawko and Towler report a prediction of  $102 \text{ kN}^{(10)}$  using their own finite element computer program. The author's own result is therefore quite encouraging and tends to bear out the author's hypothesis that MECHARCH does in fact provide good estimates of arch barrel strength for Bridgemill, Prestwood and Torksey but that arch-fill interaction would need to be allowed for to gain a better estimate of the strength of the whole arch/fill bridge system.

## 4.8 SERVICEABILITY MODEL

### 4.8.1 Introduction

It must be stated that the concept of serviceability in the context of masonry arches is a very complex one. As far as the author is aware, no other researchers in this field have directly addressed the problem, presumably instead relying upon the application of arbitrary load factors to (ultimate) mechanism analyses. Herein is a limited attempt to generate a serviceability analysis whereupon the limiting criterion is to be based on or factored on the formation of the first hinge.

A tentative flexibility analysis for an encastre segmental arch under single point loading is now described. A standard reduction procedure is developed to solve the resulting three simultaneous equations and the means of incorporating this procedure within a series of computer programs is described.

### 4.8.2 Initial Serviceability Model

To introduce FLEXARCH, it is useful to set out the basic linear elastic modelling. Noting the topology given in Figure 4.5, from statics, initially with  $Q=0$ , then

$$H_1 = H_2 \quad \dots (4.17)$$

ASSUMPTIONS:

1. Supports at same level
2. Single point loading
3. Linear flexural strain effects only
4. E, I constant

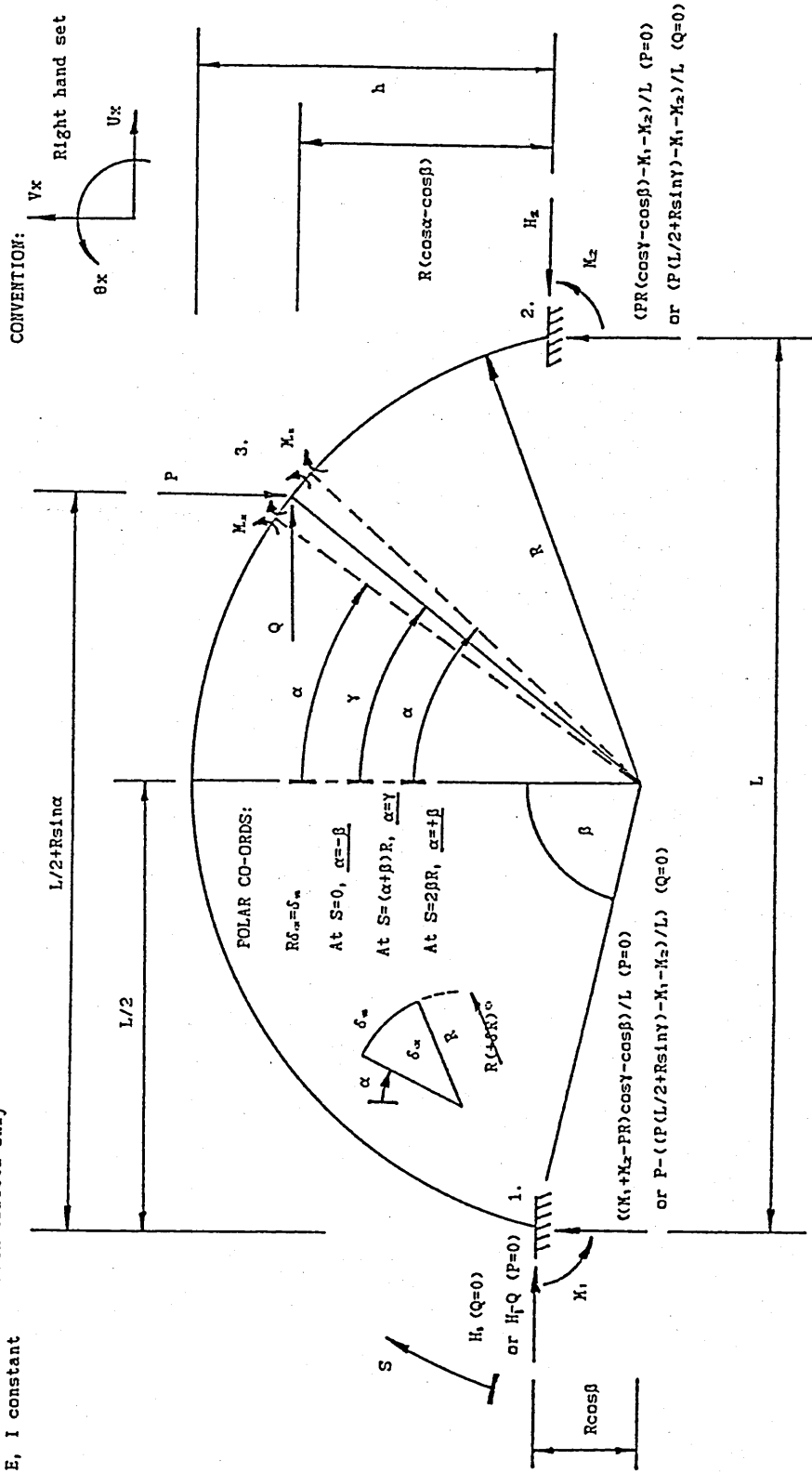


Figure 4.5

Topology

$$F_1 + F_2 = P \quad \dots (4.18)$$

$$F_2 L + M_1 + M_2 - P(L/2 + R \sin \gamma) = 0 \quad \dots (4.19)$$

$$F_2 = (P(L/2 + R \sin \gamma) - M_1 - M_2) / L \quad \dots (4.20)$$

and

$$F_1 = P - ((P(L/2 + R \sin \gamma) - M_1 - M_2) / L) \quad \dots (4.21)$$

where the three statical redundancies are taken as H (=H1, =H2), M1 and M2. Applying Castigliano's<sup>(15)</sup> for flexural strain effects only affords

$$\frac{\partial U}{\partial H} = \int_0^{(\gamma+\beta)R} \frac{M\alpha(\partial M\alpha/\partial H) ds}{EI} + \int_{(\gamma+\beta)R}^{2\beta R} \frac{M\alpha(\partial M\alpha/\partial H) ds}{EI} = 0 \quad \dots (4.22)$$

$$\frac{\partial U}{\partial M_1} = \int_0^{(\gamma+\beta)R} \frac{M\alpha(\partial M\alpha/\partial M_1) ds}{EI} + \int_{(\gamma+\beta)R}^{2\beta R} \frac{M\alpha(\partial M\alpha/\partial M_1) ds}{EI} = 0 \quad \dots (4.23)$$

$$\frac{\partial U}{\partial H_2} = \int_0^{(\gamma+\beta)R} \frac{M\alpha(\partial M\alpha/\partial H_2) ds}{EI} + \int_{(\gamma+\beta)R}^{2\beta R} \frac{M\alpha(\partial M\alpha/\partial H_2) ds}{EI} = 0 \quad \dots (4.24)$$

The null terms signify no structural "lack of fit"<sup>(33)</sup>. These equations can be rearranged in the form

$$\int_{-\beta}^{\gamma} \frac{M\alpha(\partial M\alpha/\partial H)Rd\alpha}{EI} + \int_{\gamma}^{\beta} \frac{M\alpha(\partial M\alpha/\partial H)Rd\alpha}{EI} = \partial U/\partial H = 0 \quad \dots (4.25)$$

$$\int_{-\beta}^{\gamma} \frac{M\alpha(\partial M\alpha/\partial M_1)Rd\alpha}{EI} + \int_{\gamma}^{\beta} \frac{M\alpha(\partial M\alpha/\partial M_1)Rd\alpha}{EI} = \partial U/\partial M_1 = 0 \quad \dots (4.26)$$

$$\int_{-\beta}^{\gamma} \frac{M\alpha(\partial M\alpha/\partial M_2)Rd\alpha}{EI} + \int_{\gamma}^{\beta} \frac{M\alpha(\partial M\alpha/\partial M_2)Rd\alpha}{EI} = \partial U/\partial M_2 = 0 \quad \dots (4.27)$$

Considering  $-\beta < \alpha < \gamma$ , taking moments about node 3 gives

$$M\alpha = -M_1 - H(R(\cos\alpha - \cos\beta)) + ((PL/2 - PR\sin\gamma + M_1 + M_2)/L)(L/2 + R\sin\alpha) \quad \dots (4.28)$$

which affords

$$\frac{\partial M\alpha}{\partial H} = -R(\cos\alpha - \cos\beta) \quad \dots (4.29)$$

$$\frac{\partial M_\alpha}{\partial M_1} = R \sin \alpha / L - 1/2 \quad \dots (4.30)$$

$$\frac{\partial M_\alpha}{\partial M_2}$$

$$\frac{\partial M_\alpha}{\partial M_1} = R \sin \alpha / L + 1/2 \quad \dots (4.31)$$

$$\frac{\partial M_\alpha}{\partial M_2}$$

For  $\gamma < \alpha < \beta$ , taking moments about node 3 gives

$$M_\alpha = M_2 - H(R(\cos \alpha - \cos \beta)) + ((PL/2 + PR \sin \gamma - M_1 - M_2)/L)(L/2 - R \sin \alpha) \quad \dots (4.32)$$

Which similarly leads to

$$\frac{\partial M_\alpha}{\partial H} = -R(\cos \alpha - \cos \beta) \quad \dots (4.33)$$

$$\frac{\partial M_\alpha}{\partial M_1}$$

$$\frac{\partial M_\alpha}{\partial M_1} = R \sin \alpha / L - 1/2 \quad \dots (4.34)$$

$$\frac{\partial M_\alpha}{\partial M_2}$$

$$\frac{\partial M_\alpha}{\partial M_1} = R \sin \alpha / L + 1/2 \quad \dots (4.35)$$

$$\frac{\partial M_\alpha}{\partial M_2}$$

Finally equations 4.25, 4.26 and 4.27 may ultimately be written in the form

$$f_{11}H + f_{12}M_1 + f_{13}M_2 = P_{1v} \quad \dots (4.36)$$

$$f_{21}H + f_{22}M_1 + f_{23}M_2 = P_{2v} \quad \dots (4.37)$$

$$f_{31}H + f_{32}M_1 + f_{33}M_2 = P_{3v} \quad \dots (4.38)$$

The flexibility influence coefficients  $f_{11}$  to  $f_{33}$  are given by

$$f_{11} = -R^2/2(-\beta - \sin\beta\cos\beta) + 2R^2\beta\cos^2\beta + R^2/2(\beta + \sin\beta\cos\beta) + 4R^2\sin\beta\cos\beta \quad \dots (4.39)$$

$$f_{12} = R\sin\beta - R\beta\cos\beta \quad \dots (4.40)$$

$$f_{13} = -R\sin\beta + R\beta\cos\beta \quad \dots (4.41)$$

$$f_{21} = R\sin\beta - R\beta\cos\beta \quad \dots (4.42)$$

$$f_{22} = R^2/L^2(\beta - \sin\beta\cos\beta) + \beta/2 \quad \dots (4.43)$$

$$f_{23} = R^2/L^2(\beta - \sin\beta\cos\beta) - \beta/2 \quad \dots (4.44)$$

$$f_{31} = R\beta\cos\beta - R\sin\beta \quad \dots (4.45)$$

$$f_{32} = R^2/L^2(\beta - \sin\beta\cos\beta) - \beta/2 \quad \dots (4.46)$$

$$f_{33} = R^2/L^2(\beta - \sin\beta\cos\beta) + \beta/2 \quad \dots (4.47)$$

The loading coefficients are given by

$$P_{1v} = -PR^2 \sin^2 \gamma / 2 + PR^2 \gamma \cos \beta \sin \gamma + PR^2 \cos \gamma \cos \beta + PLR \sin \beta / 2 - PR^2 \sin^2 \beta / 2 - PLR \beta \cos \beta / 2 - PR^2 \cos^2 \beta \quad \dots (4.48)$$

$$P_{2v} = -PR^2 / 2 / L (\gamma - \sin \gamma \cos \gamma) - PR \gamma \sin \gamma / 2 + PL \beta / 4 + PR \cos \beta / 2 + PR^2 \cos \beta \sin \gamma / L + PR^3 \sin \gamma / L^2 (\beta - \sin \beta \cos \beta) - PR \cos \gamma / 2 - PR^2 \cos \gamma \sin \gamma / L \quad \dots (4.49)$$

$$P_{3v} = PR \cos \gamma / 2 - PR^2 \cos \gamma \sin \gamma / L - PR^2 / 2 / L (\gamma - \sin \gamma \cos \gamma) + PR \gamma \sin \gamma / 2 - PR \cos \beta / 2 + PR^2 \cos \beta \sin \gamma / L - PL \beta / 4 + PR^3 \sin \gamma / L^2 (\beta - \sin \beta \cos \beta) \quad \dots (4.50)$$

It is noteworthy that the flexibility matrix is symmetrical about its leading diagonal and furthermore

$$f_{13} = f_{31} = -f_{12}, f_{21} \quad \dots (4.51)$$

$$f_{22} = f_{33} \quad \dots (4.52)$$

It should also be noted that the flexibility matrix is independent of the loading terms - this is to be expected for linear studies.

Returning to Figure 4.5, the foregoing is repeated for Q being present with  $P=0$ .

$$H_1 + P = H_2 = H \quad \dots (4.53)$$

$$F_2 L + M_1 + M_2 - P(R \cos \gamma - R \cos \beta) = 0 \quad \dots (4.54)$$

$$\therefore F_2 = (P(R \cos \gamma - R \cos \beta) - M_1 - M_2) / L \quad \dots (4.55)$$

$$F_1 L - M_1 - M_2 = P(R \cos \gamma - R \cos \beta) = 0 \quad \dots (4.56)$$

$$\therefore F_1 = (M_1 + M_2 - P(R \cos \gamma - R \cos \beta)) / L \quad \dots (4.57)$$

Taking the three statical redundancies as  $H$  ( $\equiv H_2$ ),  $M_1$  and  $M_2$ , and applying Castigliano<sup>(16)</sup> for flexural strain effects only affords equations identical to 4.22, 4.23 and 4.24. As before, these can be rearranged to afford equations 4.25, 4.26 and 4.27.

Considering  $\beta < \alpha < \gamma$  and taking moments about node 3 gives

$$M\alpha = -M_1 - (H - P)(R(\cos \alpha - \cos \beta)) + (M_1 + M_2 - P(R \cos \gamma - R \cos \beta)) / L (L/2 + R \sin \alpha) \quad \dots (4.58)$$

with

$$\frac{\partial M\alpha}{\partial H} = -R(\cos \alpha - \cos \beta) \quad \dots (4.59)$$

$$\frac{\partial M\alpha}{\partial M_1} = R \sin \alpha / L - 1/2 \quad \dots (4.60)$$

$$\frac{\partial M_{\alpha}}{\partial M_2} = R \sin \alpha / L + 1/2 \quad \dots (4.61)$$

$\partial M_2$

For  $\gamma < \alpha < \beta$ , taking moments about node 3 gives

$$M_{\alpha} = M_2 - H(R(\cos \alpha - \cos \beta)) + ((PR(\cos \gamma - \cos \beta) - M_1 - M_2)/L)(L/2 - R \sin \alpha) \dots (4.62)$$

with

$$\frac{\partial M_{\alpha}}{\partial H} = -R(\cos \alpha - \cos \beta) \quad \dots (4.63)$$

$\partial H$

$$\frac{\partial M_{\alpha}}{\partial M_1} = R \sin \alpha / L - 1/2 \quad \dots (4.64)$$

$\partial M_1$

$$\frac{\partial M_{\alpha}}{\partial M_2} = R \sin \alpha / L + 1/2 \quad \dots (4.65)$$

$\partial M_2$

The flexibility influence coefficients remain unchanged as befitting functions of the datum structure only. The corresponding loading terms become

$$P_{1H} = PR^2/2(\gamma + \sin \gamma \cos \gamma) - PR^2 \sin \gamma \cos \beta - PR^2 \sin \gamma \cos \gamma + PR^2 \gamma \cos \beta \cos \gamma$$

$$-PR^2/2(-\beta - \sin \beta \cos \beta) - 2PR^2 \sin \beta \cos \beta + PR^2 \beta \cos^2 \beta \quad \dots (4.66)$$

$$\begin{aligned}
P_{zn} = & -PR\gamma\cos\gamma/2 + PR^2\cos\gamma\cos\beta/L - PR^3\cos\gamma/L^2(-\beta + \sin\beta\cos\beta) \\
& + PR^3\cos\beta/L^2(-\beta + \sin\beta\cos\beta) - PR^2\cos^2\gamma/L \\
& - PR^2\sin^2\gamma/2/L + PR\sin\gamma/2 + PR^2\sin^2\beta/2/L + PR\sin\beta/2 - PR\beta\cos\beta/2 \dots \dots (4.67)
\end{aligned}$$

$$\begin{aligned}
P_{zn} = & -PR^2\cos^2\gamma/L + PR^2\cos\beta\cos\gamma/L + PR\gamma\cos\gamma/2 \\
& - PR^3\cos\gamma/L^2(-\beta + \sin\beta\cos\beta) + PR^3\cos\beta/L^2(-\beta + \sin\beta\cos\beta) \\
& - PR^2\sin^2\gamma/2/L - PR\sin\gamma/2 + PR^2\sin^2\beta/2/L - PR^2\sin\beta/2 + PR\beta\cos\beta/2 \dots (4.68)
\end{aligned}$$

Whilst the foregoing relates to established work, no reference was located containing all the key algebraic details herein set out. Relating as it does to a general analysis of the linear elastic, doubly encastred segmental arch (note the superposition of an arbitrary point load), the detail given was considered worthy of inclusion. Its development for more specific "serviceability analysis" useage is given shortly.

#### 4.8.3 General Solution Of The Matrix Equations

For either loading condition, a set of three simultaneous equations is obtained. A standard reduction procedure yields the following solution

$$\text{Let } \lambda = (f_{21}^2 f_{12} P_3) - (f_{11} f_{22} f_{12} P_3) - (f_{21} f_{12} f_{31} P_2) \\ + (f_{21} f_{32} f_{11} P_2) - (f_{21}^2 f_{32} P_1) + (f_{31} f_{22} f_{21} P_1) \quad \dots (4.69)$$

$$\text{And let } \delta = (f_{21}^2 f_{12} f_{33}) - (f_{11} f_{22} f_{21} f_{33}) \\ - (f_{21} f_{12} f_{31} f_{23}) + (f_{21} f_{32} f_{11} f_{23}) \\ - (f_{21}^2 f_{32} f_{13}) + (f_{31} f_{22} f_{21} f_{13}) \quad \dots (4.70)$$

Then

$$M_1 = ((f_{11} P_2 \delta) - (f_{11} f_{23} \lambda) - (f_{21} P_1 \delta) + (f_{11} f_{13} \lambda)) / (\delta (f_{11} f_{22} - f_{21} f_{12})) \quad \dots (4.71)$$

$$M_2 = \lambda / \delta \quad \dots (4.72)$$

$$H = (P_1 - f_{12} M_2 - f_{12} M_1) / f_{11} \quad \dots (4.73)$$

#### 4.8.4 Initial Serviceability Case Studies

The above mathematical procedure was incorporated into a computer program written in BASIC language for the B.B.C. 'B' microcomputer and termed FLEXARCH. The following data runs were made for validation

1. With reference to Figure 4.6a, taking  $W=1$ ,  $R=1$ , then the application of equations 4.39 to 4.50 yields

$$f_{11}= 1.57080 \quad f_{12}= 1.00001 \quad f_{13}=-1.00001 \quad P_{1v}= 0.500002$$

$$f_{21}= 1.00001 \quad f_{22}= 1.17810 \quad f_{23}=-0.39269 \quad P_{2v}= 0.285398$$

$$f_{31}=-1.00001 \quad f_{32}=-0.39269 \quad f_{33}= 1.17810 \quad P_{3v}=-0.285398$$

Solution by means of equations 4.69 to 4.73 provides

$$H = -0.459136$$

$$M_b = -0.110606$$

The published solution<sup>(34)</sup> is given as

$$H = -0.459W$$

$$M_b = -0.1106WR$$

2. A similar procedure may be applied to Figure 4.6b, noting though that the pinned feet in this example require only the application of the first of the three simultaneous equations, giving

$$f_{11}=320.6 \quad f_{12}=0 \quad f_{13}=0 \quad P_{1v}=6249$$

And hence

$$H = 9.4376$$

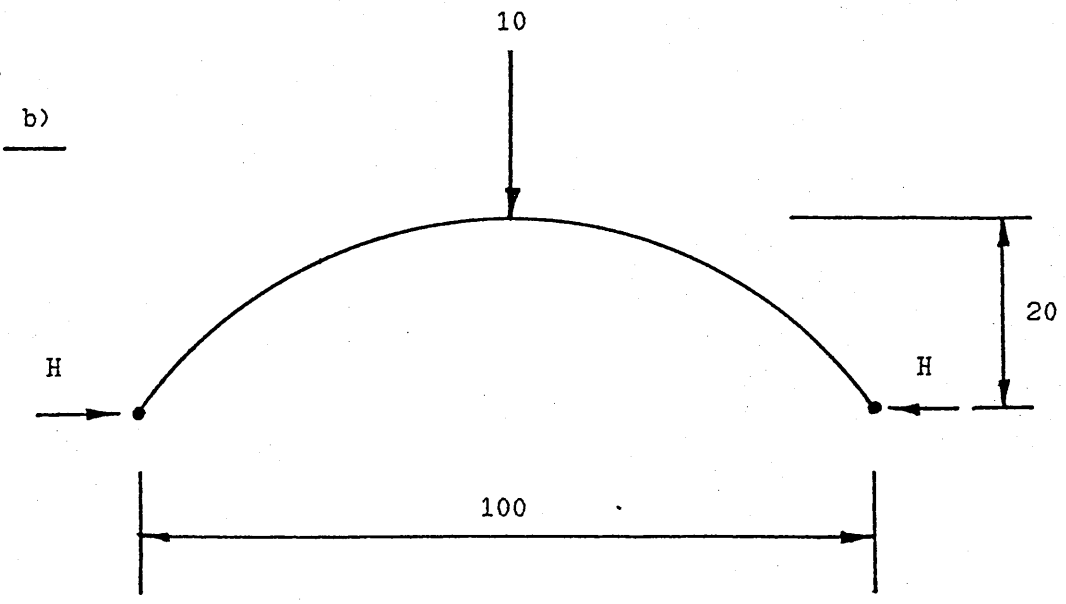
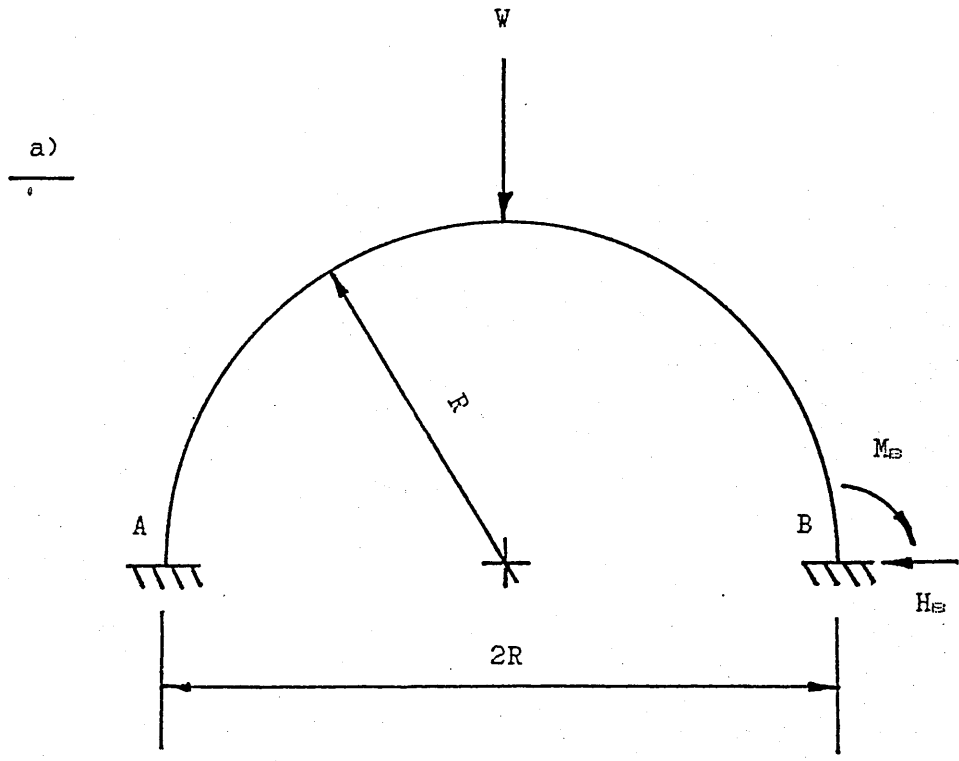


Figure 4.6  
Case Studies

By comparison, the published solution<sup>(34)</sup> is

$$H = 9.45$$

3. Finally, a series of comparisons was made against a well-tried computerised stiffness method employing forty straight beam elements<sup>(33)</sup>. These comparisons yielded similar close correlation.

#### 4.8.5 Development Of The Serviceability Model

The foregoing modelling and corresponding computer program FLEXARCH were developed continually over a period of time and gradually the following features were incorporated:

1. The arch ring was notionally divided into discrete "elements" (rather like voussoirs, each subtending an equal arc at the arch's centre of radius) and point loading was taken to act at the middle of each of these "elements". Dead loading, due to fill and arch barrel material, was taken in vertical strips, one above each element, and the load due to that strip of fill was applied to its own element below as a point load. Live loading could be applied as virtually any number of point loads at the deck surface, but was, in actuality, restricted to a single point load for simplicity. The point live load at the surface was distributed down to the level of the arch extrados using theory due to Boussinesq<sup>(32)</sup> (as previously) in two dimensions. The resulting load at extrados level was similarly apportioned as a

point load to each arch barrel element, as with dead loading. See Figure 4.7(a).

By repeated application of the elementary FLEXARCH program for each element's own point load and summing the results, the redundancies (external reactions) could be determined for the entire dead and live loading pattern. See Figure 4.7(b).

2. The next step was to revert to numerical integration of the original equations (4.25 to 4.27) enabling each integration station to possess its own 'E' and 'I' values. This, significantly, enabled each element of arch to possess its own 'E' and 'I' values rather than having fixed, constant values across the whole arch. This procedure primarily enables:

a) the use of locally variable constitutive properties (note below) with increasing load, and,

b) the variation of second moment of area as local tension cracks develop under increasing load.

Numerical integration was applied, with respect to the foregoing formal integrals, at the stages demarked by equations 4.35 to 4.36, and equations 4.65 to 4.66. At this stage the program was renamed "NIARCH" - representing Non-linear Integration of an ARCH. See Figure 4.7(c).

3. A further program module was then incorporated to determine the thrust line position at each element. It was therefore possible at this stage to determine the thrust and eccentricity at each element.

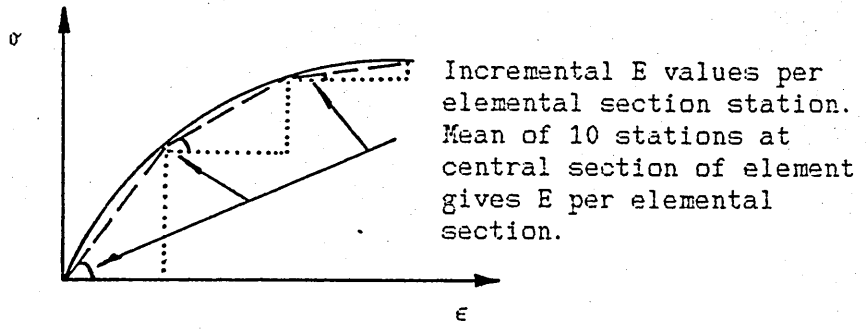
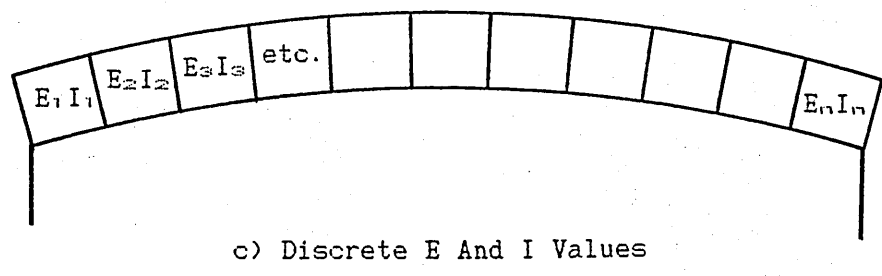
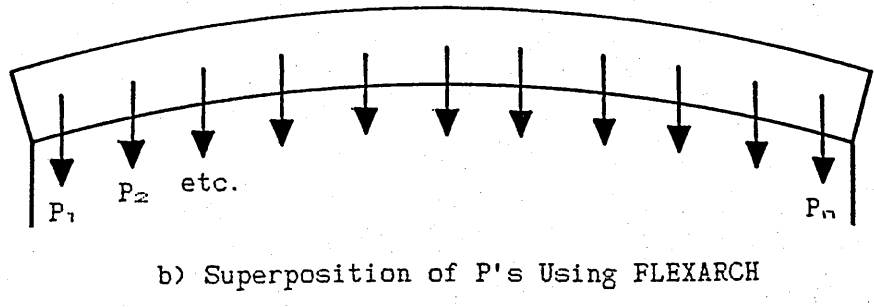
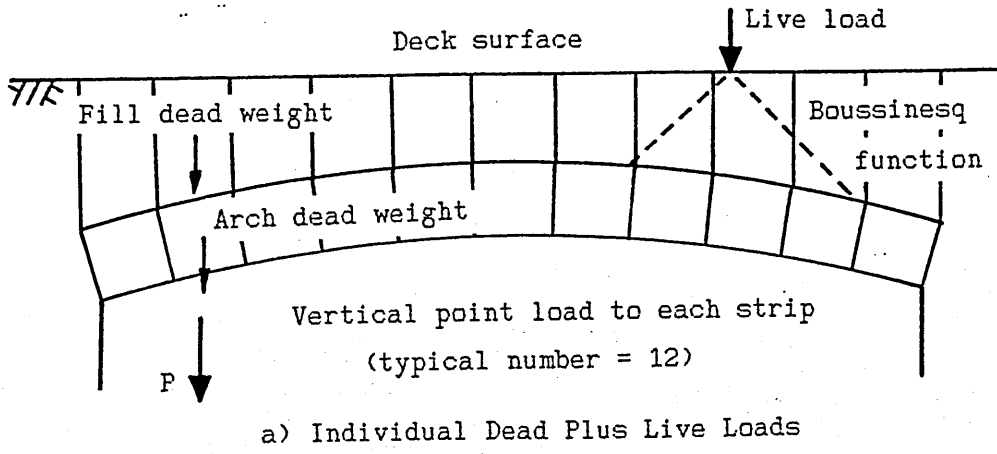


Figure 4.7

FLEXARCH → NIARCH → SERVARCH Development

4. Next to be incorporated was the constitutive theory described in the previous chapter; this was essentially program PSTRESS1 in the role of a subroutine - see equations 3.20 (uncracked section) and 3.44 (cracked section). Live loading was thus to be applied incrementally, after first applying the dead load in a similar incremental manner. At each increment, the thrust, eccentricity and stress-strain state of each element were determined. From the latter, it could be ascertained as to whether that element was uncracked or cracked and to what extent the crack had propagated, if present. This enabled the computation of a new 'I' value for that element based on the depth of section remaining together with a corresponding revised, mean, 'E' value for the same element - see Figure 4.7(d).

In summary, the final stage involved incremental loading, finding the redundancies at each stage, thus determining the thrust line at each stage and consequently the state of stress "in" each element. The revised 'E' and 'I' values were then ascribed to their respective elements to provide a new arch "stiffness" for the next load increment. This cycle would be repeated, with 'E' and 'I' gradually degrading locally until either an element failed completely or, more sensibly, until it was adjudged that an element had become so deeply cracked that it could be regarded as a "hinge" - a somewhat subjective situation, taken herein to occur when the crack depth had propagated through approximately two thirds of the section. The latter was chosen because, given the aforementioned lack of an adequate definition of serviceability, the author had originally considered that a limiting serviceability state might sensibly be based on the

formation of the first mechanical hinge. This final model/computer program was termed SERVARCH. Once a hinge had formed, the structure would, of course, lose a degree of redundancy and the basic analysis, which assumed a triply redundant structure, would no longer remain valid. For this reason the whole process could not be taken to the ultimate limit state; this was not considered to be a problem given the MECHARCH ultimate modelling developed in complement.

To summarise, the whole procedure was thus to take an original segmental arch of known, constant E and I, to apply its dead loading incrementally, then to apply its live loading incrementally (whilst distributing the live load down through the fill), adjusting E and I locally at each stage until finally a hinge was deemed to have developed. The results of this computerised process (called SERVARCH) when applied to a full scale arch bridge test will now be described.

#### 4.8.6 SERVARCH Vs Bridgemill Full-Scale Test

One of the stated objectives of the actual prototype test was to record the formation of cracks during loading. This is one of only very few tests, to the author's knowledge, to specifically set out to measure data of direct relevance to serviceability work. However, as noted earlier, the tension sensor beneath the load failed to work during the test and so the probable earliest indication of cracking was lost!

The input data to SERVARCH is as reported previously in the MECHARCH study. Additional data specific to SERVARCH is:

Number of "elements" = 12

Dead loading: Applied over ten load increments.

Live loading: A single point load (SERVARCH can handle multiple point loading) was applied to the right hand quarter point (see Figure 4.7), 13.717m into the span. This is incremented in approximately 15kN increments (with respect to the one metre strip). A total of 25 increments of this magnitude would take the bridge up to its true collapse load.

It should be noted that SERVARCH is capable of considering a horizontal component of the vertical loads applied to the arch ring. This is done by first computing the vertical load to be applied to each strip, then multiplying this load by a coefficient of earth pressure (K, typical values 0.25 to 4) to obtain a horizontal load to be applied to the same point on the arch. As this aspect of the theory is not particularly well founded, and as the value of K to be adopted should probably vary depending on whether the arch is tending to deflect towards or away from the body of the fill, this feature has not been invoked. Consequently a value of zero is used for K.

The results obtained from SERVARCH were as follows:

After application of the full dead load, over ten increments, the arch ring was found to be still wholly in compression and uncracked. However, some elements were uncomfortably close to tension, rather more so than would have been expected for a supposedly well designed arch. It is to be observed in the Bridgemill report that tension under dead load was in fact predicted by both Crisfield's finite element program and by an elastic analysis carried out by the researchers. The other assessment methods used by the researchers, M.E.X.E., mechanism analysis and model analysis were not able to yield data at all on this point<sup>(3)</sup>.

On applying live load, SERVARCH computed that after application of the first live load increment (15kN) the arch ring was still wholly in compression and sound. On application of the second live load increment it predicted that element 10 (which is approximately under the load) cracks for approximately 6% of its depth. This corresponds to an equivalent load of merely 248kN on the real bridge. On application of the third live load increment, elements 9 and 12 are also predicted to have suffered tensile cracking. The most severely affected element is 12 with cracking through approximately one third of its depth. On application of the fourth live load increment the analysis can be said to have effectively broken down in that elements 3, 4, 5, 6 and 11 are predicted to have "failed" and it would appear that possibly three hinge zones are forming. The load at this point stand at the equivalent of approximately 500kN on the real arch.

Comparison of these findings with the log of emissions<sup>(2)</sup> from the acoustic sensors affixed to Bridgemill is not especially encouraging.

SERVARCH has predicted slight tensile cracking (which would surely be accompanied by noises) under the load point, on the intrados, at about 248kN. Unfortunately, this is the location of the one acoustic sensor that failed to work! Comparison here is therefore not possible.

By the time the load has reached 500kN, SERVARCH is predicting distress under the load, plus distress at, and to the far side of, the crown. The acoustic emission log at around the same load reveals a response from the crown intrados sensor (though slight), and nothing elsewhere - remembering, though, that the crucial load point intrados sensor is still inoperative. The real bridge load has to be increased to around 800kN before anything approaching the situation predicted appears to occur, and even then the emissions are very small compared with the responses obtained later in the full-scale test when substantial cracking occurred.

Accepting that the major theoretical thrust herein is towards ultimate limit state prediction for well established reasons - system variability, lack of understanding of a complex system - and that this is the modern trend in design, then the present serviceability studies are of a lesser importance. However, something has to be done about defining serviceability and this represents an initial attempt to investigate the phenomenon. It is considered too complex a matter to present herein a full treatment, but the foregoing does serve to

illustrate the problems associated with masonry arch bridges. Taking, say, 450kN as the predicted serviceability limit for Bridgemill (in comparison with the hinge zones forming at 500kN noted above), then this represents a load factor of almost 7 on the collapse load. Clearly this seems very high and it is concluded that further work is required in this area.

#### 4.9 SUMMARY

A fundamental study of the constitutive properties of masonry, using the latest parabolic form of modelling for its stress-strain response, has been incorporated into a mechanism-type model. By this means, it has been possible to allow for true compressibility effects, in contrast to established techniques where an infinite compressive strength approximation has needed to be employed<sup>(5,6,7,8)</sup>. The resulting procedure has been computerised and tested against full-scale arch tests, against a comparability study and against a laboratory model test. Against the latter, a very good result has been achieved. In the case of the comparison against the full-scale tests the program yielded somewhat low results, as with other mechanism methods<sup>(9)</sup>. This effect is believed to be due largely to the effect of arch-fill interaction, a complex effect not modelled by the present computer program.

A further limited study has been undertaken with respect to the serviceability limit state. Compared against acoustic emissions and observed cracking in the one full-scale test for which suitable data was available, the analysis suggests that hinge formation may occur very early in the loading regime, although the validity of the analysis has not been well proven. If the analysis were shown to be reliable, it would lead to the postulation that the formation of a first hinge may not be a realistic criterion on which to base permissible service loading for a masonry arch bridge.

## CHAPTER 5

### COMMENTS AND CONCLUSIONS

#### 5.1 PRELIMINARY ASSESSMENT

The continuing abundance and yet inevitable gradual deterioration of the masonry arch bridge components of the national bridge stock, combined with the continuous demands of increasingly heavy traffic loading, clearly constitute a problem bound to grow more severe as time passess. The problem is compounded by the inadequacy of the analytical techniques presently available for these 'rule of thumb' designed structures together with the almost universal absence of as-built drawings and an ignorance of the basic properties of their natural and highly variable constituent materials.

It is widely accepted that the present utilitarean arch assessment tool, MEXE, is over-conservative, particularly so in the case of longer spans. Furthermore, it is not applicable to many real life structures, such as skewed bridges, for example. The consequences of this are that the authority responsible for the safety and maintenance of a particular masonry arch bridge may be forced prematurely to apply weight restrictions or to carry out unnecessary "strengthening" works. Given that there is a need to develop modern techniques aimed at determining the strength of these existing structures when subjected to present day loading, contemporary work in this field has been

primarily directed along two paths - the first being almost entirely due to the work of Professor Heyman<sup>(S.E.7.8)</sup>, his approach assuming infinite compressive strength and deeming failure to occur upon the formation of four mechanistic hinges - and the second being concerned with evaluation of the full load-displacement path history employing finite element analysis<sup>(4.10.11)</sup>. Of the two, "mechanism analysis" has shown the most promise to date, hardly surprising given the highly non-linear behaviour involved.

In making a contribution to work in this field, the author initially undertook a study of masonry bridge stock, work considered to be invaluable. Then a detailed theoretical study of the fundamental engineering properties of masonry was undertaken and the results, apart from being novel and of value in their own right, have been utilised in the remainder of the work. This ultimately enabled a refinement of the mechanism-type analysis to be developed whereby the "infinite compressive strength" assumption was replaced by actual masonry constitutive properties. Computer software (named MECHARCH) was written to carry out the analysis and to arrive at ultimate collapse load predictions. Given the limited data against which to test such predictions, promising results have been obtained.

## 5.2 SECONDARY FACTORS

Contemporary research in this field has been primarily devoted to the prediction of an ultimate collapse load for an arch, whereas in practice it is the service load capacity of the arch that is of relevance to the bridge owner. It is possible that the latter may be determinable from a collapse value by simply factoring down, but at present the magnitude(s) of such a factor is a matter for conjecture.

With this in mind, the author sought to develop an iterative, piecewise linear flexibility analysis, adjustments being made to the arch model during each increment to allow for the attendant degradation of structural stiffness, in order to estimate a serviceability limit state (ie. SERVARCH). This work, drawing upon less data for validation, has produced limited results to-date but serves to demonstrate key features required of such an approach.

With respect to computer analyses in general, it was found that the serviceability software (SERVARCH) stretched the BBC's available memory capacity to the limit and the switching of separate blocks of program in and out of memory became necessary. Additionally, both with SERVARCH and MECHARCH, processing time became extremely extended and in particular the solution of equations in the latter program could often take perhaps thirty minutes. This is to be expected of non-linear algorithms in the micro-computer context with floating

point arithmetic being undertaken by software emulation - mainframes employ specific hardware for the task.

### 5.3 SUGGESTIONS FOR FURTHER WORK

Whilst claiming that the MECHARCH analysis is quite sophisticated in its treatment of true constitutive properties, it remains relatively undeveloped in other areas. Further work should be directed towards generalisation of the applied live loading and extension of the treatment to arches possessing profiles other than segmental. Furthermore, an optimisation routine could be incorporated to establish the mechanistic hinge positions with more accuracy. Another development, though perhaps requiring a programme of study in its own right, would be to incorporate some form of modelling for the aforementioned arch-fill interaction effect.

The above enhancements to MECHARCH would necessitate an improvement in computer power and together with this improved "packaging" of the product would prove beneficial.

At a later stage other arch forms remain to be studied - skewed arches and multispan viaducts, for example. However, before any of this ultimate limit state work becomes of true benefit, a relationship between collapse and serviceability must be established and this is an area offering considerable scope for innovation and research.

## A P P E N D I X 'A'

### SOFTWARE LISTING

An example of the software produced is herein presented for completeness. This program - PSTRESS1 - graphically displays sectional stresses and strains for a specific rectangular section under combined uniaxial compression and flexure. See pages 75, 77 and 78 for typical examples of the output.

```

>L.
10REM PROGRAM PSTRESS1
20:
30REM P. A. MALLINDER. DECEMBER 1986
40:
70REM NOTE - NEWTON & METRE UNITS
80:
90:
100REM----- DATA INPUT
T -----
110:
120@%=&20509:MODEO:CLS
130PRINT"PROGRAM 'PSTRESS1':PRINT
"-----":PRINT:PRINT
140PRINT"To solve a rectangular masonry section.
of parabolic stress-strain law.":PRINT
150PRINT"subject to thrust and uniaxial bending
moment.":PRINT:PRINT:PRINT
160PRINT"MATERIAL PROPERTIES:":PRINT:INPUT"Sigma
max. (N/mm2 units, typical value 16 N/mm2) ".SIGm
:SIGm=SIGm*1E6:REM CONVERT TO N/m2 UNITS
170PRINT:INPUT"E max. (typical value 0.0024) ";E
m
180PRINT:PRINT:PRINT"SECTION DIMENSIONS:":PRINT:
INPUT"Section depth (metres) ".d
190PRINT:PRINT"(unit metre strip assumed)":PRINT
:b=1:REM UNIT METRE STRIP ASSUMED
200PRINT:PRINT"LOADING:":PRINT
210INPUT"Axial thrust (kN units) ".P:P=P*1000:RE
M CONVERT TO NEWTONS
220PRINT:INPUT"Bending moment (kNm units) ".M:M=
M*1000:REM CONVERT TO NEWTON METRES
230CLS
240:
250PROCaxisdraw
260:
270REM----- UNCRACKED ANAL
YSIS -----
280:
290REM PLOTTING POLYNOMIAL
300:
310I=0
320FOR E2=-1.5*Em TO 1.5*Em STEP 3*Em/50
330I=I+1
340X=(2*(E2/Em)^2-5*E2/Em+3*P/SIGm/b/d-12*M/SIGm
/b/(d^2))/(1-E2/Em)
350ANSWER=SIGm*b*d^2/6*(-.5*X^2+X-E2/Em+.5*(E2/E
m)^2)-M
360PRINT TAB(20.4); "E2=";E2; " E1=";X*Em; " poly.=
";ANSWER; "
370IF500+ANSWER/1000>1200 OR500+ANSWER/1000<-120

```

```

O GOTO390
380DRAW I/52*1200.500+ANSWER/1000
390NEXT E2
400:
410REM P L O T T I N G E 2
420:
430VDU5
440MOVE0.500
450I=0
460FOR E2=-1.5*Em TO 1.5*Em STEP 3*Em/50
470I=I+1
480X=(2*(E2/Em)^2-5*E2/Em+3*P/SIGm/b/d-12*M/SIGm
/b/(d^2))/(1-E2/Em)
490ANSWER=SIGm*b*d^2/6*(-.5*X^2+X-E2/Em+.5*(E2/E
m)^2)-M
500DRAW I/52*1200.500+E2/(1.5*Em)*500
510NEXT E2
520:
530:
540REM P L O T T I N G E 1
550:
560MOVE0.500
570I=0
580FOR E2=-1.5*Em TO 1.5*Em STEP 3*Em/50
590I=I+1
600X=(2*(E2/Em)^2-5*E2/Em+3*P/SIGm/b/d-12*M/SIGm
/b/(d^2))/(1-E2/Em)
610E1=X*Em
620IF500+E1/(1.5*Em)*500 >1200 OR500+E1/(1.5*Em)
*500 <-1200 GOTO640
630DRAW I/52*1200.500+E1/(1.5*Em)*500
640NEXT E2
650VDU4
660:
670:
680REM S O L V E F O R U N C R A C K E D S
E C T I O N
690:
700IFP>0THEN720
710CLS:PRINT"SECTION IN TENSION!":STOP
720E2=1.5*Em+0.00010001:STIP=Em/24
730X=(2*(E2/Em)^2-5*E2/Em+3*P/SIGm/b/d-12*M/SIGm
/b/(d^2))/(1-E2/Em)
740RLAST=SIGm*b*d^2/6*(-.5*X^2+X-E2/Em+.5*(E2/Em
)^2)-M
750E2=E2-STIP:IF E2>-0.0024 GOTO770
760FORDD=1TO3000:NEXT:CLS:PRINT"NO SOLUTION FOUN
D - SECTION BEYOND SQUASH LOAD OR PLASTIC MOMENT":
STOP
770MOVE E2/(1.5*Em)*600+600.400
780DRAW E2/(1.5*Em)*600+600.600
790X=(2*(E2/Em)^2-5*E2/Em+3*P/SIGm/b/d-12*M/SIGm
/b/(d^2))/(1-E2/Em)
800RNOW=SIGm*b*d^2/6*(-.5*X^2+X-E2/Em+.5*(E2/Em)
^2)-M
810IF ABS(RNOW)<10 GOTO850
820IF SGN(RLAST)=SGN(RNOW) GOTO840
830STIP=-STIP/2

```

```

840RLAST=RNOW:GOTO750
850E1=X*Em
860PRINTTAB(10.5);"*** Solution: E1=";E1;" E2=";
E2;" , at poly.=";X;" ***
870PRINT"CHECK:
880KK=SIGm*b*d*(-1/3*(E1/Em)^2+E1/Em-1/3*(E1*E2/
Em^2)+E2/Em-1/3*(E2/Em)^2)
890PRINT"COMPUTED P=";KK/1000;" kN"
900JJ=SIGm*b*d^2/6*(-1/2*(E1/Em)^2+E1/Em-E2/Em+1
/2*(E2/Em)^2)
910PRINT"COMPUTED M=";JJ/1000;" kNm"
920IF ABS(KK-P)<ABS(5/100*P) AND (ABS(JJ-M)<ABS(
5/100*M) OR ABS(JJ-M)<50) THEN 940:REM CHECK THAT
CORRECT P & M FOUND TO WITHIN 5% OR .05 kNm
930PRINT"COMPUTED P AND M NOT CORRECT":VDU4:STOP
940PROCcopy
950:
960:
970REM D R A W   S T R E S S   &   S T R A I N   D I
A G S.
980:
990CLS:VDU5
1000MOVE0.950:PLOT21,1279,950
1010MOVE0.400:PLOT21,1279,400
1020MOVE300.400:DRAW300,950
1030MOVE900.400:DRAW900,950
1040MOVE220.300:PRINT"S T R E S S"
1050MOVE830.300:PRINT"S T R A I N"
1060MOVE280.50:PRINT"*** U N C R A C K E D   A N A
L Y S I S ***"
1070MOVE900.950:DRAW 900+E1*150000.950:DRAW 900+E
2*150000.400:DRAW900.400
1080MOVE820.990:PRINTE1
1090MOVE820.390:PRINTE2
1100MOVE300,950
1110FORI=0TO10
1120J=E1-(1/10)*(E1-E2)
1130J=SIGm*(2*J/Em-(J/Em)^2)/1E6:REM STRESS IN N/
mm^2
1140DRAW J*20+300,950-1/10*550
1150NEXTI
1160DRAW300,400
1170MOVE220,990:PRINT SIGm*(2*E1/Em-(E1/Em)^2)/1E
6;" N/sq.mm"
1180MOVE220,390:PRINT SIGm*(2*E2/Em-(E2/Em)^2)/1E
6;" N/sq.mm"
1190:
1200REM F I N D   M E A N   'E'
1210K=0
1220FORI=0TO10
1230J=ABS(E1-(1/10)*(E1-E2)):REM STRAIN
1240K=K+SIGm*(2*J/Em-(J/Em)^2)/J:REM STRESS/STRAI
N = E
1250NEXTI
1260Elocal=K/11:REM MEAN 'E'
1270MOVE300,200:PRINT"Averaged local 'E' = ";Eloc

```

```

al: " N/sq.m"
1280MOVE0.30
1290PROCcopy
1300:
1310REM  D E C I D E  I F  C R A C K E D  A N A
L Y S I S  R E Q D.
1320:
1330IF E1<0 OR E2<0 THEN 1380
1340VDU4:CLS:STOP
1350:
1360REM----- C R A C K E D  A N A L
Y S I S -----
1370:
1380CLS:J=SGN(M):M=ABS(M)
1390PROCaxisdraw
1400I=0
1410FOR E1=-1.5*Em TO 1.5*Em+3*Em/50 STEP 3*Em/50
+1E-9
1420I=I+1
1430dd=3*P/(SIGm*b*(3*E1/Em-(E1/Em)^2))
1440ANSWER=4*SIGm*b*P*(M/P-(d-dd)/2)*(3*E1/Em-(E1
/Em)^2)^2-3*P^2*(2*E1/Em-(E1/Em)^2)
1450IF500+ANSWER/1E10>1200 OR 500+ANSWER/1E10<-12
00 GOTO1480
1460DRAW I/52*1200.500+ANSWER/1E10
1470PRINT TAB(20,4);" E1=";E1;" d'=";dd;"m, poly.
=";ANSWER:"
1480NEXT E1
1490:
1500REM  P L O T T I N G  E 1
1510:
1520MOVE0.500
1530I=0
1540FOR E1=-1.5*Em TO 1.5*Em STEP 3*Em/50
1550I=I+1
1560DRAW I/52*1200.500+E1/(1.5*Em)*500
1570NEXT E1
1580:
1590REM  S O L V E  F O R  C R A C K E D  S E C
T I O N
1600:
1610E1=0.0000001:STIP=Em/24:REM J=SGN(M):M=ABS(M)
<- NEED IN PSTRESS2
1620dd=3*P/(SIGm*b*(3*E1/Em-(E1/Em)^2))
1630RLAST=4*SIGm*b*P*(M/P-(d-dd)/2)*(3*E1/Em-(E1/
Em)^2)^2-3*P^2*(2*E1/Em-(E1/Em)^2)
1640E1=E1+STIP:IF E1<1.5*Em GOTO1660
1650VDU4:CLS:PRINT"NO SOLUTION FOUND - SECTION BE
YOND SQUASH LOAD OR PLASTIC MOMENT":STOP
1660MOVE E1/(1.5*Em)*600+600.400
1670DRAW E1/(1.5*Em)*600+600.600
1680dd=3*P/(SIGm*b*(3*E1/Em-(E1/Em)^2))
1690RNOW=4*SIGm*b*P*(M/P-(d-dd)/2)*(3*E1/Em-(E1/E
m)^2)^2-3*P^2*(2*E1/Em-(E1/Em)^2)
1700IF ABS(RNOW)<1E5 GOTO1740
1710IF SGN(RLAST)=SGN(RNOW) GOTO1730

```

```

1720STIP=-STIP/2
1730RLAST=RNOW:GOTO1640
1740VDU4
1750dd=3*P/(SIGm*b*(3*E1/Em-(E1/Em)^2))
1760PRINTTAB(10,5);"*** Solution: d'=";dd;" E1=";
E1;" at poly.=";RNOW;" ***
1770PRINT"Check: "
1780PRINT"Computed P=";SIGm*b*dd/3*(3*E1/Em-(E1/E
m)^2)/1000;" kN"
1790XX=SIGm*b*dd^2/12*(2*E1/Em-(E1/Em)^2)
1800PRINT"Computed M'=";XX/1000;" kNm"
1810PRINT"Giving a computed M =";(XX/P+(d-dd)/2)*
P/1000*SGN(J);" kNm"
1820PROCcopy
1830:
1840REM D R A W   S T R E S S   &   S T R A I N   D I
A G S.
1850:
1860CLS:VDU5
1870MOVE0.950:PLOT21,1279,950
1880MOVE0.400:PLOT21,1279,400
1890MOVE300,400:DRAW300,950
1900MOVE900,400:DRAW900,950
1910MOVE220,300:PRINT"S T R E S S"
1920MOVE830,300:PRINT"S T R A I N"
1930MOVE280,50:PRINT"*** C R A C K E D   A N A L Y
S I S ***"
1940MOVE900,950:DRAW 900+E1*100000,950:DRAW 900,9
50-dd/d*550:DRAW900,400
1950MOVE820,990:PRINTE1
1960MOVE770,370:PRINT"Crack depth = ";d-dd;" m"
1970MOVE300,950
1980FORI=0T010
1990J=E1-(I/10)*E1
2000J=SIGm*(2*J/Em-(J/Em)^2)/1E6:REM STRESS IN N/
mm^2
2010DRAW J*20+300,950-I/10*dd/d*550
2020NEXTI
2030DRAW300,400
2040MOVE220,990:PRINT SIGm*(2*E1/Em-(E1/Em)^2)/1E
6;" N/sq.mm"
2050:
2060REM F I N D   M E A N   'E'
2070:
2080K=0
2090FORI=0T09
2100J=ABS(E1-(I/10)*E1):REM STRAIN
2110K=K+SIGm*(2*J/Em-(J/Em)^2)/J:REM STRESS/STRAI
N = E
2120NEXTI
2130Elocal=K/10:REM MEAN 'E'
2140MOVE300,200:PRINT"Averaged local 'E' = ";Eloc
al;" N/sq.m"
2150Ilocal=b*dd^3/12:REM LOCAL 'I'
2160MOVE300,150:PRINT"Local 'I' = ";Ilocal;" m4"
2170MOVE300,100:PRINT"ALL MOMENTS ASSUMED +VE"
2180MOVE0,30

```

```

2190PROCcopy
2200:
2210VDU4:CLS:PRINT"PROGRAM FINISHED
":STOP
2220:
2230REM  HARD COPY SUBROUTINE
2240:
2250DEFPROCcopy
2260INPUT"C FOR COPY",A#
2270IFA#="C"THEN2290
2280ENDPROC
2290*FX5.1
2300*FX6.0
2310VDU2
2320*GDUMP1,1,3,1.0
2330VDU3
2340ENDPROC
2350:
2360REM  SUBROUTINE TO DRAW AXE
S Et C.
2370:
2380DEFPROCaxisdraw
2390MOVE0.500
2400DRAW1200.500
2410VDU5
2420I=0
2430FOR E2=-1.5*Em TO 1.5*Em STEP 1.5*Em/6
2440I=I+1
2450MOVE I/6*1200.505
2460DRAW I/6*1200.495
2470MOVE0.500+E2/(1.5*Em)*500
2480PRINTE2
2490MOVE150.500+E2/(1.5*Em)*500
2500DRAW1200.500+E2/(1.5*Em)*500
2510NEXT E2
2520VDU4
2530@%=&20109:PRINT"  Axial force = ";P;" Newton
s. Bending moment = ";M;" Newton metres  ":PRINT
"  *****
*****":@%=&20509
2540MOVE0.0
2550ENDPROC

```

## DISCUSSION ON TECHNICAL NOTE 381

### On the stiffness properties of masonry

F. Sawko and M. A. Rouf

Dr N. W. Taylor, Sheffield City Polytechnic, Mr. P. A. Mallinder and Mr. B. L. Davies, South Yorkshire County Council

The Authors have presented an interesting study with regard to the analysis of masonry materials subject to axial loading in the presence of bending moment. The following points are, perhaps, worthy of consideration.

36. Do the discrete points denoted on the curves in Fig. 1 relate to actual experimental readings or to curve fitting empiricism? The peak stress values given do not concur with stress ordinate values.

37. It would be interesting to receive the Authors' comments regarding the nature of the stress-strain curves equivalent to those of Fig. 1 for natural stone types. This bears directly on the study of masonry arches constructed of stone, a common structural form.

38. The adoption of a parabolic stress-strain distribution negates the well established middle third rule. Surely this is to be noted. Indeed, employing an approach equivalent to that given in the Technical Note, it can be shown that the eccentricity  $e$  at which a compressive load will cause the onset of cracking is given by

$$e = f(T)/6$$

where  $T$  is the depth of the section and  $f$  is a parabolic factor of the form

$$f = 6 - 3(\epsilon_1/\epsilon_m)/6 - 2(\epsilon_1/\epsilon_m)$$

where  $\epsilon_1$  and  $\epsilon_m$  are as defined by the Authors. This expression has been programmed on a micro-computer and the corresponding graphical output is depicted in Fig. 12. Clearly, care must be taken in its interpretation at high strain ratios.

#### Professor Sawko and Mr Rouf

In reply to the specific points raised by the contributors, the Authors would like to make the following comments.

40. The empirical curves in Fig. 1 are based on mean curves obtained from twenty-six pillar tests carried out by Powel and Hodgkinson at the laboratories of the British Ceramic Research Association at Stoke-on-Trent. The individual curves are presented as Figs 3-6 in reference 1. The peak stress values used by the Authors are numerically approximate; more accurate values are 27.4, 19.2 and 9.3 for the three brickwork types considered.

41. In the opinion of the Authors, stress-strain curves for natural stone and also for concrete blockwork are certainly comparable to those in Fig. 1, and would, therefore, be applicable to stone masonry arches.

## DISCUSSION

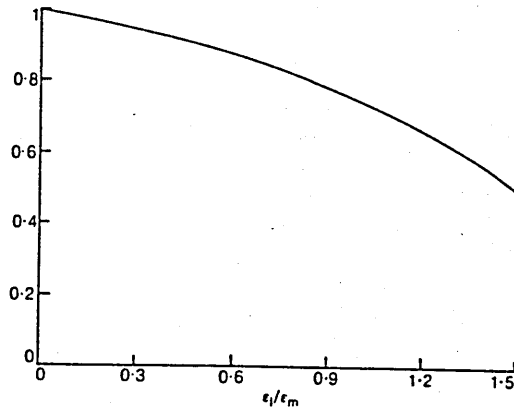


Fig. 12. Middle third factor

42. The adoption of the parabolic stress-strain law does indeed negate many well-known concepts derived on the basis of linear elasticity, such as the middle third rule and the parabolic shear stress distribution in masonry sections. The expressions for  $f$  quoted by the contributors are derived from the zero tension criterion. At the onset of cracking the strain distribution in a section is as shown in Fig. 13.

43. From simple geometry, centroidal strain  $\epsilon_c = \epsilon_1/2$  and curvature  $C = \epsilon_1/T$ . Substituting these expressions into equations (24) and (25), the corresponding expressions for axial force and bending moment at the onset of cracking are

$$P = \frac{E_0 A_0 \epsilon_m}{2} \left( \frac{\epsilon_1}{\epsilon_m} - \frac{\epsilon_1^2}{3\epsilon_m} \right)$$

$$M = \frac{E_0 I_0 \epsilon_m}{2T} \left( 2 \frac{\epsilon_1}{\epsilon_m} - \frac{\epsilon_1^2}{\epsilon_m^2} \right)$$

Thus the eccentricity at the onset of cracking is

$$e = \frac{M}{P} = \left[ \frac{6 - 3(\epsilon_1/\epsilon_m)}{6 - 2(\epsilon_1/\epsilon_m)} \right] \left( \frac{T}{6} \right)$$

where the expression in square brackets is the contributors' value of  $f$ .

44. The Authors are grateful to the contributors for pointing out the practical significance of this result.

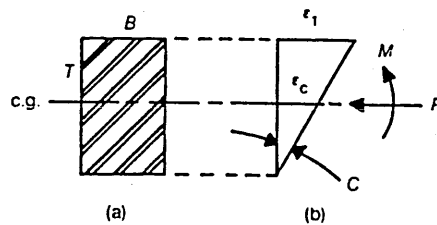


Fig. 13. Strain distribution at the onset of cracking: (a) section; (b) strain

## On the limit state properties of masonry

N. TAYLOR, BTech, MSc, PhD\*

P.A. MALLINDER, BEng, MICE†

An axial force/bending moment interaction diagram for the limit state of rectangular masonry sections is presented. The strain distribution across the section is taken to be linear, and the stress-strain relationship for the material is assumed to be parabolic. Tensile strength is taken to be insignificant in comparison with the compressive strength. The interaction curve generated represents the limit state configurations of axial thrust and bending moment; this curve is discussed in the context of masonry design to BS5628 Part 1.

### Notation

$b$	breadth of section
$d$	depth of section
$d'$	effective depth of cracked section
$e$	eccentricity, $e _{zz} = 0$
$m$	non-dimensional bending moment parameter, $m = M_m/M_s$
$M$	bending moment
$M_m$	limit state bending moment
$M_s$	maximum limit state bending moment
$M_t$	tensile component of bending moment
$n$	non-dimensional axial compression parameter, $n = P_m/P_s$
$P$	axial compression
$P_m$	limit state axial compression
$P_s$	squash load
$y$	sectional spatial co-ordinate, $y _{zz} = 0$
$y_m$	distance from centroid to fibres suffering maximum stress
$zz$	flexural axis
$\epsilon$	compressive strain
$\epsilon_m$	compressive strain accompanying maximum compressive stress
$\epsilon_{om}$	centroidal strain at limit state
$\epsilon_1$	top fibre strain
$\epsilon_2$	bottom fibre strain
$v_m$	curvature at limit state
$\sigma$	compressive stress
$\sigma_m$	maximum compressive stress
$\sigma_1$	top fibre stress
$\sigma_2$	bottom fibre stress

### Introduction

Developments in the use of masonry in new structural forms<sup>1,2</sup> and concern with the safe-load assessment of existing and often elderly structures such as the vous-

---

Written discussion closes 15 May 1987; for further details see p. ii.

\* Senior Lecturer, Department of Civil Engineering, Sheffield City Polytechnic.

† Assistant Structural Engineer, Sheffield Metropolitan City Council.

## TAYLOR AND MALLINDER

soir arch<sup>3,4</sup> have led to considerable research on the structural behaviour of masonry. Recent studies have included investigation into the fundamental properties of structural masonry.<sup>5-8</sup> This has resulted in the adoption of a parabolic stress-strain relationship acting in conjunction with a linear strain distribution across a rectangular masonry section subject to a singly-eccentric compressive normal load.

2. Employing equations relating sectional strain response to any specified loading combination of axial thrust and bending moment so established,<sup>8</sup> the respective limit state combinations can be derived for both cracked and uncracked sectional topologies; tensile strength is considered to be negligible in the context of limit state configurations.

### Non-linear theory

3. An idealized parabolic stress-strain locus is shown in Fig. 1. The relationship is of the form

$$\sigma/\sigma_m = 2\varepsilon/\varepsilon_m - (\varepsilon/\varepsilon_m)^2 \quad (1)$$

where  $\sigma$  and  $\varepsilon$  are the general stress and strain parameters,  $\sigma_m$  is the maximum stress, and  $\varepsilon_m$  is the corresponding strain.

4. A masonry section subject to a compressive normal force  $P$  acting at an eccentricity  $e$  is shown in Fig. 2(a); the corresponding uncracked strain distribution is shown in Fig. 2(b). Incorporation of equation (1) gives the stress distribution shown Fig. 2(c). The equivalent cracked section configurations are given in Fig. 3. Stresses  $\sigma_m$  are present at the limit state (see below). However, the general stress responses of Figs 2(c) and 3(c), noting equation (1), are given by

$$\frac{\sigma}{\sigma_m} = \left[ \left( \frac{\varepsilon_1 + \varepsilon_2}{2\varepsilon_m} \right) + \frac{y}{d} \left( \frac{\varepsilon_1 - \varepsilon_2}{\varepsilon_m} \right) \right] \left\{ 2 - \left[ \left( \frac{\varepsilon_1 + \varepsilon_2}{2\varepsilon_m} \right) + \frac{y}{d} \left( \frac{\varepsilon_1 - \varepsilon_2}{\varepsilon_m} \right) \right] \right\} \quad (2)$$

for the uncracked case, with  $\varepsilon_2 \geq 0$  ( $\varepsilon_2 \leq \varepsilon_1 \leq 1.5\varepsilon_m$ ), and by

$$\frac{\sigma}{\sigma_m} = \frac{\varepsilon_1}{\varepsilon_m} \left( 1 + \frac{y}{d} - \frac{d}{2d'} \right) \left\{ 2 - \left[ \frac{\varepsilon_1}{\varepsilon_m} \left( 1 + \frac{y}{d} - \frac{d}{2d'} \right) \right] \right\} \quad (3)$$

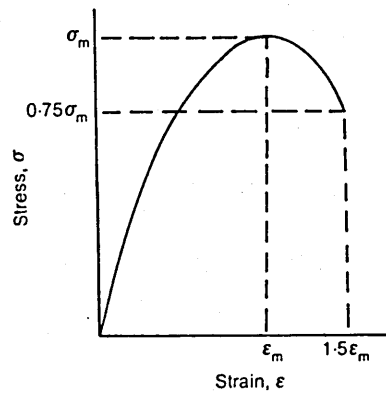


Fig. 1. Idealized stress-strain locus for masonry (compression)

LIMIT STATE PROPERTIES OF MASONRY

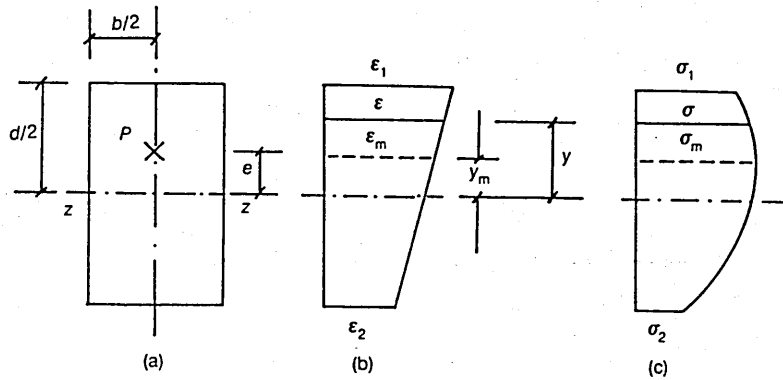


Fig. 2. General strain and stress distributions in an uncracked section: (a) section; (b) strain; (c) stress

for the cracked case, with  $\epsilon_1 \leq 1.5\epsilon_m$  ( $0 \leq d' \leq d$ ).  $d$  denotes the full depth of the section,  $d'$  denotes the effective depth in the cracked case,  $y$  is the sectional spatial co-ordinate, and  $\epsilon_1$  and  $\epsilon_2$  represent the extreme fibre strains.

5. Interpreting the eccentric loading  $P$  as being statically equivalent to an axial thrust  $P$  and a bending moment  $M$  acting about the flexural ( $zz$ ) axis (i.e.  $M = Pe$ ), then for the uncracked configuration, integration across the section, incorporating equation (2), gives

$$P = \int_{-d/2}^{d/2} \sigma b \, dy = \sigma_m b d \left( \frac{(\epsilon_1 + \epsilon_2)(3\epsilon_m - \epsilon_1 - \epsilon_2) + \epsilon_1 \epsilon_2}{3\epsilon_m^2} \right) \quad (4)$$

(where  $b$  is the breadth of the section), and

$$M = \int_{-d/2}^{d/2} \sigma b y \, dy = \sigma_m b d^2 \left( \frac{(\epsilon_2 - \epsilon_1)(\epsilon_1 + \epsilon_2 - 2\epsilon_m)/2}{6\epsilon_m^2} \right) \quad (5)$$

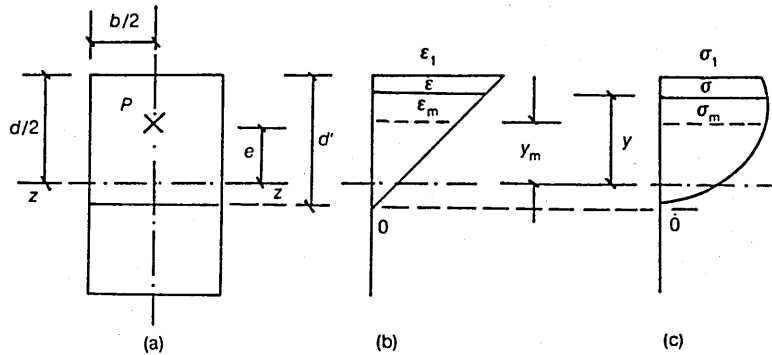


Fig. 3. General strain and stress distributions in a cracked section: (a) section; (b) strain; (c) stress

TAYLOR AND MALLINDER

Similarly, for the cracked configuration, noting equation (3)

$$P = \int_{d/2-d'}^{d/2} \sigma b \, dy = \sigma_m b d' \left( \frac{\varepsilon_1 \varepsilon_m - \varepsilon_1^2/3}{\varepsilon_m^2} \right) \quad (6)$$

and

$$M = \int_{d/2-d'}^{d/2} \sigma b y \, dy = \sigma_m b d' \left( \frac{\varepsilon_1 (6\varepsilon_m d - 2\varepsilon_1 d + \varepsilon_1 d' - 4\varepsilon_m d')}{12\varepsilon_m^2} \right) \quad (7)$$

Sagging bending moments ( $0 \leq e \leq d/2$ ) will be considered first.

**Limit state configuration: uncracked section**

6. The limit state is determined by obtaining the maximum force  $P_m$  that the section can withstand at any given value of bending moment  $M$ . This is achieved by employing  $\partial P/\partial \varepsilon_1 = 0$  in conjunction with prescribed values of  $M(\varepsilon_2)$  with respect to equations (4) and (5). Differentiating equation (4) accordingly generates the limiting condition

$$\varepsilon_1 = (3\varepsilon_m - \varepsilon_2)/2 \quad (8)$$

recalling  $\varepsilon_1 \leq 1.5\varepsilon_m$ ,  $\varepsilon_2 \geq 0$ . The appropriate expressions for  $P_m$  and the corresponding limit state bending moment  $M \equiv M_m$  are obtained by back-substituting equation (8) into equations (4) and (5):

$$P_m = \frac{\sigma_m b d}{4} [3 + 2(\varepsilon_2/\varepsilon_m) - (\varepsilon_2/\varepsilon_m)^2] \quad (9)$$

and

$$M_m = \frac{\sigma_m b d^2}{16} [1 - 2(\varepsilon_2/\varepsilon_m) + (\varepsilon_2/\varepsilon_m)^2] \quad (10)$$

Equations (9) and (10) thus give the requisite limit state interaction locus, subject to the delineation of the range of validity of the uncracked case studies.

7. Intuition demands that the squash load  $P_s$  represents an upper bound on  $P_m$ , with

$$P_m \Big|_{M_m=0} \equiv P_s = \sigma_m b d \quad (11)$$

wherein, noting Fig. 2(c), a uniform axial stress distribution  $\sigma_1 = \sigma_2 = \sigma_m$  acts across the entire section. Equation (11) can also be obtained using  $\partial P_m/\partial \varepsilon_2 = 0$  with respect to equation (9), such that

$$\varepsilon_2 \Big|_{P_m=P_s} = \varepsilon_m \quad (12)$$

which gives equation (11) on back-substitution into equations (9) and (10). The lower bound value for  $P_m$  with respect to the uncracked section studies is obtained by setting  $\varepsilon_2 = 0$ . At this state, equation (8) gives  $\varepsilon_1 = 3\varepsilon_m/2$ , which accords with the limiting permissible extreme fibre strain. Furthermore, substitution into equa-

## LIMIT STATE PROPERTIES OF MASONRY

tion (9) identifies the lower bound of  $P_m$  to be  $P_m = 0.75\sigma_m bd$ , at which state equation (10) gives  $M_m = \sigma_m bd^2/16$ . Introducing the non-dimensional parameter  $n = P_m/P_s$ , then equations (9) and (10) afford the limit state locus for the section in the range  $0.75 \leq n \leq 1$ .

8. Finally, it is instructive to determine the position,  $y_m$ , at which the maximum stress,  $\sigma_m$ , occurs under limit state conditions. This can be achieved employing the geometry of the corresponding strain distribution, with  $\varepsilon_1$  in Fig. 2(b) being defined by equation (8), such that

$$y \Big|_{\sigma_m} = y \Big|_{\varepsilon_m} = y_m = d/6 \quad (13)$$

for  $0.75 \leq n < 1$ . That is, at the limit state the most highly stressed fibres occur at  $d/6$  above the centroidal axis, while the most highly strained fibres occur at the top of the section (note Fig. 2(c)). This separation of maximum effects relates directly to the presence of the falling branch in the stress-strain curve given in Fig. 1. For completeness, the centroidal strain  $\varepsilon_{om}$  and the sectional curvature  $v_m$  corresponding to the uncracked limit state configuration can also be obtained from Fig. 2(b),  $\varepsilon_1$  being as defined in equation (8)

$$\varepsilon_{om} = (\varepsilon_1 + \varepsilon_2)/2 = (3\varepsilon_m + \varepsilon_2)/4 \quad (14)$$

$$v_m = (\varepsilon_1 - \varepsilon_2)/d = 3(\varepsilon_m - \varepsilon_2)/(2d) \quad (15)$$

### Limit state configuration: cracked section

9. The approach used to determine the limit state locus for  $0 \leq n \leq 0.75$  is similar to that employed in the previous section. Employing the limiting criterion  $\partial P/\partial \varepsilon_1 = 0$  in conjunction with prescribed values of  $M(d')$  with respect to equations (6) and (7) gives the explicit limiting condition  $\varepsilon_1 = 1.5 \varepsilon_m$ , which when back-substituted into equations (6) and (7) gives

$$P_m = 3\sigma_m bd'/4 \quad (16)$$

and

$$M_m = \sigma_m bd'(6d - 5d')/16 \quad (17)$$

respectively. These expressions define the limit state interaction locus for  $0 \leq n \leq 0.75$ ; they interface with equations (9) and (10) at  $n = 0.75$  ( $d' = d$ ), with a lower bound at  $n = 0$  ( $d' = 0$ ), whereupon equations (16) and (17) afford  $n = P_m = d' = M_m = 0$ .

10. Intuition suggests that a turning point is present in the interaction locus  $0 \leq n \leq 0.75$ . Employing

$$\frac{\partial M_m}{\partial P_m} = \frac{\partial M_m}{\partial d'} \cdot \frac{\partial d'}{\partial P_m} = 0 \quad (18)$$

then, from equations (16) and (17),

$$d' \Big|_{\partial M_m/\partial P_m = 0} = 3d/5 \quad (19)$$

with a maximum turning point at  $n = 0.45$ . The absolute maximum bending moment the section can resist,  $M_s$ , is therefore, from equation (17)

$$M_m \Big|_{n=0.45} \equiv M_s = 9\sigma_m bd^2/80 \quad (20)$$

11. Employing the geometry of Fig. 3(b) with  $\epsilon_1 = 1.5 \epsilon_m$  gives the location of the fibres undergoing maximum stress, with

$$y \Big|_{\sigma_m} = y \Big|_{\epsilon_m} = y_m = (3d - 2d')/6 \quad (21)$$

which interfaces with equation (13) at  $n = 0.75$ . As the tension crack develops, the location of these fibres moves towards the top of the section (Fig. 3(c)). Again employing Fig. 3(b) with  $\epsilon_1 = 1.5 \epsilon_m$ , the centroidal strain  $\epsilon_{om}$  and the sectional curvature  $v_m$  corresponding to the cracked limit state configuration take the form

$$\epsilon_{om} = 0.75\epsilon_m(2d' - d)/d' \quad (d/2 \leq d' \leq d) \quad (22)$$

$$v_m = 3\epsilon_m/(2d') \quad (23)$$

both interfacing with equations (14) and (15) at  $n = 0.75$ .

#### Axial force/bending moment interaction diagram

12. Noting the identities of equations (11) and (20), and introducing the non-dimensional parameter  $m = M_m/M_s$ , then the interaction diagram can be conveniently presented in  $n$ - $m$  space. For this purpose, equations (9), (10), (16) and (17) are written in the form

$$n = [3 + 2(\epsilon_2/\epsilon_m) - (\epsilon_2/\epsilon_m)^2]/4 \quad (24)$$

$$m = 5[1 - 2(\epsilon_2/\epsilon_m) + (\epsilon_2/\epsilon_m)^2]/9 \quad (25)$$

$$n = 0.75(d'/d) \quad (26)$$

and

$$m = 5[d'(6d - 5d')/d^2]/9 \quad (27)$$

respectively. The interaction diagram (Fig. 4) can thus be constructed for  $0 \leq e \leq d/2$  using equations (24) and (25) for  $0.75 \leq n \leq 1$  and equations (26) and (27) for  $0 \leq n \leq 0.75$ . These equations are in parametric form, and are most conveniently evaluated in increments of  $\epsilon_2$  and  $d'$  respectively. For  $-d/2 \leq e \leq 0$  (hogging moment) the interaction diagram is simply a mirror image of Fig. 4 about the abscissa.

13. As the axial compression reduces from  $P_s$  to  $0.75 P_s$ , the falling branch effect is immediately realized as maximum strains in excess of  $\epsilon_m$  (see Fig. 1) are experienced ( $\epsilon_m < \epsilon_1 \leq 3\epsilon_m/2$ ). The maximum stress occurs at the 'middle third'. These two effects are intimately connected with a degradation in the minimum compressive strain  $\epsilon_2$ . Compressive stress response is thereby critical for  $0.75 \leq n \leq 1$ . Details of the interface state (0.75, 0.55) are given in Fig. 5. All parameters interface smoothly. Maximum compressive strain now becomes crucial, with  $\epsilon_1 = 3\epsilon_m/2$  as  $n$  decreases. Flexural resistance increases up to a maximum at (0.45, 1), whereupon crack propagation becomes crucial, resulting in a degradation of sectional strength. Fig. 6 shows a detail of the maximum flexural

### LIMIT STATE PROPERTIES OF MASONRY

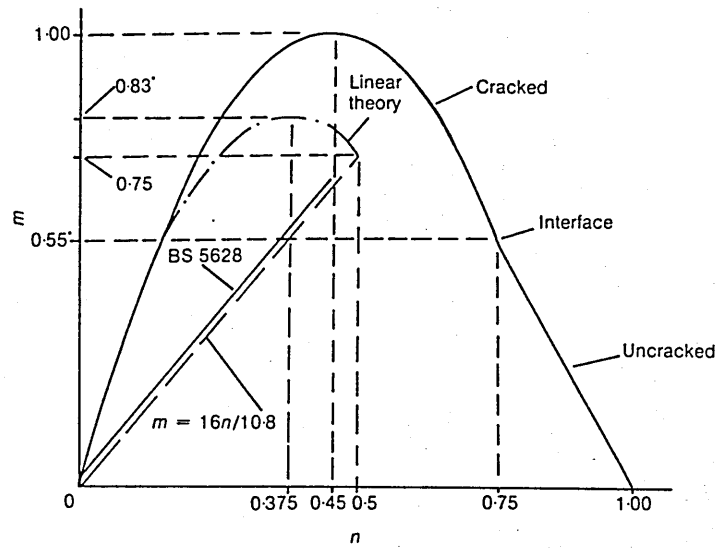


Fig. 4. Limit state masonry moment-thrust interaction diagram

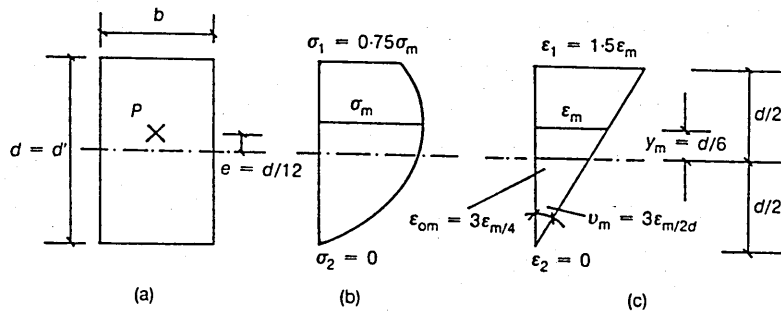


Fig. 5. Stress-strain states at  $n = 0.75$

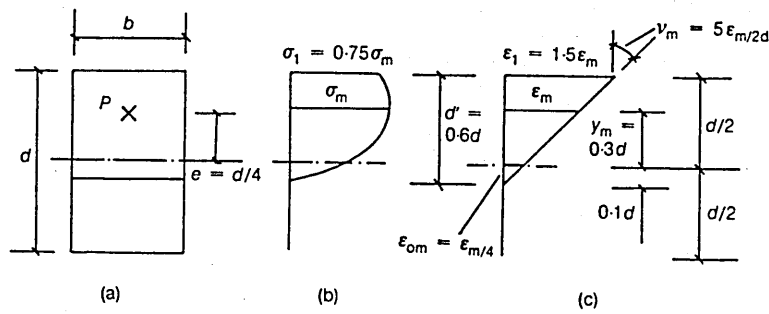


Fig. 6 Stress-strain states at  $n = 0.45$

## TAYLOR AND MALLINDER

response state; the tension crack extends to 40% of the section depth at this state. The movement of the location of the fibres undergoing maximum compressive stress  $\sigma_m$  as  $n$  decreases from 0.75 can be seen by comparing Figs 5 and 6. The extreme fibre compressive stress remains unaltered throughout  $0 < n \leq 0.75$  at  $\sigma_1 = 0.75 \sigma_m$ . Curvature  $v_m$  increases throughout as  $n$  decreases from unity, while crack depth  $d - d'$  increases as  $n$  decreases from 0.75. Centroidal strain  $\epsilon_{om}$  decreases from  $\epsilon_m$  at  $n = 1$  to zero at  $n = 0.375$ ; this lower limit is readily determined from equations (16) and (22) with cracking reaching up to the centroidal axis. The (0, 0) state is effectively trivial; it is predictable, since zero tensile strength has been assumed.

### Design considerations

14. The relationship between axial compression and moment of resistance with regard to present design practice<sup>9</sup> includes the section modulus term  $bd^2/6$ . This suggests a linear interpretation of the appropriate stress-strain characteristics, and the respective  $n, m$  limit state moment-thrust interaction locus corresponding to the cracked configuration is included in Fig. 4. This locus is derived from the familiar elastic basis, with stress-strain characteristics being linear up to the limiting case of  $\sigma_m, \epsilon_m$  (Fig. 1). While the expressions for squash load are the same for both the elastic theory and the non-linear theory discussed here, it is important to note that the maximum moment in the latter exceeds that in the former by 20% (Fig. 4); i.e.  $m = 1$  corresponds to  $M_m = M_s = 9\sigma_m bd^2/80$ .

15. For design practice, the expression for the respective moment of resistance,<sup>9</sup>  $M_m$ , can be written in the form

$$M_m = M_t + Pd/6 \quad (28)$$

where  $M_t$  is the permitted tensile resistance (and is not a function of  $P$ ). Neglecting this tensile component, then the relationship  $M_m = Pd/6$  conforms to the unique linear theory limit state  $n = 0.5, m = 0.75$ , corresponding to the respective cracked/uncracked interface state.

16. Interpreting equation (28) as a design limit state locus, initially for  $0 \leq P \leq P_s/2$  and neglecting the tensile component, generates the non-dimensionalized expression  $m = 16n/10.8, 0 \leq n \leq 0.5$ , which is also depicted in Fig. 4. Including the variable tensile component and noting code constraints<sup>9</sup> on  $n$ ,

$$m = \left( \frac{96M_t}{P_s d} + 16n \right) / 10.8 \quad (0 \leq n \leq 0.44) \quad (29)$$

is the  $n$ - $m$  equivalent of equation (28); this is sketched in Fig. 4 with the tensile term being, typically, responsible for a few percent of the total resistance moment at the prescribed upper limit value of  $n$ . This upper limit has an 'absolute' maximum value of 0.44 ( $= [0.9 \times 2.5]^{-1}$ ) as denoted in equation (29). The relationship between this design locus and that corresponding to the non-linear theory presented previously can be seen in Fig. 4. It is suggested that some relaxation of present design criteria, leading to more economic design practice, could be considered; the availability of constitutive loci of the form typified by Fig. 1 would be an essential prerequisite, however.

### Conclusions

17. An axial force/bending moment interaction diagram for masonry employing a parabolic stress-strain relationship has been produced, and the effect of the

## LIMIT STATE PROPERTIES OF MASONRY

falling branch demonstrated. The diagram provides appropriate data with respect to the limit state characteristics of masonry. The area enclosed by the limit state locus and the abscissa defines 'safe' combinations of axial force and bending moment with regard to a rectangular masonry section. The study affords insight into masonry mechanics and invites further consideration of present design practice.

### Acknowledgements

18. The Authors thank J. Ducker, J. Ducker and Associates, Consulting Engineers, Rotherham, and B. L. Davies, formerly Chief Engineer, Bridges and Structures, South Yorkshire County Council, for their advice and assistance.

### References

1. CURTIN W. G. Brick diaphragm walls in tall single storey buildings. *Design guide No. 3* (revised edition), The Brick Development Association, 1979.
2. CURTIN W. G. *et al.* Design of brick fin walls in tall single storey buildings. *Design Guide No. 8*, The Brick Development Association, 1980.
3. HEYMAN J. *The masonry arch*. Ellis Horwood Ltd, Chichester, 1982.
4. WALKLATE R. P. and MANN J. W. A method for determining the permissible loading of brick and masonry arches. *Proc. Instn Civ. Engrs*, Part 2, 1983, 75, Dec., 585-597.
5. TOWLER K. D. S. *The structural behaviour of brickwork arches*. PhD thesis, University of Liverpool, 1981.
6. POWELL B. and HODGKINSON H. R. *Determination of stress-strain relationship of brickwork*. TN249, British Ceramic Research Association, Stoke-on-Trent, 1976.
7. TOWLER K. and SAWKO F. Limit state behaviour of brickwork arches. *Proc. 6th Int. Conf. on Brick Masonry, Rome, 1982*. ANDIL, Rome, 412-421.
8. SAWKO F. and ROUF M. A. On the stiffness properties of masonry. *Proc. Instn Civ. Engrs*, Part 2, 1984, 77, Mar., 1-12.
9. BRITISH STANDARDS INSTITUTION. *Code of practice for structural use of masonry*. BSI, London, 1978, BS 5628, Part 1.

b	breadth of section
d	depth of section
d'	effective depth of cracked section
e	eccentricity
m	non-dimensional bending moment parameter, $m=M_m/M_s$
M	bending moment
$M_m$	limit state bending moment
$M_s$	maximum limit state bending moment
$M_t$	tensile component of bending moment
n	non-dimensional axial compression parameter, $n=P_m/P_s$
P	axial compression
$P_m$	limit state axial compression
$P_s$	squash load
y	sectional spatial co-ordinate
$y_m$	distance from centroid to fibres undergoing maximum stress
zz	flexural axis
$\epsilon$	compressive strain
$\epsilon_m$	compressive strain accompanying maximum compressive stress
$\epsilon_{sm}$	centroidal strain at limit state
$\epsilon_1$	top fibre strain
$\epsilon_2$	bottom fibre strain
$v_m$	curvature at limit state
$\sigma$	compressive stress

$\sigma_m$  maximum compressive stress  
 $\sigma_1$  top fibre stress  
 $\sigma_2$  bottom fibre stress

1. McKenning, Bridge Assessments for Heavy Loads, County Surveyor's Society, Panel Meeting Conference Manual, November 1985.
2. Technical Memorandum BD21/84, Department of Transport, 1984.
3. Technical Memorandum BA16/84, Department of Transport, 1984.
4. Crisfield, A Finite Element Computer Program for the Analysis of Masonry Arches, Transport and Road Research Laboratory, Laboratory Report LR 1115, 1984.
5. Heyman, Hobbs & Jermy, The Rehabilitation of Teston Bridge, Proceedings of The Institution of Civil Engineers, Part 1, August 1980.
6. Heyman, The Masonry Arch, Ellis Horwood, 1984.
7. Heyman, The Estimation of the Strength of Masonry Arches, Proceedings of The Institution of Civil Engineers, Part 2, December 1980.
8. Heyman, The Safety of Masonry Arches, International Journal of Mechanical Science, 1969.
9. Hendry, Davies & Royles, Test on Stone Masonry Arch at Bridgemill - Girvan, Department of Transport, 1985.
10. Towler, K. D. S., & Sawko, F., Limit State Behaviour of Brickwork Arches, Proceedings of The 6th International Brick Masonry Conference, Rome, 1982.
11. Towler, Structural Behaviour of Masonry Arches, PhD Thesis, University of Liverpool, 1982.

12. Harvey, Arches Stand The Test of Time, New Scientist, 15th May 1986.
13. Dowrick & Beckmann, York Minster Structural Renovation, Proceedings of The Institution of Civil Engineers, Paper 7415S, June 1971.
14. Dales Bridge Collapses With Frostbite, New Civil Engineer, 28th February, 1985.
15. Barlow, On the Presence (practically) of The Line of Equal Thrust in Arches and The Mode of Determining it by Geometrical Construction, Proceedings of The Institution of Civil Engineers, Volume 5, 1846.
16. Castigliano, C. A. P., Theorie de L'equilibre des Systemes Elastiques et ses Applications, Augusto Frederico Negro, Turin, 1879.
17. Pippard et al, The Mechanics of The Voussoir Arch, Journal of The Institution of Civil Engineers, Volume 4, 1936.
18. Page, Mechanism Computer Programmes for The Prediction of Masonry Arch Bridge Collapse Loads, Department of Transport, April 1986.
19. Walklate & Mann, A Method for Determining The Permissible Loading of Brick and Masonry Arches, Proceedings of The Institution of Civil Engineers, Part 2, December 1983.
20. Hendry et al, Load Test to Collapse on a Masonry Arch Bridge at Bargower, Strathclyde, Contractor Report 26, Transport & Road Research Laboratory, 1986.

21. Sawko & Towler, Structural Behaviour of Brickwork Arches, Proceedings of The 7th International Loadbearing Brickwork Conference, November 1981.
22. Hodgkinson & Powell, The Determination of The Stress Strain Relationship for Brickwork, Proceedings of The 6th International Brick Masonry Conference, Brugge, April 1976.
23. Science & Engineering Research Workshop on Masonry Arch Bridge Assessment, Edinburgh University, July 1986.
24. Technical Memorandum BE3/73, Department of Transport, 1973.
25. Curtin, Shaw, Beck & Bray, Structural Masonry Designer's Manual, Granada, 1982.
26. Hudson, Crouch & Fairhurst, Soft, Stiff and Servo Controlled Testing Machines: A Review with Reference to Rock Failure, Engineering Geology, Vol. 6, 1972.
27. Sawko & Rouf, On The Stiffness Properties of Masonry, Proceedings of The Institution of Civil Engineers, Part 2, March 1984.
28. Taylor & Mallinder, On The Limit State Properties of Masonry, Proceedings of The Institution of Civil Engineers, Part 2, March 1987.
29. Code of Practice for Use of Masonry, B.S. 5628:Parts 1 to 3:1985, B.S.I.
30. Pease, J, Wanted - Arch Bridges For Demolition Testing, Construction News, October 22, 1987.
31. Taylor & Davies, Discussion on Paper 8677, Proceedings of The Institution of Civil Engineers, Part 2, September 1984.

32. Terzaghi & Peck, Soil Mechanics in Engineering Practice, Wiley, 1967.
33. Marshall & Nelson, Structures, Pitman, Second Edition, 1977.
34. Mills, Theory of Structures, Macmillan, 1965.
35. Chettoe & Henderson, Masonry Arch Bridges: A Study, Proceedings of The Institution of Civil Engineers, Volume 7, 1957.
36. Jennings, Use and Misuse of Fuller's Construction for The Analysis of Masonry Arches, The Structural Engineer, Volume 63A/Number 11, November 1985.
37. Taylor, Mallinder & Davies, Discussion on Technical Note 381, Proceedings of The Institution of Civil Engineers, Part 2, December 1984.
38. Frisch-Fay, Influence of Tensile Additives to The Stability of Masonry Structures, International Journal of Masonry Construction, Volume 1, Part 2, 1980.
39. Tellett & Hodgkinson, The Structural Performance of Brickwork Arches, 8th International Symposium on Loadbearing Brickwork, British Ceramic Society, November 1983.
40. Vilnay, Buckling of Masonry Arches, Proceedings of The Institution of Civil Engineers, Part 2, March 1984.
41. Tellett, A Review of The Literature on Brickwork Arches, British Ceramic Research Association, Technical Note 338, 1982.

42. McDowell, McKee & Sevin, Arching Action Theory of Masonry Walls, Proceedings of The American Society of Civil Engineers, Paper 915, March 1956.
43. Anderson, Arching Action in Transverse Laterally Loaded Masonry Wall Panels, Structural Engineer, Volume 62B, March 1984.
44. Parme & Holland, Parabolic Arches of Variable Thickness, Journal of The Structural Division of The American Society of Civil Engineers, December 1964.
45. Lightfoot & Hutchinson, Optimum Design Considerations for Arch Bridges, Proceedings of The Institution of Civil Engineers, Part 2, December 1979.
46. Calhoun & DaDeppo, Non-linear Analysis of Clamped Arches, Journal of Structural Engineering (America), March 1983.
47. Pedreschi & Sinha, Deformation and Cracking of Post Tensioned Brickwork Beams, The Structural Engineer, December 1985.
48. McKay, Retaining Wall Design: The Determination of Lateral Earth Pressure, Civil Engineering Technology, October 1983.
49. Davies & Smith, Conference on Large Ground Movements and Structures, U.W.I.S.T., July 1977.
50. Code of Practice for Stone Masonry, B.S. 5390:1976, B.S.I.
51. Dadson, Destruction Tests Bend Loading Laws, New Civil Engineer, 17th October 1985.
52. Bridge Test Bears out Model Estimates, New Civil Engineer, 31st May 1984.

53. The Pitztal Arch Bridge, Construction Industry International, November 1983.
54. A Chance for Old Bridges, New Civil Engineer Editorial, 19th April 1984.
55. Chatterjee, Assessment of Old Bridges, Highways & Transportation, February 1985.
56. Bridge Busts Under Pressure, Construction News, February 1986.
57. Cracks Corrected, New Civil Engineer, September 1985.
58. Metal Bridge Loading Failures on a Huge Scale, New Civil Engineer, 30th January 1986.
59. Low Cost Rehabilitation Using Curved Steel Sections, The Structural Engineer, December 1983.
60. Ferguson, Bridge Checks to be Huge and Costly, New Civil Engineer, 23rd June 1983.
61. Jones, The Inspection and Maintenance of Highway Structures, Municipal Engineer, January 1984.
62. Fuller, Curve of Equilibrium for a Rigid Arch Under Vertical Forces, Proceedings of The Institution of Civil Engineers, Volume 40, 1875.
63. Lancaster, The Strengthening of The Weycroft Bridge Axminster, The Highway Engineer, January 1982.
64. Davies & Kemsley, Structural Renovation of Pont Lima, Civil Engineering, April 1981.
65. Tests on Road Bridges (Research Paper Number 16), National Building Studies, H.M.S.O., 1953.

66. Mallett, Bridge Maintenance Value for Money, Institute of Highways & Transportation, April 1986.24.
67. Vilnay & Cheung, Stability of Masonry Arches, Journal of Structural Engineering (America), February 1985.